**Magnetic Separation Nanotechnology for Wastewater Treatment and Used Nuclear**

**Fuel Recycle**

A Dissertation

Presented in Partial Fulfillment of the Requirements for the

Degree of Doctorate of Philosophy

with a

Major in Environmental Science

in the

College of Graduate Studies

University of Idaho

by

Huijin Zhang

Major Professor: You Qiang, Ph.D.

Committee Members: Batric Pesic, Ph.D.; Ruprecht Machleidt, Ph.D.; Shenghan Xu, Ph.D.

Department Administrator: Robert Mahler, Ph.D.

May 2016

**Authorization to Submit Dissertation**

This dissertation of Huijin Zhang, submitted for the degree of Doctorate of Philosophy with a major in Environmental Science and titled "**Magnetic Separation Nanotechnology for Wastewater Treatment and Used Nuclear Fuel Recycle**," has been reviewed in final form. Permission, as indicated by the signatures and dates below, is now granted to submit final copies to the College of Graduate Studies for approval.

Major Professor:          _____Date_____
                                            You Qiang, Ph.D.

Committee Members:    _____Date_____
                                            Batric Pesic, Ph.D.

                                     _____Date_____
                                            Ruprecht Machleidt, Ph.D.

                                     _____Date_____
                                            Shenghan Xu, Ph.D.

Department
Administrator:              _____Date_____
                                            Robert Mahler, Ph.D.

**Abstract**

Magnetic separation nanotechnology is an upcoming technology in the field of wastewater and nuclear waste treatment and environmental remediation for heavy metal and radioactive contaminants. Traditional separation methods such as centrifugation and filtration are usually labor-consumptive, uneconomical and thus impractical for large-scale water treatment. From this point of view, magnetic nanosorbents exhibit special superiority due to convenient separation by an external magnetic field. Other advantages of magnetic nanosorbents are low inventory utilization of nanosorbents, enhanced metal sorption efficiency and selectivity, and low production of secondary waste. This dissertation presents the study on our lab-made magnetic nanosorbents (referred to as dMNP-DTPA) – double coated magnetic nanoparticles (dMNP) coupled with diethylene triamine pentaacetic acid (DTPA) and their potential to be used as effective sorbent materials to remove metal ions (bivalent heavy metals and trivalent lanthanides) from aqueous solutions. The metal sorption results show that the magnetic nanosorbents developed in our study possess a high stability, fast kinetics, and high sorption efficiency in harsh environments. The metal sorption on the dMNP-DTPA nanosorbents is reversible so that the metal-loaded dMNP-DTPA can be fast and effectively regenerated by the dilute acids. The sorption/desorption cycle experiments demonstrate that the dMNP-DTPA nanosorbents can be reused for a long time which helps to offset the synthesis cost and makes this technique cost-effective. To better explore the dynamic behavior of MNPs in a continuous flow, a simulation tool, Computational Fluid Dynamics (CFD), is applied in this study. The CFD models will help us to design a separation system that can be operated under continuous flow conditions.

**Curriculum Vitae**

**Huijin Zhang**

Room 333, Engineering/Physics Building
University of Idaho, Moscow, ID 83844
Phone: 208-596-9186
E-mail: zhan3921@vandals.uidaho.edu

## EDUCATION

- Ph.D. in Environmental Science, University of Idaho, Moscow, Idaho, USA – May 2016
- M.S. in Environmental Science, University of Idaho, Moscow, Idaho, USA – May 2012
- B.S. in Environmental Science, Liaoning University, Shenyang, Liaoning, China – July 2008

## WORK EXPERIENCE

▶ **Research Assistant,** University of Idaho (Aug. 2009 – Dec. 2015, Moscow, ID)
- Worked on the magnetic separation nanotechnology project
- Guided undergraduates in the research lab

▶ **Teaching Assistant,** University of Idaho (Aug. 2011 – Dec. 2015, Moscow, ID)
- Set-up and taught environmental science labs, course website design and maintenance
- Coordinated students' service learning opportunities with different organizations

▶ **Summer Intern,** Idaho National Laboratory (Jun. 2014 – Aug. 2014, Idaho Falls, ID)
- Worked on the lanthanide extraction project
- Worked on the Am/Eu separation project

▶ **Research Assistant,** Liaoning University (Oct. 2007 – Jun. 2008, Shenyang, China)
- Worked on the biological toxicity of the ionic liquid project
- Worked on the hydroponic culture of wheat

## PUBLICATIONS

- **H. Zhang**, R. McDowell, L. Martin, Y. Qiang, "Selective Extraction of Heavy and Light Lanthanides from Aqueous Solution by Advanced Magnetic Nanosorbents." *ACS Applied Materials & Interfaces*, 2016, 8(14): 9523–9531.
- **H. Zhang**, H. Zhou, Y. Qiang, "Thermodynamic, and Reusability of DTPA-Functionalized Magnetic Nanosorbents for Cadmium Removal from Wastewater." Submitted to Water Research.
- M. Kaur, **H. Zhang**, L. Martin, T. Todd, Y. Qiang, "Conjugates of Magnetic Nanoparticle - Actinide Specific Chelator for Radioactive Waste Separation," *Environmental Science & Technology,* 2013, 47(21): 11942-11959.
- M. Kaur, **H. Zhang**, Y. Qiang, "Magnetic Separation Dynamics of Colloidal Magnetic Nanoparticles," *Magnetics Letters, IEEE*, 2013, 4:4000204-4000204.

- **H. Zhang**, A. K. Johnson, M. Kaur, A. J. Paszczynski, and Y. Qiang, "Fast Separation of Cadmium and Lead Ions from Contaminated Water using Conjugates of Magnetic Nanoparticle-DTPA," *11th International Conference on Nanotechnology*, 2011, 1504-1507.
- S. K. Rastogi, J. M. F. Jabal, **H. Zhang**, C. M. Gibson, K. J. Haler, Y. Qiang, D. E. Aston, and A. L. Branen. "Antibody@silica coated Iron Oxide nanoparticles: synthesis, capture of E. coli and SERS titration of biomolecules with antibacterial silver colloid". *Journal of Nanomedicine & Nanotechnology*, 2011, 2(7):121.
- S. K. Rastogi, J. M. F. Jabal, **H. Zhang**, C. M. Gibson, K. J. Haler, Y. Qiang, D. E. Aston and A. L. Branen. "Silica Coated Magnetic Nanoparticles (SMNPs): Capture and Identification of Escherichia coli using Surface Enhanced Raman Spectroscopy". NSTI-Nanotech 2011, www.nsti.org, ISBN 978-1-4398-17138-6, vol. 3, 68-71.
- W. Guan, W. Xue, **H. Zhang**. "Research and the developing direction of the toxicity of ionic liquids (in Chinese)". *Journal of Liaoning University,* 2008, 35(2):127-132.

## CONFERENCE-PRESENTATIONS

- **H. Zhang**, R. McDowell, L. Martin, Y. Qiang, "Removal of actinides and lanthanides from aqueous solution by DTPA-functionalized magnetic nanosorbents," American Physical Society (APS) Northwest Section Meeting, May 14-16, 2015, Pullman, WA, USA.
- **H. Zhang**, and Y. Qiang, "Magnetic Separation nanotechnology for heavy metal treatment in industrial wastewater," Environment, Agriculture, Resources, Technology and Society (EARThS) Interdisciplinary Conference, April 11, 2015, Pullman, WA, USA.
- **H. Zhang**, L. Martin, Y. Wu, Y. Qiang, "Magnetic nanosorbents for recycling spent nuclear fuel," 2015 TMS Annual Meeting & Exhibition, March 15-19, 2015, Orlando, FL, USA.
- **H. Zhang**, T. Xing, and Y. Qiang, "Magnetic nanosorbents for heavy metal and radioactive waste treatment," Materials Science & Technology 2014 Conference & Exhibition, October 12-16, 2014, Pittsburgh, PA, USA.
- **H. Zhang**, M. Kaur, Y. Qiang, "Magnetic Nanosorbents for Fast Separation of Radioactive Waste". ANS Global 2013, September 29 – October 3, 2013, Salt Lake City, UT, USA.
- **H. Zhang**, A. K. Johnson, M. Kaur, A. J. Paszczynski, and Y. Qiang. "Fast Separation of Cadmium and Lead Ions from Contaminated Water using Conjugates of Magnetic Nanoparticle-DTPA". IEEE NANO 2011, 11th International Conference on Nanotechnology, August 15-18, 2011, Portland, OR, USA.
- **H. Zhang**, A. K. Johnson, M. Kaur, A. J. Paszczynski, and Y. Qiang. "Synthesis and evaluation of conjugates of magnetic nanoparticle-DTPA for fast separation of cadmium ions from contaminated water". 53rd Annual Symposium of the Idaho Academy of Science, March 31 – April 2, 2011, Meridian, ID, USA.
- **H. Zhang**, A. K. Johnson, M. Kaur, A. J. Paszczynski, and Y. Qiang. "Separation of heavy metal ions from wastewater using conjugates of magnetic nanoparticle-chelator". Joint 65th Northwest/22nd Rocky Mountain Regional Meeting of the ACS, June 20-23, 2010, Pullman, WA, USA.

**Acknowledgements**

During the career of a graduate student, I feel a deep gratitude to many people for their assistance and support on the approach to my PhD degree. Of those people, the most important person to acknowledge is my advisor Dr. You Qiang. I would like to thank Dr. Qiang for his tremendous time and effort spent on guiding, supporting, and encouraging me during my graduate study. Without his abundant knowledge of science and stimulating suggestions, my study and research would not proceed so smoothly and effectively. I also would like to thank Dr. Batric Pesic, Dr. Ruprecht Machleidt, and Dr. Shenghan Xu for serving on the committee, and valuable comments and suggestions on my defense and dissertation.

I would like to express my appreciation to Dr. Andrzej Paszczynski for offering me the opportunity to work in his lab. I am also grateful to Dr. Ray von Wandruszka and Dr. Sofie Pasilis for their support on the atomic absorption spectrophotometer (AAS), Dr. Tao Xing and his student Mr. Joseph George for sharing their knowledge on the magnetic separation CFD project, Dr. Eric Aston for his assistance on the zeta potential analyzer, Dr. Armando McDonald and his student Dr. Liqing Wei for help in the FTIR measurements. Additionally, special thanks are given to Dr. Leigh Martin, Dr. Rocklan McDowell, Dr. Catherine Riddle and many other people at the Idaho National Laboratory (INL) for both their time spent working with me at INL on the lanthanide separation project. They made my 2014 summer intern at Idaho Falls such memorable.

I owe great thanks to my academic advisor Chris Dixon and Alecia Hoene for their assistance with the logistics of my graduate education. Additionally, I would like to specially thank my colleagues and friends Dr. Maninder Kaur, Dr. Jennifer Anand

Sundararajan, Joseph  George, Lokendra Khanal for their constant concern and endless help during my time at the University of Idaho.

I feel grateful to all my friends in Moscow, ID. They have made my life here delightful and memorable. I also want to thank all the professors, staff and students in Environmental Science Program and Department of Physics at UI for offering me such a joyful studying and working environment.

My deepest gratitude goes to my parents and my husband for their unconditional love and support throughout my life. And finally my son, Miles, it was difficult to have you near the end of my graduate study when life was so busy. But thank you for showing up and becoming the sweetest burden and blessing in my life.

**Table of Contents**

## List of Figures

## List of Tables

**Chapter 1: Introduction to Magnetic Separation Nanotechnology**

**1.1 Magnetic separation**

**1.1.1 History and basic principle**

The history of magnetic materials can be traced back to as early as the 6th century BC. However, the field of magnetic separation, which applies the properties of magnetic materials to the actual practices, is only about 200 years old. The physics behind the magnetic phenomenon remained mysterious until the late 18th century. In 1792, the first patent on magnetic separation, issued to William Fullarton, describing the separation of iron minerals by magnetic attraction, heralded the birth of the field of magnetic separation.[1,2] In the mid-1800s, Faraday demonstrated in a series of experiments that materials react quite differently to the presence of an applied magnetic field, either increasing or decreasing to a varying degree the magnetic field passing through them. Such variation of magnetic susceptibility of different materials in response to an applied magnetic field makes possible the phenomenon of magnetic separation. Since then, numerous magnetic devices have been developed utilizing differences in magnetic susceptibility to achieve physical separation of mineral products.[3] In the 1950s, a new technology – high gradient magnetic separation (HGMS) – was introduced that could generate fairly large field gradients around the loosely packed ferrous wires in the column, and thus produce large enough magnetic forces to attract and trap even weakly magnetic particles in the flow stream. HGMS offered a faster and more universal separation process, and gave a rise to a great expansion of the field of magnetic separation to broader applications, especially to separation problems where the subject of interest has relatively low magnetic susceptibility.[4,5]

Over these two hundred years of development, the basic principle behind magnetic separation has remained very simple and unchanged. This basic principle states that materials with different magnetic susceptibility experience different forces under the magnetic field gradients. In other words, magnetic separation is a process in which a magnetic force, generated by an applied external magnetic field, extracts materials with distinctive magnetic properties from a mixture.[6]

Based on its magnetic susceptibility, a material can be classified as ferromagnetic, paramagnetic, or diamagnetic. Ferromagnetic materials have a large, positive susceptibility to an external magnetic field. They are strongly attracted to magnetic fields and retain their magnetic properties in the absence of an applied magnetic field. Also such materials have a magnetic saturation point beyond which increasing the magnetic field strength with not increase the magnetization of the material. Paramagnetic materials have a small, positive susceptibility, which are weakly attracted by a magnetic field. Although it is difficult to magnetize, the induced magnetization is proportional to the magnetic field strength applied, and usually it cannot be magnetically saturated. Diamagnetic materials have a weak, negative susceptibility and slightly repelled by a magnetic field. Both paramagnetic and diamagnetic materials do not retain the magnetic properties when the external field is removed. Materials that are negligibly affected by magnetic fields are classified as non-magnetic. Different strengths of magnetic force can be generated by permanent magnets, electromagnets, or superconducting magnets.

In the presence of an external magnetic field, magnetic particles experience tractive magnetic forces, the principal force that the magnetic separation exploits to remove particles from solution, which is expressed as[7]

$$F_{\mathrm{m}} = V_{\mathrm{p}} \Delta\chi \nabla(\frac{1}{2} B \cdot H) \qquad (1\text{-}1)$$

in which $V_{\mathrm{p}}$ denotes the volume of the particle, $\Delta\chi$ denotes the effective volumetric magnetic susceptibility of the particle relative to the solution, $B$ denotes the magnetic induction, and $H$ denotes the strength of the magnetic field. So the magnetic force is proportional to the particle volume and magnetic properties, as well as the differential of the magnetostatic field energy density, $\frac{1}{2} B \cdot H$.

In fact, in addition to the magnetic force, there are several competing forces simultaneously acting on the magnetic nanoparticle during flow in a magnetic field, such as the hydrodynamic drag force ($F_{\mathrm{d}}$) due to the flow velocity, the gravitational force ($F_{\mathrm{g}}$) for large and dense particles, diffusive forces ($F_{\mathrm{B}}$) from Brownian motion of particles, and other forces such as the inertial force and Helmholtz double layer interaction.

The drag force acts against magnetic separation, which can be obtained from Stocks' equation:

$$F_{\mathrm{d}} = 6\pi\eta R(v_{\mathrm{f}} - v_{\mathrm{p}}) \qquad (1\text{-}2)$$

where $\eta$ is the dynamic viscosity of the fluid, $R$ is the particle radius, and $v_{\mathrm{f}}$ and $v_{\mathrm{p}}$ are velocities of the fluid and particle respectively.

The gravitational force considering the buoyant force on the particle is expressed as:

$$F_{\mathrm{g}} = (\rho_{\mathrm{p}} - \rho_{\mathrm{f}})V_{\mathrm{p}}g \qquad (1\text{-}3)$$

where $\rho_{\mathrm{p}}$ and $\rho_{\mathrm{f}}$ are the density of particle and solution respectively, and $g$ is the acceleration due to gravity.

Equations for other interacting forces can be found in the References.[8–10] Those competing forces tend to reduce the degree of separation. Therefore, for a successful magnetic separation, the magnetic force must dominate other competing forces as the magnetic particles flow through the separator.

## 1.1.2 Advantages

Speaking of separation processes, standard methods such as filtration, sedimentation, centrifugation, evaporation, etc., are well-developed and well-established in diverse industrial applications. Therefore, it is not always obvious that magnetic separation could or should be used for a given problem while alternatives are present. Certainly, magnetic separation has a lot of remarkable advantages over these standard methods. Generally speaking, if part of the mixture is intrinsically magnetic, compared to equivalent centrifugation and filtration methods, magnetic separation can offer a faster, simpler and more efficient process to deal with large sample volumes by virtue of its higher throughput with greater specificity. Even for non-magnetic components, magnetic separation can be targeted to a specific product of interest and feasibly applied to almost any system, especially aqueous systems, by using engineered and functionalized magnetic particles or beads. Such selectivity and flexibility can hardly be achieved by traditional standard methods.

Regarding the economic consideration, magnetic separation offers many key advantages. Magnetic separation is generally a low cost or cost effective process and has been reported so by some studies. For instance, Yano *et al.* evaluated and compared the HGMS and the sand filtration applied to steel mill wastewater treatment (see Table 1.1).[11]

They reported that, with almost the same installation cost, HGMS excelled sand filtration in speed and space requirement, as well as in operating cost. Moreover, if a permanent magnet is used, operating cost will be further reduced since no external power is needed to generate the magnetic field. The rare earth magnetic separators are much cheaper compared to the electro-magnetic high intensity separators, but can still produce a magnetic field around 6,000 gauss. In addition, maintenance is less needed for a magnetic separator than for column-based or membrane-based separators since the fouling and clogging problems are greatly reduced. The modern design of superconducting separator operates continuously, 24 hours per day, 7 days per week, with less than a 12-hour shutdown per year for essential maintenance.[12] According to Vedavyasan's report, by adopting an electromagnetic separator there was a 30% reduction in down time owing to the saving in membrane cleaning.[13] Last but not least, most magnetic separation systems could operate with minimal supervision due to high levels of reliability and automation as demonstrated in the china clay industry since the late 1980s.[12] In brief, magnetic separation offers great savings in time, space, and cost and labor in various applications as opposed to conventional methods. This promises a wide field of applications with great prospects.

**Table 1.1** Comparison between HGMS and sand filtration methods used in steel mill wastewater streams.[11]

|  | **HGMS** | **Sand filter** |
|---|---|---|
| Flow rate | $6*10^{-2}$ m/s | $8*10^{-3}$ m/s |
| Feed time | 20 min | 8 h |
| Space | 4.5 $m^2$ | 8 $m^2$ |
| Relative operating cost | 0.7 | 1 |
| Relative installation cost | 1.1 | 1 |

**1.1.3 Applications**

Up till now, the applications of magnetic separation have spanned increasingly complex and diverse industrial processes and scientific research, ranging from mineral benefication to food processing, from clay decolorization to protein/DNA purification, from steel production to water purification.[14] Numerous applications are closely related to environmental protection and remediation. For example, sulfur in coal is an important source of sulfur dioxide that contributes to the production of acid rain and other air pollution. Magnetic separation has, for decades, been applied to the coal desulfurization process to effectively remove pyrite ($FeS_2$) owing to the magnetic nature of pyrite and its derivatives.[15,16] In another example, several studies reported that HGMS can be used to capture fly ash containing iron magnetic faction, i.e. iron oxides, from power plants.[17,18] The captured fly ash can also offer a way to recycle iron oxides in industries.

Moreover, with respect to environmental applications, magnetic separation provides a very promising and clean technology for water treatment and purification. Various impurities or contaminants in water can be removed using magnetic assistance.[19]

First, a magnetic separator can be directly applied to water streams to remove impurities on the basis of their ferromagnetic or paramagnetic properties in nature without adding any carrier magnetic component. This can be seen in the removal of magnetic particulates and other iron-containing impurities from a steel mill or metal finishing wastewater,[20] the removal of radionuclides in waste sludge,[21] and the removal of corrosion products from a pressurized water nuclear reactor.[22]

Second, magnetic seeding flocculation combined magnetic separation techniques are widely used for general removal of non-magnetic water pollutants, such as coliform

bacteria, suspended solids, and specific elements like phosphate and heavy metal ions.[23–25] In this process flocculant cations, such as Fe(III) and Al(III), and magnetic seeds, such as fine magnetite powder, are added, yielding insoluble but magnetic flocs. At the same time, contaminants such as oil, suspended solids, and metal ions co-precipitate with these flocs and are together separated from the water body by means of magnetic separation.

Last but not the least, magnetic sorbents enable an effective solid liquid separation technology for wastewater treatment where the direct HGMS or magnetic flocculation is difficult to apply or has low efficiency. By a successful attachment of specific functional groups to magnetic particles or beads, engineered or functionalized magnetic sorbents not only possess high sorption efficiency to attract and remove non-magnetic materials but also greatly improve selectivity for target species. Therefore, magnetic sorbents, as a more flexible and versatile technique, lead to a hot field of environmental research on magnetic separation, extraction and remediation of inorganic pollutants such as heavy metal ions [26,27] and radioactive elements,[28,29] as well as organic pollutants like spilled oil contaminant.[30] Given the significance of magnetic sorbents in magnetic separation applications and the ongoing need for more efficient, universal, and magnetically responsive sorbents to meet industrial requirements, extensive research on design, synthesis and evaluation of such magnetic sorbents is necessary and worth the effort.

## 1.2 Magnetic nanoparticles

Magnetic nanoparticles are a class of particles within nanoscale (typically 1-500 nm in diameter) that can be manipulated by an external magnetic field. Their magnetic properties can be determined by studying the hysteresis loop, i.e. *M-H* curve, as shown in

Figure 1.1. $M$ is the magnetic moment per unit volume, and $H$ is the strength of a magnetic field. Ferromagnetic particles, once being magnetized, show remnant magnetization ($M_r$) after the external field is removed (Figure 1.1a). The strength of the reverse magnetic field required to bring the magnetization to zero is called coercivity ($H_c$). Such particles exhibit ordered magnetic states and are magnetic even without a field applied.

However, when scaling the particle size down to nanosize, especially when it is below a threshold size, i.e. the critical diameter, magnetic particles may display a remarkably unique property – superparamagnetism – that arises from their single magnetic domain structure. A superparamagnetic nanoparticle exhibits a large magnetization in the presence of an applied magnetic field, but has little to no $M_r$ or $H_c$ after the magnetic field is removed (see Figure 1.1b). These features make superparamagnetic nanoparticles very attractive to a broad range of applications because magnetic agglomeration will not happen to such nanoparticles at room temperature, which further means that such nanoparticles can be easily and well dispersed in aqueous solution in absence of applied magnetic field.[31,32]

This superparamagnetic behavior is both size- (Figure 1.2a) and temperature-dependent (Figure 1.2b). Typically, the critical diameter lies in the range of a few tens of nanometers depending on the material. For example, the critical diameter of a spherical Fe particle is ~15 nm and $Fe_3O_4$ is ~25 nm. At temperatures above the blocking temperature ($T_B$), the thermal energy flips the atomic spins of single-domain particles rapidly, causing the atomic magnetic moment to fluctuate randomly, so that in zero external field, the net moment of the particles is zero (no remnant magnetization).

In addition to specific magnetic properties, magnetic nanoparticles also possess other distinctive attributes, such as large specific surface area as well as their reactivity for surface

functionality that directly contribute to the improvement of sorption capacity and selectivity, making them an excellent sorbent candidate for magnetic separation.
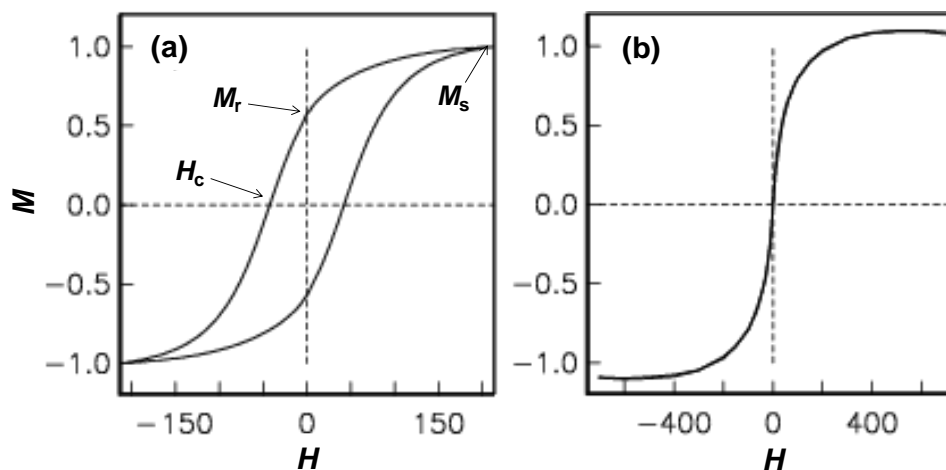


**Figure 1.1** Hysteresis loops magnetic nanoparticles. (a) Ferromagnetism ($M_r$ - remnant magnetization; $H_c$ - coercivity; $M_s$ - saturation magnetization); (b) superparamagnetism with $M_r$=0 and $H_c$=0.
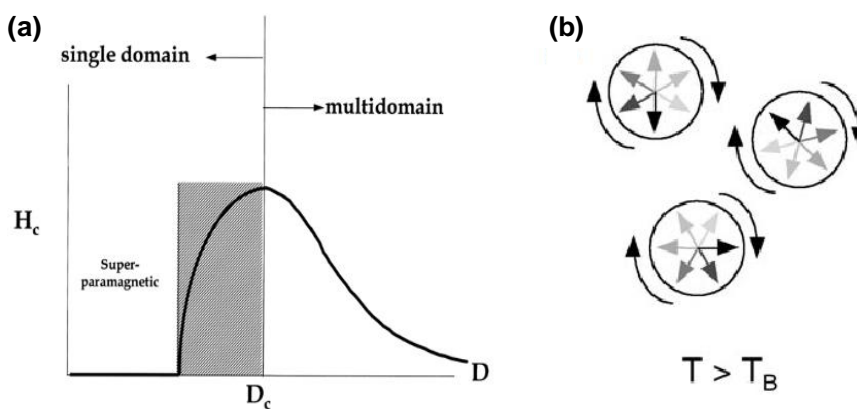


**Figure 1.2** Illustration of the concept of superparamagnetism. (a) Relationship between particle size and coercivity;[31] (b) randomly atomic spins at zero external field when above blocking temperature ($T_B$) (circles depict three magnetic nanoparticles, and the arrows represent the magnetization direction in those particles).[7]

**1.3 Magnetic nanosorbents**

During the last few decades, numerous works have been done on nanosized materials in adsorption process due to their unique physical and chemical properties. With the large ratio of specific surface area to volume, nanoparticles have become a promising adsorbent candidate in adsorption process and been widely used in the chemical, biological, analytical, and environmental fields. On the other hand, because nanoparticles are quite small, the adsorption process is performed preferentially in a stirred suspension system instead of a conventional packed bed. Therefore, removing the nanosorbents from the suspension system after the adsorption is completed become a key issue in the application practice. By incorporating magnetism to nanosorbents, fast and effective separation of nanosorbents can be easily achieved by utilizing the external magnetic field. Recently, magnetic nanosorbents have made accessible an immense area of new functional materials that promise large markets. Due to their bifunctional properties of magnetic core and surface-functionalized shell, magnetic nanosorbents possess the ability of selective adsorption and rapid separation in external magnetic field. Since the early 1970s, considerable efforts have been made on the surface modification of core-shell nanosorbents to increase their surface area for high loading capacities and selective ability.[33] Applications of magnetic nanosorbents can be found in fields as diverse as biological cell separation, drug delivery, wastewater treatment, mineral separation, and food processing.

In general, magnetic nanosorbent materials should fulfill four requirements:[34] (1) large surface area to increase the adsorption ability; (2) good stability in severe condition during the sorption and separation steps; (3) highly selective attachment to the target species; and (4) quick magnetic response to be effectively separated.

**1.3.1 Selection of magnetic nanoparticles**

In nanosorbent-based magnetic separation, the selection of a right magnetic nanoparticle is of great significance to enable the best sorption and separation performance. So far, a wide range of synthetic methods has been established to produce magnetic nanoparticles with the following desirable properties:[35–39]

- A high magnetic susceptibility, so that they can be easily manipulated and captured by the applied magnetic field after mixing with the sample of interest.

- Paramagnetic or good superparamagnetic properties to limit irreversible magnetic agglomeration between magnetic nanoparticles.

- A high dispersibility in aqueous systems.

- An ability to easily functionalize the magnetic nanoparticle with specific ligands for binding the target species of interest.

Based on the requirements, superparamagnetic iron oxide nanoparticles have shown the most promise as potential magnetic nanosorbent materials for magnetic separation due to their well-established synthesis and surface functionalization processes.[35] Compared to oxides, metallic magnetic nanoparticles such as zero valent iron (ZVI) have much higher magnetic moments which are favorable for magnetic separation. However, metallic magnetic nanoparticles are highly reactive: they can be rapidly and completely oxidized in the presence of the solution, therefore losing their magnetic moments. To solve this dilemma, surface functionalization is used to enable the synthesis of magnetic nanosorbents with both high magnetic moment and high chemical stability.

**1.3.2 Surface functionalization of magnetic nanoparticles**

In a magnetic separation system used for naturally non-magnetic target species, such as metal ions in aqueous solution, the magnetic nanosorbent's utility lies in both its magnetic property and its surface functionality. The addition of specific coating/ligands to the surface of the magnetic nanoparticles is of great importance for tailoring the magnetic sorbents for specific applications. Figure 1.3 illustrates some of the commonly used methods for surface functionalization, including direct organic ligand modification, stabilization with polymers, inorganic stabilization with silica or carbon coating, precious metal (silver or gold) encapsulations, etc.[40] By tailoring the physical, chemical, and surface properties of magnetic nanoparticles, surface functionalization can enhance the sorption performance of magnetic nanosorbents. However, it also has a mild to dramatic effect on the core magnetic properties. Therefore, the selection of an appropriate surface coating is very important for a given application.
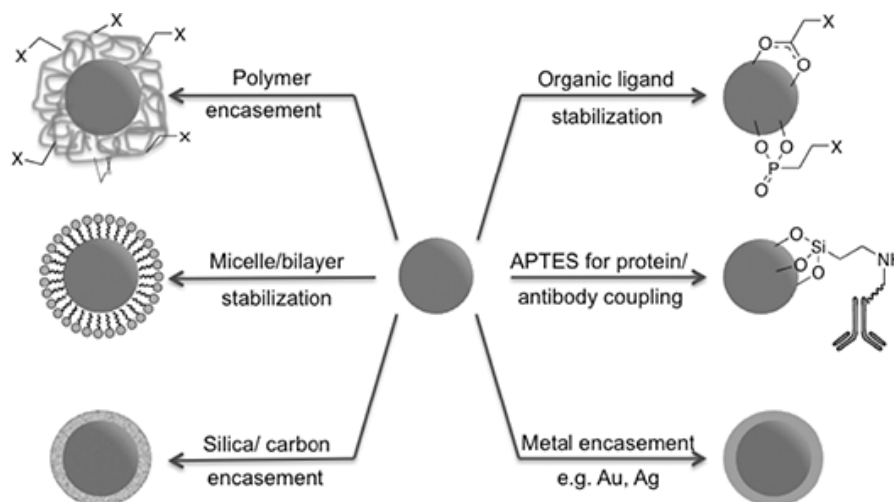
**Figure 1.3** Some of commonly used methods for surface functionalization of magnetic nanoparticles.[40]

For example, the silica coating made by the sol-gel process is by far the most common inorganic coating method.[41] As a chemically inert material, the silica shell increases the nanoparticle's stability in a harsh acid or base environment by preventing its dissolution, therefore maintaining its magnetization. The surface of silica coated magnetic nanoparticles can be easily modified with other functional groups via well-known silane chemistry. However, many studies also demonstrated the dramatic effect of the silica coating thickness on the final saturation magnetization.[42,43] As Han *et al.* reported, [43] the saturation magnetization of the silica coated MNPs drops from 60 emu/g to 44 emu/g by increasing the concentration of tetraethoxysilane (TEOS), the silica precursor, from 0 to 10%.

Another example is the polymer encasement. The polymer coating on magnetic nanoparticles can create repulsive (mainly as steric repulsion) forces between particles, therefore stabilizing the particles, enhancing dispersibility, as well as preventing particle agglomeration.[44,45] In addition, the polymer encasement usually causes the formation of larger particles or very large aggregates, but the intrinsic magnetic properties, such as superparamagnetism of the starting nanoparticles, can be retained. Moreover, the functional groups introduced with the polymer coating can be used for further surface modification.

## 1.4 Project scope and objectives

Nanosorbent based magnetic separation represents an emerging area of research in verious applications. Given the increasing generation of heavy metal containing wastewater and nuclear waste, this research mainly focuses on developing the magnetic separation process using magnetic nanosorbents, i.e. surface functionalized magnetic nanoparticles

conjugated with specific metal chelators (MNP-Che), to remove metal ions from aqueous systems. The basic process of treatment is illustrated in Figure 1.4. In this separation process, magnetic nanosorbents are added to the wastewater containing various contaminants in a reaction chamber and mixed thoroughly. To maintain the sorbents suspended, the system can be mixed by mechanical stirring. After the metal sorption, the magnetic nanosorbents absorbed with target metal species are separated by applying an external magnetic field. The supernatant is decontaminated and can be released. The metal ions absorbed on the nanosorbents can then be washed off with a small amount of stripping agent (compared to original wastewater). After that, the magnetic nanosorbents can be separated by magnetic assistance from the concentrated heavy metal solution, and reused for another treatment process. The concentrated heavy metals can be moved into further treatment or recycling.
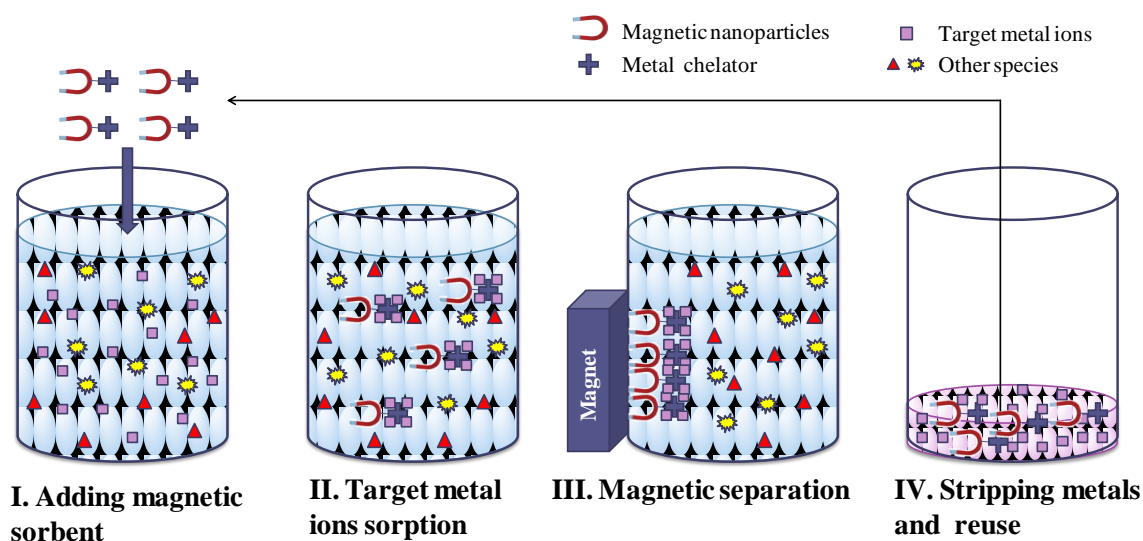


**Figure 1.4** Basic concept of magnetic separation process using magnetic nanosorbents.

This research work proceeds according to the flow chart in Figure 1.5. The main objective of this research is to develop a simple, fast, cost-effective, and environmentally benign technique that can be applied in industrial wastewater treatment and used nuclear fuel separation to reduce the volume of the liquid waste, reuse the sorbent materials, and recycle the useful metal ions in a closed-cycle. The results obtained from this investigation will be useful to generate data for scientific assessment in sorption performance and separation behavior of magnetic nanosorbents in aqueous solutions and to recommend candidate magnetic sorbents for metal extraction as well as design of continuous flow separation device utilized this magnetic separation nanotechnology.

```
        ┌─────────────────────────────────────────┐
        │      Commercial or lab-made MNPs         │
        └─────────────────────────────────────────┘
                          │
        ┌─────────────────────────────────────────┐
        │         Surface functionalization        │
        └─────────────────────────────────────────┘
                          │
        ┌─────────────────────────────────────────┐
        │   Characterizations of magnetic nanosorbents │
        └─────────────────────────────────────────┘
                          │
        ┌─────────────────────────────────────────┐
        │      Metal sorption: batch experiments    │◄──┐
        └─────────────────────────────────────────┘   │
                          │                             │
        ┌─────────────────────────────────────────┐   │  Reuse of
        │ Magnetic separation of sorbent-metal complex │   │  Magnetic
        └─────────────────────────────────────────┘   │  sorbents
                          │                             │
        ┌─────────────────────────────────────────┐   │
        │   Stripping metal ions from the complex   │───┘
        └─────────────────────────────────────────┘
```
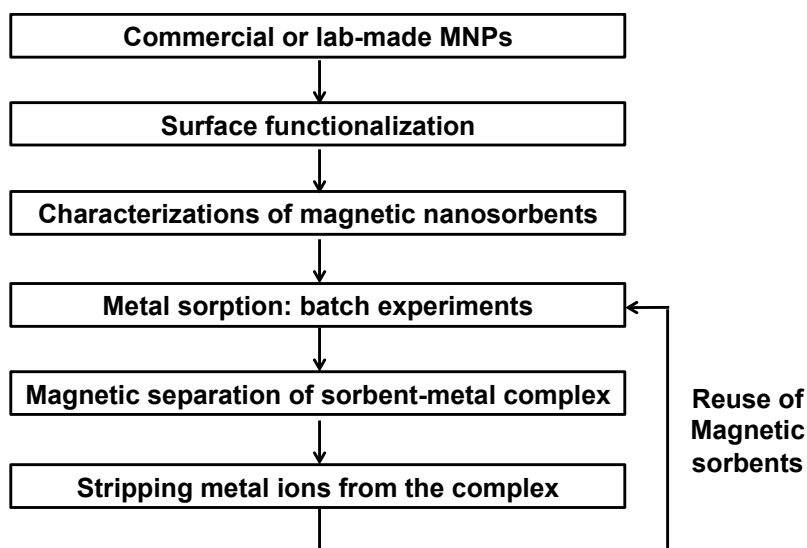
**Figure 1.5** Main research steps of magnetic separation using MNP-Che conjugates.

Previously, our lab-made magnetic nanosorbents, double coated iron/iron-oxide nanoparticles (dMNPs) conjugated with diethylenetriaminepentaacetic acid (DTPA), were synthesized and the batch sorption experiments had demonstrated that the dMNP-DTPA

nanosorbents were an excellent sorbents for the fast removal of cadmium ($Cd^{2+}$) and lead ($Pb^{2+}$) ions from contaminated water. The major factors affecting the metal sorption and magnetic separation effectiveness were evaluated, to be specific, the physical properties of magnetic nanosorbents, contact time, pH values, and the initial metal concentration. However, there were several issues that have not been addressed in our previous study, including (1) reusability of our lab-made nanosorbents; (2) multi-metal competitive sorption on dMNP-DTPA nanosorbents; (3) sorption potential study on other elements, such as actinides/lanthanides; and (4) continuous operation of the magnetic separation system. Based on these issues, this research focuses on addressing the following objectives:

- Evaluate the stability and reusability of the dMNP-DPTA nanosorbents by performing the Cd sorption/desorption cycle tests using the strong acid as the stripping agent.

- Study the sorption performance of dMNP-DTPA across the lanthanide series (as non-radioactive surrogates of actinides) for their possible applications for nuclear waste treatment.

- Examine the hydrodynamic behavior of MNPs in the applied magnetic field with the help of Computational Fluid Dynamics (CFD). In addition, a new magnetic separation device that can be operated under continuous flow condition will be proposed.

**Chapter 2: Literature Review**

**2.1 Introduction to heavy metal contaminated wastewater treatment**

**2.1.1 Heavy metal pollution in aqueous systems**

The term "heavy metals", from the perspective of environmental pollution, refers to any metallic or semimetallic element that has a relatively high density, usually with a specific gravity greater than 5 g/cm$^3$, and is of toxicity even at a low concentration.[46,47] Examples include mercury (Hg), cadmium (Cd), arsenic (As), chromium (Cr), nickel (Ni), and lead (Pb). As natural constituents of the Earth's crust, heavy metals are commonly existing and linked to human society. Some of them, such as copper (Cu) and zinc (Zn), are necessary as trace elements to maintain the metabolism of living organisms. However, a large amount of any heavy metal can cause acute or chronic toxicity or ecotoxicity, causing heavy metals to become metabolic poisons and enzyme inhibitors.[47,48] Since they are stable in the environment and cannot be degraded or destroyed by chemical or biological remediation processes, heavy metals are classified as persistent environmental pollutants.[49]

Heavy metal pollution in aqueous systems has already become a serious environmental issue on a local, regional, and even a global scale. For example, countries in Asia such as India, Bangladesh and China have experienced recent and severe problems of groundwater contamination with arsenic (As).[50] Bolivia and Berlin have also experienced heavy metal pollution (e.g., Cd, Pb, Cu and Zn) in drinking water sources.[51–53]

Heavy metals in aquatic systems come from both natural and anthropogenic sources. But currently the major causes of the pollution are human activities, such as the burning of fossil fuels, mining operations, municipal waste and sewage disposal, and agriculture practices.[54] In particular, wastewater discharges from mining activities and industries have

become a primary source of heavy metal release to the environment. This leads to a high concentration of toxic heavy metals such as Cd(II), Pb(II), Hg(II), and Cu(II) accumulating in rivers and lakes.[55,56]

The presence of heavy metals in aquatic systems, particularly in surface water, is of great concern for two reasons. On one hand, in water, heavy metals can be chemically or biologically converted into more soluble forms, making them easily transportable through rivers and streams to a long distance from their sources or seep into underground water, thereby contaminating the sources of drinking water. On the other hand, the soluble forms of heavy metals are usually more toxic and dangerous mainly because of their bioaccumulation, maybe over a million-fold, in the bodies of animals or human beings through the food chain. For humans, the accumulation of toxic heavy metals through drinking water and food can cause developmental retardation, kidney failure, various cancers, nervous system disorder, bone damage, as well as other serious illness, and even death in some cases of exposure to very high concentrations.[57,58] The "Minamata disease" and "Itai-Itai disease" were cases of heavy metal pollution caused by wastewater containing high concentrations of Hg and Cd, respectively.[59]

Many heavy metals have been categorized as hazardous substances and priority pollutants by the US Environmental Protection Agency (US-EPA) based on a combination of their frequency, toxicity, and potential for human exposure. During the past few decades, environmental regulations have been instituted by US federal and state governments to protect the quality of surface and ground water and, more importantly, human health from heavy metal pollutants such as Cd, Cu, Pb, Hg, and Zn.[60]

Given the more and more stringent regulatory limitations, increasing discharges, persistent toxicity and other adverse effects of heavy metals on receiving water, removing heavy metals from wastewater has become an urgent issue in order to protect the environment and human health.

**2.1.2 Heavy metal treatment in wastewater**

Heavy metals in wastewater have traditionally been treated by ion exchange, adsorption, chemical precipitation, membrane filtration, flotation, etc.

An ion exchange process is achieved by using either synthetic ion exchange resins like polymer-bound metal chelators or natural solid resins such as zeolites.[61,62] When wastewater goes through the ion exchange column, heavy metals can be separated by exchanging with cation ions held on the resin. Ion exchange processes have been widely applied to industrial applications owing to their advantages, such as high treatment capacity, high removal efficiency, and fast kinetics.[63] However, the efficiency of ion exchange with respect to heavy metals is limited by the flow rate.[64] Also, the large amounts of regenerant or eluent needed to reuse the resin causes secondary pollution.

The process of adsorption is based on mass transfer of soluble metal ions in solution onto solid sorbents that are usually packed in a column. A widely used sorbent material for heavy metal removal is activated carbon.[65] Other low cost sorbents such as clay, fly ash, seed shells, and coffee husks are also being investigated as potential sorbents for heavy metals.[66] Most adsorption processes function as a column, so they experience similar drawbacks to that of ion exchange processes. For example, prefiltration of suspended solids is required to prevent the clogging problem.

Chemical precipitation is effective and by far the most widely used treatment method in the industry, due to its simplicity and relatively low operating costs. In this process, precipitants, such as hydroxide[67] or sulfide,[68] convert dissolved heavy metal salts to insoluble metal hydroxides or sulfides, facilitating the subsequent removal of heavy metals from the liquid phase by sedimentation or filtration. However, the major disadvantages with precipitation are slow solid-liquid separation; large sludge production that is likely to cause secondary contamination; non-selectivity; and unsuitability for low-concentrated effluents.

Membrane filtration technologies such as ultrafiltration,[69] reverse osmosis,[70] and electrodialysis[71] show promise for heavy metal removal due to their high efficiency, easy operation and space saving. However, they are not economically appealing due to their high operating costs. Industrial membrane filtration units require not only energy-intensive pumping systems to accelerate the passage of the solution through the membrane filters,[60] but also expensive and high performance fittings and valves. Besides, membranes tend to be fouled or clogged by a wide variety of contaminants, leading to the low removal efficiency and high maintenance costs.

## 2.2. Introduction to nuclear waste treatment

### 2.2.1 Used nuclear fuel and reprocessing

Used (or spent) nuclear fuel is nuclear fuel that has been irradiated in a nuclear reactor. As shown in Figure 2.1,[73] the used nuclear fuel typically consists of 95-96% uranium (~0.8% U-235), ~1% plutonium, ~0.1% minor actinides, and 3-4% fission products. Uranium is the primary component in used nuclear fuel. Uranium and plutonium are called major actinides, which are fissile materials that undergo fission chain reaction

when hit by a neutron of any energy. Minor actinides are the actinide elements in used nuclear fuel other than uranium and plutonium, such as neptunium-237, americium-241, americium-243, curium-242, which are major contributor to the long-term radiotoxicity in spent fuel. Many of the fission products are either stable (non-radioactive) or only short-lived radioisotopes, but a considerable number are medium to long-lived radioisotopes. For example, most heat production is from cesium-137 and strontium-90 with half-lives of ~30 years, and technetium-99 and iodine-129 can remain radioactive for hundreds of thousands of years. On the other hand, due to their high thermal neutron absorption cross sections, some fission products (such as lanthanides) have a poisoning effect on reactor operation. Therefore, used fuel is discharged not because fissile material is fully used-up, but because the neutron-absorbing fission products have built up so that the fuel becomes significantly less able to sustain the nuclear reaction in an ordinary thermal reactor. There is still considerable amount of the energetic component (uranium and plutonium) in the spent fuel that can be extracted (i.e. reprocessed) for reuse. With reprocessing in the close fuel cycle, the originally mined uranium can gain potentially up to 30% more energy contributing to national energy security. On the other hand, since it is still highly radioactive and continues to generate significant heat for decades due to the decay of the radioactive elements, the used nuclear fuel needs to be managed in a safe, responsible and effective way. Reprocessing can also benefit the spent fuel management by either reducing the volume of high-level waste to about one-fifth, or reducing the level of radioactivity in the waste to be disposed.

Stable fission
products

**0.9%**
Plutonium

**0.1%**
Minor actinides

**0.1%**
Iodine and
technetium

**0.1%**
Other fission
products

**0.3%**
Cesium and
strontium

Uranium
95.6%

Other

2.9%

Source: GAO analysis of DOE data.
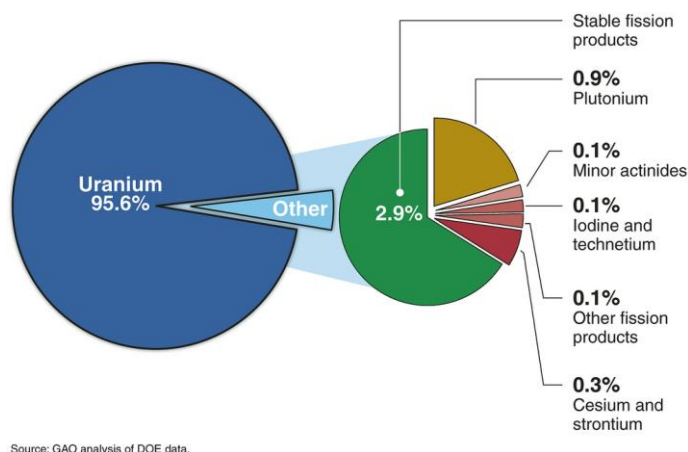
**Figure 2.1** Composition of used nuclear fuel.

From today's 437 operating nuclear power plant in 30 countries, over 10000 metric tons heavy metal (tMH) spent fuel are unloaded every year from nuclear power reactor. So far, the total amount of spent fuel cumulatively generated from commercial power reactors worldwide is approximately 290000 tMH of which 90000 tHM has been reprocessed. The world commercial reprocessing capacity is about 5370 tons per year.[74] By the year 2020, the time when most of the presently operated nuclear power reactors approach the end of their licensed operation life time, a total of approximately 445000 tMH spent fuel is expected to be generated worldwide (Figure 2.2).[75] In addition, as shown in Figure 2.2, although the amount of discharged spent fuel is continuously increasing, the reprocessing capacity stays low and does not grow proportionally. Consequently, more and more spent fuel goes to the direct disposal/storage, which putting a huge pressure on the storage capacity and nuclear waste management.
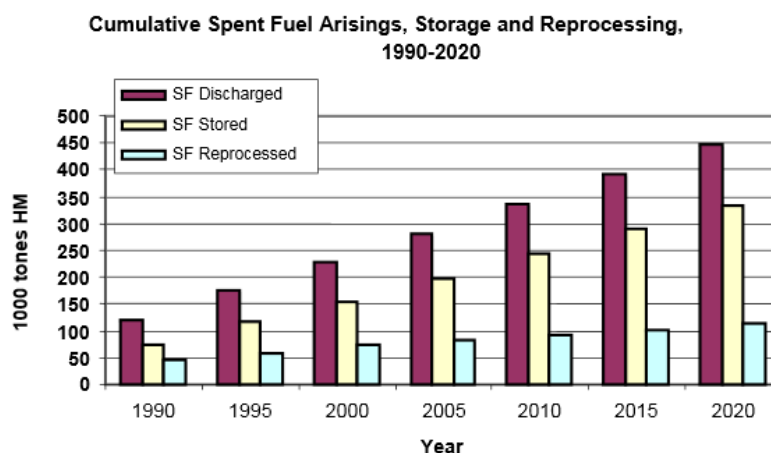
**Figure 2.2** Global statistics in spent fuel (SF) management.[75]

The U.S. does not reprocess used fuel, but uses a uranium once-through fuel cycle which leads to the placing of used fuel in direct disposal and final storage. Unfortunately, despite more than 30 years of study, Yucca Mountain repository project was shut down in 2010 and permanent geologic disposal in Yucca Mountain is no longer an option. Nearly 60,000 metric tons of spent nuclear fuel that wait for permanent geologic disposal have to be piled up at the country's 104 commercial nuclear power plants.[76] Since the spent nuclear fuel is highly hazardous, any failure or leakage of the storage container will cause severe soil and groundwater contamination, posing a potential risk and threat to the environment and public health. On the other hand, nuclear energy demand has never stopped. As it is a key tool to achieve the greenhouse reduction strategies and a potential alternative to fossil fuels, use of nuclear energy continues to increase worldwide. The spent fuel inventory is expected to be doubled, growing to more than 140,000 metric tons by 2055.[73] However, it is estimated that the spent fuel storage pools at the U.S. reactors will reach their maximum capacity soon.[77] Therefore, intensive scientific efforts has been put into nuclear waste

treatment technologies to resolve the disposal issues, to protect the environment and human health, and to maximize the future use of nuclear energy.

**2.2.2 Aqueous nuclear waste treatment**

The main purposes of nuclear waste treatment are: (1) to recycle the unused fissile and fertile materials that have been disposed as a waste; (2) to extract valuable fission products or other byproducts from the high level waste; (3) to reduce the volume and/activity of the waste to be disposed to enhance the safety and/or reduce the costs of further management phase; (4) to minimize the impact on the environment.

Similar to heavy metal treatment in wastewater, in order to remove radionuclides of interest, aqueous nuclear waste can be treated using ion exchange,[78] adsorption,[79] chemical precipitation,[80] membrane filtration (i.e. reverse osmosis, microfiltration, ultrafiltration, etc.),[81] and/or evaporation.[82] The main advantage and disadvantage of those treatment processes are listed in Table 2.1.[83–85]

**Table 2.1** Comparison of different aqueous radioactive waste treatment options.

| Method | Advantages | disadvantages |
|---|---|---|
| **Ion exchange** | 1. Good chemical, thermal and radiation stability | 1. Limited by the flow rate |
| | 2. High capacity and efficiency | 2. Blockage problem |
| | 3. Large choice of products ensuring high selectivity | 3. Affected by high salt content |
| | 4. Low running costs | 4. Regeneration and recycling often difficult employed |
| **Adsorption** | 1. Low costs of sorbent | 1. Regeneration of sorbent |
| | 2. Good for low/trace concentration | 2. Clogging of column |
| | | 3. Pre-filtration required |
| **Precipitation** | 1. Suitable for large volumes and high salt content waste | 1. Slow separation kinetics |
| | 2. Simplicity | 2. Great generation of toxic sludge |
| | 3. Low operating costs | 3. Low selectivity |
| | | 4. Not for low metal concentration |
| **Membrane filtration** | 1. No special regeneration required | 1. High capital cost |
| | 2. High recovery efficiency | 2. High operating cost |
| | 3. Easy operation | 3. Member fouling or clogging |
| | 4. Space saving | 4. Organic membranes subject to radiation damage |
| **Evaporation** | 1. Well established technology | 1. Process limitations (scaling, foaming, corrosion) |
| | 2. High volume reduction factor | 2. Not suitable for volatile radionuclides |
| | 3. Suitable for variety of radionuclides | 3. Intense energy required |

Commercially, solvent extraction has been exclusively used in all spent fuel reprocessing plants. The PUREX (Plutonium Uranium Recovery by Extraction) process invented by Anderson and Asprey in 1940s[86] has become a standard nuclear reprocessing method to effectively and selectively recover plutonium and uranium from aqueous spent fuel.[87] This process involves dissolving the spent fuel in concentrated nitric acid, after which chemical separation of uranium and plutonium is taken place by liquid-liquid exaction steps between aqueous and organic phase. Specifically, using tributyl phosphate (TBP) dissolved

in high boiling hydrocarbon diluents such as kerosene or dodecane, U(VI) and Pu(IV) are extracted into the organic phase while the fission products and minor actinides remain in the aqueous nitric acid. In the second step, U is separated from Pu by reducing Pu(IV) to Pu(III) with excess U(IV) in a new aqueous phase, so that Pu is stripped into the new aqueous phase while the mixture U(VI) and U(IV) remains in the organic phase. Based on the same principle, other solvent extraction processes has been developed for different radionuclide separation. For example, by adding octyl(phenyl)-N,N-dibutyl carbamoylmethyl phosphine oxide(CMPO), the TRUEX (TRansUranic EXtraction) process was invented in the Argonne National Laboratory to remove minor actinides (Am/Cm) from the nuclear waste which largely reduces the radioactivity of the waste.[88] The TALSPEAK (Trivalent Actinide Lanthanide Separations by Phosphorus-reagent Extraction from Aqueous Complexes) process developed in the Oak Ridge National Laboratory is considered the best solvent extraction process to separate trivalent lanthanides (Ln(III)) from the minor actinides (Am(III) and Cm(III)).[89] This separation relies on the slightly greater strength of interaction of trivalent actinides with ligand donor atoms that is softer than oxygen. Compared to other methods, solvent extraction has high selectivity and is better suited to continuous, large scale, remote operation, and can facilitate a 3-way separation of uranium, plutonium and fission products. However, during the processes, large quantities of aqueous and organic secondary waste are generated.

## 2.3 Removal of metal ions using nanosorbent based magnetic separation

In the late 1990s, magnetic assisted chemical separation (MACS) process was developed in the Argonne National Laboratory for radioactive waste remediation and

treatment.[90–93] This process utilize magnetic carrier microparticles (rear earth or

ferromagnetic materials embedded in a polymer material) coated with selective chemical

extractants (CMPO, TBP, etc.) that have a high affinity for the target elements. The MACS

process combined the selective and efficient separation afforded by chemical sorption with

magnetic recovery. The concept using MNP-Che (surface functionalized magnetic

nanoparticles conjugated with specific metal chelators) nanosorbents to separate metal target

metal ions from contaminated aqueous solution is similar to the MACS process. However,

the MNP-Che separation, using our research as an example, has many advantages over the

MACS process as shown in the

. For example, high surface area to volume ratio of MNPs provides better kinetics for

the sorption of metal ions from aqueous solution; high magnetic moment aids in fast

separation of particles from waste solution; with the surface functionalization, the MNP-Che

conjugates have a better acid and radiation resistance. As a simple, versatile, and compact

process, the MNP-Che separation has been effectively utilized to remove target metal ions,

including heavy metal and radioactive elements, from aqueous solution.

The distribution coefficient ($K_d$, in mL g$^{-1}$) is usually used to evaluate the sorption

effectiveness of a sorbent for a given metal ion, which is defined by the following equation:

$$K_d = \frac{(c_i - c_f)}{c_f} \frac{V}{m} \tag{2-1}$$

where $c_i$ and $c_f$ are the initial and final metal concentrations, $V$ (in mL) is the volume of the

solution and $m$ (in g) is the dry weight of the sorbent. The sorption performance of different

sorbents can be compared via the $K_d$ value. A higher $K_d$ value implies a greater effectiveness

of the sorbent in capturing and holding the metal ions. In general, $K_d$ values above a few

thousands are considered good, and those above ten thousands are outstanding.[94]

**Table 2.2** Comparison between MACS process and MNP-Che separation.

| | MACS[90–93] | MNP-Che (in our research) |
|---|---|---|
| **Particle size** | Microsize (0.1 to 25 μm) | Nanosize (20-100 nm) |
| **Surface coating** | Commercially purchased particles with a polymeric coatings (charcoal in a cross-linked N,N-methylene bis-acrylamide) Particles are partially covered, leading to the acid dissolution problem | Customized surface coating: Silica coating: dense coating for acid protection, and facilitate further functionalization Polyamine coating: Increase the density of bonding sites for chelators |
| **Bond between particle and ligand** | Physical adsorption (electrostatic attractive force) by evaporation of the volatile diluents): weak bond and reversible | Chemical adsorption by covalent bond (charge sharing or charge transfer from the organic molecules to the metal surface in order to form a coordinate bond): increased long-term stability |
| **Magnetic moment** | For noncoated particle: $M_s$=16 emu/g CMPO coated particle before radiation: $M_s$=13 emu/g CMPO coated particle after $3.43*10^6$ gamma radiation: $M_s$ less than 3 emu/g (so high gradient magnetic field is needed) | Uncoated core-shell MNPs before radiation: $M_s$=89 emu/g Uncoated core-shell MNPs after radiation (5.5 MeV $Si^{2+}$ ion): $M_s$=77 emu/g Final products MNP-DTPA: $M_s$=~25 emu/g |
| **Acid resistance** | ~1.2% (wt) of iron dissolved after settling in 1 M $HNO_3$ for 2 weeks, and the dissolved iron in the supernatant steadily increased with increasing $HNO_3$ concentration | No iron leaching after incubation in 1 M HCl for 25 days (due to the dense silica coating) |
| **Chelator/Ligand** | CMPO/TBP Diethylhexyl phosphoric acid ($D_2EHPA$) Trioctyl phosphine oxide (TOPO) | Diethylene triamine pentaacetic acid (DTPA) |
| **Sorption capacity** | Americium $K_d$=3000-5,000 mL/g Plutonium $K_d$=18,000-26,000 mL/g | Americium $K_d$=~10,000 mL/g Plutonium $K_d$=~1200 mL/g |

**2.3.4 Research on removal of heavy metal ions using MNP-Che**

In a detailed study conducted by Yantasee *et al.* in 2007, DMSA (dimercaptosuccinic acid) modified $Fe_3O_4$ nanoparticles (around 6 nm in diameter), DMSA- $Fe_3O_4$, were employed to remove Hg, Ag, Pb, Cd and Tl from natural water (i.e. river, ground, and ocean water).[95] The scheme was illustrated in Figure 2.3. The magnetic nanosorbents used in this study were highly dispersible in aqueous solution, but could be removed with relative ease by exposing them to an external magnetic field.
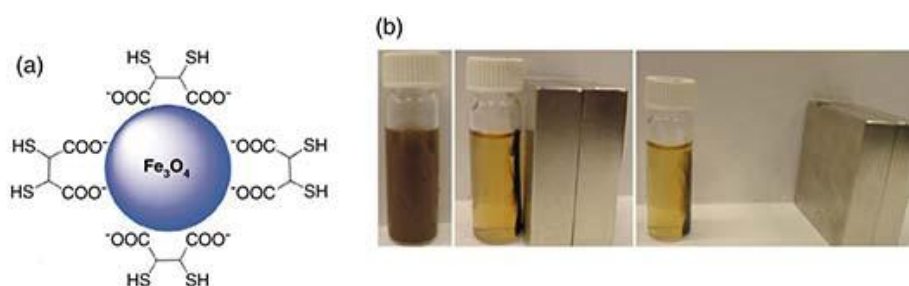


**Figure 2.3** (a) Schematic of a DMSA-modified $Fe_3O_4$ nanoparticles; (b) removal of nanoparticles from the liquid phase using NdFeB magnets (~1.2 T); initial solution (left), after 10 s with magnet (middle), and when the magnet was moved to a distant position (right).[95]

In this study, it was shown that over 99 wt % of 1 mg $L^{-1}$ Pb could be removed by DMSA- $Fe_3O_4$ after 1 min of contact time. The Hg sorption on DMSA- $Fe_3O_4$ followed the Langmuir adsorption model, with a sorption capacity of 227 mg of Hg/g. Table 2.3 summarized the comparison of the metal removal efficiency of DMSA- $Fe_3O_4$ against other sorbents containing thiol ligands. In terms of the $K_d$ value, the DMSA- $Fe_3O_4$ nanoparticles were significantly superior to the commercial GT-73 and activated carbon (Darco KB-B) for capturing Hg, Cd, Ag, Pb, and Tl. The massive improvement in $K_d$ values clearly showed the excellent utilization of the metal chelating ligands for improved sorption efficiency of

the target metal species. The data in Figure 2.4 illustrated that, at near-neutral pH, the thiol-modified magnetic nanoparticles were proven to be outstanding sorbent materials for soft metals such as Hg, Ag, Pb, Cu, and As ($K_d > 50000$), and also a good sorbent for harder metals such as Cd, Co, and Tl. In a word, compared to the commercial sorbents tested, the surface functionalized magnetic nanosorbents surpassed with respect to the chemical affinity, capacity, kinetics, and ease of separation.

**Table 2.3** $K_d$ (mL/g) of metal ions on selected sorbents in groundwater.[95]

| Sorbent[a] | Final pH | Cobalt | Copper | Arsenic | Silver | Cadmium | Mercury | Thallium[b] | Lead |
|---|---|---|---|---|---|---|---|---|---|
| $Fe_3O_4$-DMSA | 6.91 | 3000 | 270 000 | 5400 | 3 600 000 | 10 000 | 92 000 | 14 000 | 2 300 000 |
| Bare $Fe_3O_4$ | 6.93 | 1600 | 7 400 | 5800 | 13 000 | 2 400 | 16 000 | 4 000 | 78 000 |
| SH-SAMMS | 6.80 | 430 | 1 700 000 | 950 | 67 000 000 | 66 000 | 1 100 000 | 15 000 | 350 000 |
| GT-73 | 6.76 | 890 | 6 300 | 1200 | 16 000 | 1 500 | 10 000 | 2 200 | 41 000 |
| Darco KB-B | 6.90 | 790 | 26 000 | 750 | 27 000 | 1 300 | 31 000 | 21 | 190 000 |

[a] Each magnetic nanosorbent was measured at $10^4$ liquid-to-solid (L/S) ratio in 0.45 μm filtered groundwater
[b] Thallium added as $Tl^{+1}$.
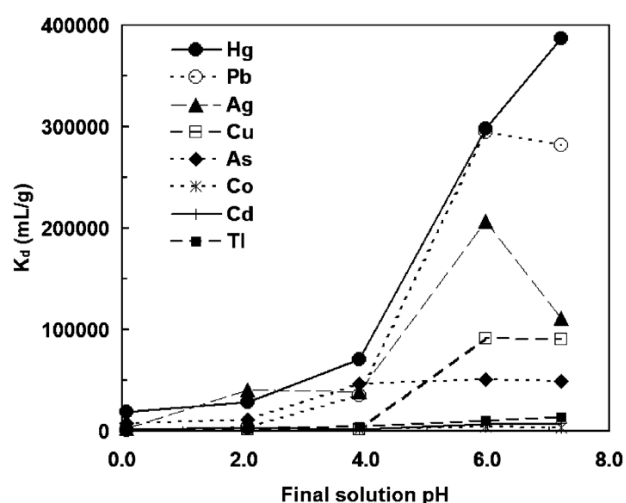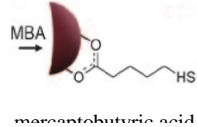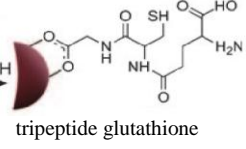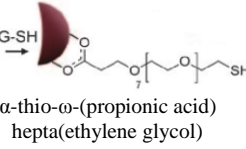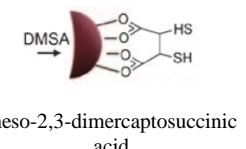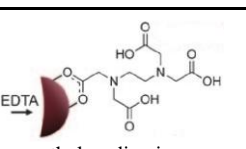


**Figure 2.4** Effect of pH on $K_d$ values, measured in $HNO_3$-spiked unfiltered river water [liquid/solid ratio (L/S) = $10^5$].[95]

Warner *et al.* investigated several superparamagnetic $Fe_3O_4$ nanoparticle-based sorbents functionalized with different ligands (with $M_s$ ranging from 47-66 emu/g) to remove heavy metal ions from natural water in batch sorption equilibrium experiments.[96] Each affinity ligand was introduced onto the nanoparticle surface by a simple, one-step ligand exchange reaction. A summary of $K_d$ results was shown in Table 2.4, which clearly showed that, compared to the bare iron oxide nanoparticles, the surface functionalized nanosorbents almost always had higher $K_d$ values. The results demonstrated the essential value of surface functionalization to increase and tune the chemical activity of the magnetic nanosorbent material. The $K_d$ data also clearly showed that the selectivity of the magnetic nanosorbents depended on the ligand/chelator. For example, the order of selectivity for $Fe_3O_4$-MBA was Pb>Cu>Ag>Cd, Co>Hg, Tl; for $Fe_3O_4$-EDTA the order was significantly different: Hg, Pb, Ag>Cu, Co, Tl>Cd. In addition, the results confirmed that the orientation of the thiol affinity moiety on the nanoparticle surface could have a significant effect on the binding potential towards a specific metal ion.[97] In brief, thiol containing ligands or EDTA installed on $Fe_3O_4$ nanoparticles were shown to be highly effective magnetic nanosorbent materials.

**Table 2.4** $K_d$ values of selected sorbents for heavy metal in river water [adopted from Ref. [96]].

| Sorbent | Chelator/Ligand | $K_d$ (mL/g) | | | | | | |
|---|---|---|---|---|---|---|---|---|
| | | Co | Cu | Ag | Cd | Hg | Pb | Tl |
| Bare Fe₃O₄ | -- | 1600 | 7400 | 13000 | 2400 | 16000 | 78000 | 4000 |
| Fe₃O₄-MBA |  mercaptobutyric acid | 20000 | 440000 | 27000 | 20000 | 7800 | 1800000 | 6400 |
| Fe₃O₄-GSH |  tripeptide glutathione | 2600 | 80000 | 12000 | 9000 | 95000 | 265000 | 2100 |
| Fe₃O₄-PEG-SH |  α-thio-ω-(propionic acid) hepta(ethylene glycol) | 26000 | 400000 | 86000 | 37000 | 330000 | 1200000 | 12000 |
| Fe₃O₄-DMSA |  meso-2,3-dimercaptosuccinic acid | 3200 | 91000 | 110000 | 7400 | 390000 | 280000 | 13000 |
| Fe₃O₄-EDTA |  ethylenediamine tetraacetic acid | 10000 | 15000 | 150000 | 320 | 300000 | 200000 | 6800 |

[a] Each magnetic nanosorbent was measured at $10^5$ liquid-to-solid (L/S) ratio (equates 0.1 mg sorbent in 10 mL).
[b] pH of filtered Columbia River water was 7.8.

An article published by Huang and Chen in 2009 reported a novel magnetic nanosorbent synthesized by the covalent binding of polyacrylic acid (PAA) on the surface of Fe₃O₄ nanoparticles and the followed amino-functionalization using diethylenetriamine (DETA), as illustrated in Figure 2.5.[98] By this amino-functionalization, nitrogen-containing complex ligands were introduced on the surface of the nanoparticles. The sorption results

shown in demonstrated that this novel magnetic nanosorbent not only had excellent adsorption capability for mono- or polyvalent metal cations, such as $Ag^+$, $Cu^{2+}$, $Cd^{2+}$, and $Fe^{3+}$, due to the strong affinity between the nitrogen atom and metal cations, but also was capable of adsorbing anionic metal species such as $PdCl_4^{2-}$ and $HCrO_4^-$ after protonation. This anion sorption was seldom discussed in similar research papers. In addition, Huang and Chen revealed the different pH effects on the sorption of Cu(II) and Cr(VI) ions by the amino-functionalized nanoparticles: the sorption capacity for cationic Cu(II) ions increased with increasing the solution pH; in contrast, the higher sorption capacity for Cr(VI) in various anionic forms (i.e., $Cr_2O_7^{2-}$, $HCrO_4^-$, $CrO_4^{2-}$, $HCr_2O_7^-$) was observed at lower pH (pH <3). The phenomenon was explained by the pH-dependent protonation and deprotonation reaction of the amino groups which may be expressed by the following equation:

$$- NH_2 + H^+ = -NH_3^+ \tag{2-2}$$

At a lower pH, the above equation favored the protonation of $-NH_2$ to form $-NH_3^+$. When more $-NH_2$ groups were converted to $-NH_3^+$, there were fewer $-NH_2$ sites available on the surface for cationic Cu(II) ion sorption. Also, the increased electrostatic repulsion between $Cu^{2+}$ ions and the $-NH_3^+$ groups could reduce the Cu(II) sorption. However, the formation of $-NH_3^+$ favored the electrostatic attraction with the negatively charged Cr(VI) ions according to an anionic exchange mechanism, leading to the increase in Cr(VI) sorption with decreasing the solution pH. A similar pH-dependent sorption phenomenon was reported by Chang and Chen.[99,100] Our research also evaluated the pH effect on the sorption efficiency as described in Chapter 5, which can be in part explained by the similar protonation mechanism.
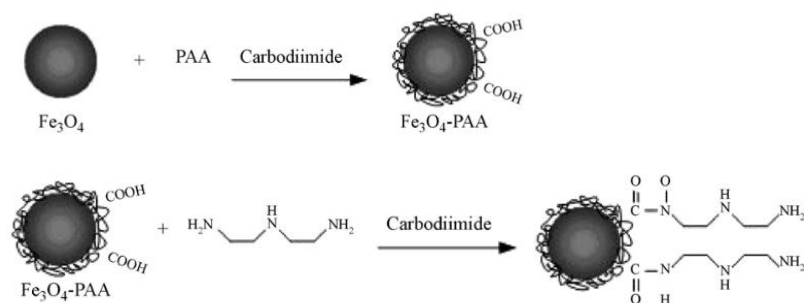
**Figure 2.5** A scheme for the binding and amino-functionalization of PAA on $Fe_3O_4$ nanoparticles as a novel magnetic nanosorbent for both metal cations and anions.[98]

As discussed above, the use of iron oxide nanoparticles has given rise to appealing applications of magnetic separation in heavy metal treatment, but the limited stability prohibits the use of iron oxide based nanosorbents in combination with functional ligands in acidic media which would immediately dissolve the particles. More recently, the silica or carbon coating has opened access to chemically stable magnetic nanosorbents.[43,101]

In 2009, Koehler *et al.* combined the stability of carbon-encapsulated nanomagnets and the complexing power of ethylenediaminetetraacetic acid (EDTA) like chelators to study the capabilities of such a functionalized magnetic nanosorbent (referred to as Fe/C-PEI-DTPA) for the fast removal of Cd, Cu and Pb from wastewater.[102] Figure 2.6 showed the results of the sorption tests where contaminated model solutions were decontaminated within 5 min to concentrations as low as $\mu g\ L^{-1}$, which demonstrates the fast kinetics. In strongly diluted concentrations (1 $\mu g\ L^{-1}$) the removal efficiency decreased for all tested heavy metal ions, as the system was limited by the chelating power of the ligand, by diffusion or kinetics.
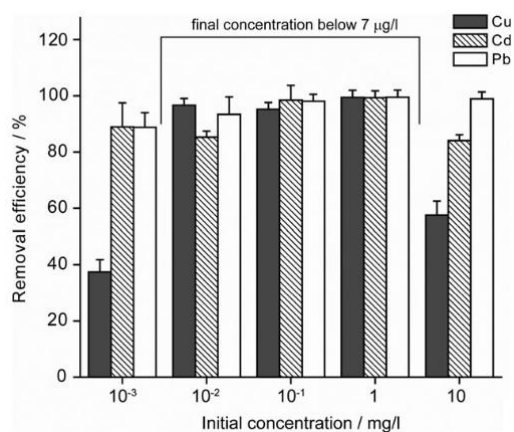
**Figure 2.6** Heavy metal removal from model waste waters using Fe/C-PEI-DTPA enables purification down to drinking water standards.[102]

In this study, stripping experiments were also conducted to study the possibility of recycling Fe/C-PEI-DTPA. The results showed that, due to irreversibly bound metals or loss of chelator, the sorption capacity decreased to 65% after the first washing but stayed constant afterwards. The ability to remove adsorbed metal ions by stripping process without adversely affecting the MNP-che's sorption efficiency is one of the most important criteria to make this separation method economical and cost-effective. Numerous studies have reported that dilute acids and deionized water (DW) can be used to effectively remove the metal ions from the functional groups on the particle surface, as summarized in Table 2.5. Our research also evaluated the reusability of our lab-made magnetic nanosorbents using HCl or $HNO_3$ as the stripping agent, and the details were discussed in Chapter 4.

**Table 2.5** Stripping processes for the desorption of metal ions.

| Ligand-Metal | Stripping Agent | Process | Conclusion |
|---|---|---|---|
| EDTA-Cu[102] | DTPA-Buffer solution and DW | 2 times with DTPA-Buffer solution; 3 times with Buffer solution; 2 times with DW | - Stripping ratio for the first washing was 29% and nearly 100% afterward;<br>- Binding capacity decreases from 93% to 65% after the first washing, and stays constant afterwards |
| Poly(ethylene glycol dimethacrylate-vinyl imidazole) – Pb, Cd, Zn, Cu[103] | 0.1 M HNO$_3$ | Recirculated in a column for 1 hr with 50 ml HNO$_3$ | - Elution ratio ~95%<br>- Binding capacity remained at 97% for 10 cycles |
| Polystyrene sulfonic acid-Ni, Cu, Pb, Ag[104] | 0.1 M HNO$_3$ | Mixing with HNO$_3$ at 600 rpm for 16 h at 25$^{o}$C; several times with DW | - Completely reversible sorption<br>- 5 cycles without significant binding power loss |
| Polymer with COOH-Zn[26] | 1 M HCl | No details | - Completely reversible sorption<br>- Less stripped if initial conc. is low<br>- 10 cycles without significant binding power loss |
| EDTA-Cu, Zn, Mn[105] | 1 M HCl | Introduce HCl into the top of the column | - High elution ratio |

## 2.3.5 Research on removal of actinide and/or lanthanide ions using MNP-Che

Kaur *et al.* [106] reported the separation of actinides using MNPs functionalized with

diethylene triamine pentaacetic acid (DTPA) . DTPA chelators were covalently attached to

MNP surface using silica coating, followed by coupling with ployamine groups. The surface

modification of particle showed the increment in the particle size (both the dry particle size

observed in the TEM and the hydradynamic size measured by the DLS), variation of surface

charge, and drop of magnetization without changing the crystal structure of the particle. The uptake for various actinides using DTPA-MNP conjugates at different pH values showed that the immobilized DTPA had a high affinity to Am(III) at pH 3 ($K_d$ >10000) and medium affinity towards Pu(IV) at pH 1 ($K_d$ ~1500), as shown in Figure 2.7. In addition, the results showed that the actinide sorption process on the DTPA-MNP surface was highly dependent on the solution pH, and the actinides with higher oxidation states (U(VI) and Np(V)) showed a much weaker interaction with DTPA-MNP.
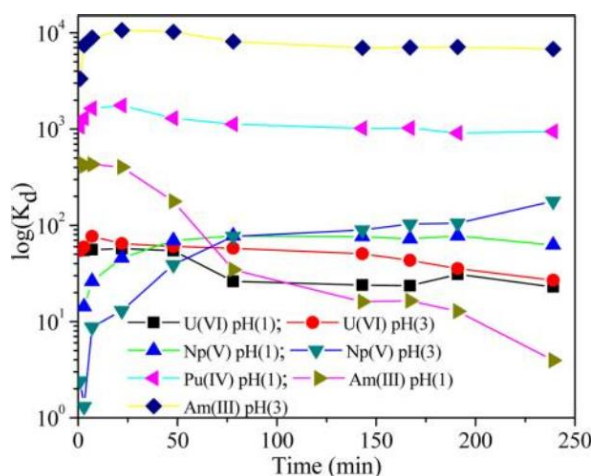


**Figure 2.7** Distribution coefficient ($K_d$) as a function of various actinides such as Am(III), Pu(IV), U(VI), and Np(V) by DTPA-MNPs.[106]

To effectively extract the higher oxidation states of uranium, U(VI) as $UO_2^{2+}$, amidoxime-functionalized magnetic mesoporous silica (MMS-AO) microspheres were synthesized by Zhao *et al.*[107] The synthesized MMS-AO nanosorbents exhibited a sandwich structure with an inner core of MNP, a middle layer of nonporous silica and an outer layer of amidoxime-functionalized mesoporous silica. The reported U(VI) sorption capacity, 277.3 mg g$^{-1}$,in this work was much higher than the results previously reported for other magnetic

materials under the similar conditions (Table 2.6), which was attributed to strong

complexation of amidoxime with U(VI) and high surface area provided by mesoporous

structure. The sorption results (in Figure 2.8) also showed that selectivity of MMS-AO for

U(VI) over a wide range of competitive ions was remarkably improved in comparison with

that of MMS, indicating that the effectiveness and necessity of amidoxime functionaliztion.

This study also demonstrated that complete desorption of U(VI) can be achieved using 1 M

or more concentrated HCl solution. The regenerated MMS-AO nanosorbents can be

effectively used for at least five sorption-desorption cycles with a slight decrease of sorption

capacity.

**Table 2.6** Comparison of U(VI) sorption capacity of different magnetic sorbents

| Magnetic sorbents | Experimental conditions | $Q_{max}$ (mg g$^{-1}$) | Ref. |
|---|---|---|---|
| MMS-AO | T = 298 K, pH = 5.0 | 277.3 | 107 |
| $Fe_3O_4$@$SiO_2$-salicylaldehyde | Ambient temperature, pH = 7.0 | 49.0 | 108 |
| $Fe_3O_4$@$SiO_2$-quercetin | T = 298 K, pH = 3.7 | 12.3 | 109 |
| $Fe_3O_4$@$SiO_2$-amidoxime | T = 298 K, pH = 5.0 | 105.0 | 110 |
| $Fe_3O_4$@$SiO_2$ | T = 298 K, pH = 6.0 | 52.4 | 111 |
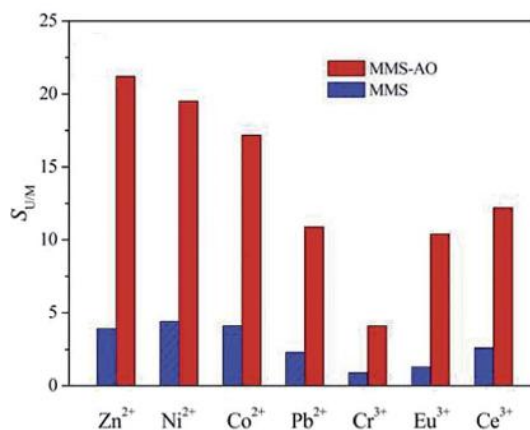


**Figure 2.8** Selectivity coefficients of U(VI) sorption by MMS and MMS-AO.[107]

Recently, Afsar *et al.*[112,113] have demonstrated the utility of BTPhen(bis-triazinyl-phenanthroline (*N*-donor) ligands in the magnetic separation nanotechnolgy for their applications in nuclear waste treatment. The distribution ratios and separation factors for the extraction of Am(III) and Eu(III) from different concentrations of nitric acid solution were examined using the different surface functionalized magnetic nanosorbents. In one of their studies,[112] C1-BTPhen molecules covalently attached to $ZrO_2$ coated maghemite MNPs exhibited their ability to co-extract Am(III) and Eu(III) from highly acidic solutions. The lack of selectivity may arise because the linker between the ligand and the MNP is too short to allow two BTPhen groups to bind to the Am(III) as is the case in the solvent extraction. In the other study,[113] $CyMe_4$-BTPhen-functionalized silica-coated maghemite MNPs were synthesized according to the scheme illustrated in Figure 2.9. The results in Figure 2.10 indicated that distribution radios for both Am(III) and Eu(III) decreased with increasing nitric acid concentration, but a significantly higher separation factor resulted at a higher nitric acid concentration. The strongly bound water molecule in the central cavity may play an important role in the separation of Am(III) from Eu(III). The high selectivity for Am(III) over Eu(III) (a separation factor in excess of 1300 at 4 M $HNO_3$) is far superior to that observed for $CyMe_4$-BTPhen ($SF_{Am/Eu} = 400$)[114,115] in solvent extraction experiments under similar conditions. Therefore, Afsar *et al.* proposed that the development of magnetic nanosorbents by attaching various BTPhen ligands may provide a potential platform for developing a new route for lanthanides/actinides extraction from nuclear waste.
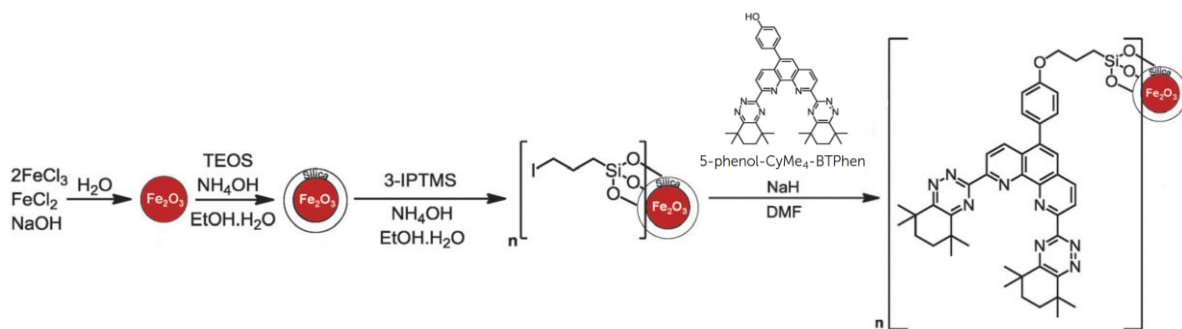
**Figure 2.9** Synthesis scheme of CyMe-BTPhen-MNP. [113]
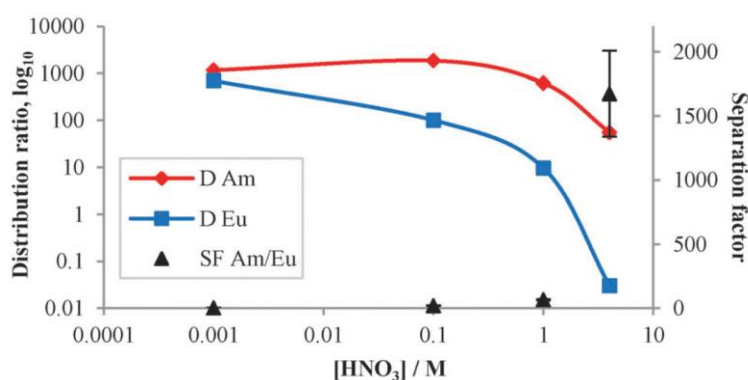


**Figure 2.10** Extraction of Am(III) and Eu(III) by CyMe-BTPhen-MNP as a function of nitric acid concentration. [113]

Organic-extractant derived from varying phosphoric acids appears to be very promising for achieving the extraction and separation of lanthanide ions from aqueous solutions. For example, traditional TALSPEAK organic phase is comprised of the monoacidic dialkyl bis(2-ethylhexyl)phosphoric acid extractant (D2EHPA or HDEHP) in diisopropyl benzene (DIPB). In the work presented by *Basualto et al.*,[116] magnetic nanosorbents were prepared based on the attachment of organophosphorus acid extractants, namely, D2EHPA, CYANEX 272, and CYANEX 301, onto the surface of oleic acid coated MNPs. Sorption tests in Figure 2.11 indicated that CYANEX-272-MNPs exhibited the best sorption ability with a sorption capacity of 12-14 $mg_{La}/g_{MNP}$, which doubled that observed

for D2EHPA and CYANEX 301 functionalized MNPs. The functionalized MNPs exhibited no significant selectivity for a given lanthanide element due to the similar chemical activities of the lanthanide group, which is consistent with the observation in our research as discussed in Chapter 5.
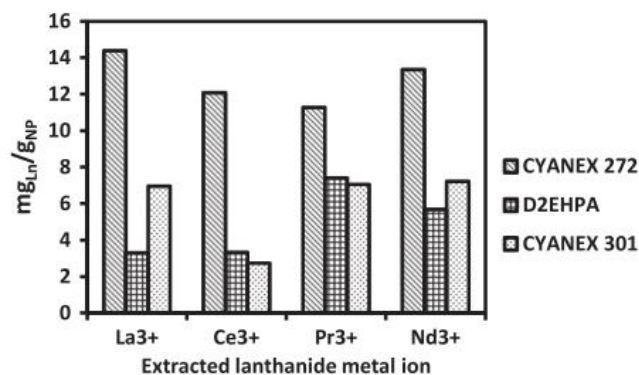


**Figure 2.11** Sorption capacities of functionalized magnetite nanoparticles for lanthanum, cerium, praseodymium, and neodymium.[116]

In another work presented by Dupont *et al.*,[117] N-[(3trimethoxysilyl)propyl]-ethylenediamine triacetic acid (TMS-EDTA) chelators were attached onto the surface of magnetic ($Fe_3O_4$) and non-magnetic ($SiO_2$ and $TiO_2$) MNPs, which were used to investigate the uptake of trivalent lanthanides from aqueous solutions. As shown in Figure 2.12 (left), in absence of competition between different ions, the uptakes of different Ln(III) ions were quite similar. However, Figure 2.12 (right) showed that if more than one element in the solutions, TMS-EDTA functionalized exhibited a higher affinity toward the heavier (smaller) Ln(III) ions. Similar selectivity results were also discovered and discussed in our research (Chapter 5). Moreover, it was found that the sorption capacity and selectivity toward smaller rare-earth ions increased in the same order as the density of EDTA-saline on

the NP surface, in the order $Fe_3O_4 < TiO_2 < SiO_2$. This could originate from the fact that a dense EDTA-silane (multi)layer is more impenetrable for larger ions, or from the fact that the size of the EDTA cage is reduced due to sterical hindrance (or crowding) caused by the high density of EDTA groups on the surface of NPs. On the other hand, although $SiO_2$ and $TiO_2$ nanoparticles held larger quantities of TMS-EDTA on their surface and therefore adsorbed more rare-earth ions, but their removal from solution was more tedious. Therefore, hybrid nanosorbents were proposed with a magnetic $Fe_3O_4$ and nonmagnetic shell that could combine the convenience of magnetic retrieval with the high sorption capacity and selectivity of $SiO_2$-based nanoparticles.
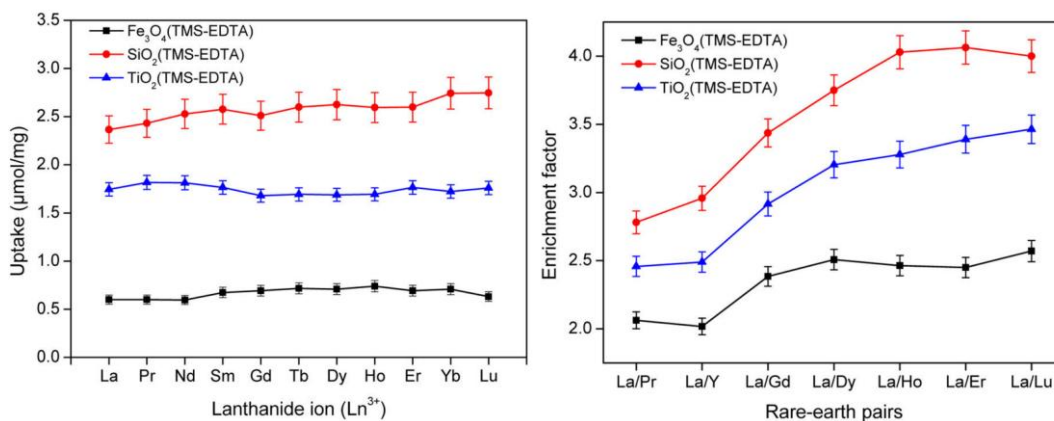


**Figure 2.12** Left: Uptake of rare-earth ions from single-element solutions by $Fe_3O_4$ -TMS-EDTA, $TiO_2$-TMS-EDTA and $SiO_2$-TMS-EDTA at pH 6.3. Right: Separation of La(III)/Ln(III) rare-earth pairs (pH 6.5) with increasingly different ionic radii from left to right.[117]

## 2.5 Summary

This literature review explains the current situation of heavy metal pollution and nuclear waste management. Traditional methods to remove heavy metal ions or radioactive elements from their waste streams were discussed in details. Sorption is one of the most

widely used recovery methods because of its low cost, easy operation and wide adaptability. Convenient separation of sorbents from aqueous phase is of special importance considering the recycling and recovering abilities of sorption methods. Traditional separation methods such as centrifugation and filtration are usually labor-consumptive, uneconomical and thus impractical for large-scale water treatment. From this point of view, magnetic nanosorbents exhibit special superiority due to convenient separation by an external magnetic field. The advantages of magnetic nanosorbents are: (1) better kinetics for the contaminations sorption due to extremely small size and high surface area to volume ratio; (2) efficient particles separation from waste solution aided by magnetic susceptibility; and (3) the minimization of disposal costs and storage area because of the low production of secondary waste.

Substantial studies have proved that magnetic nanosorbents modified with a wide variety of chelators/ligands are highly effective for removal or recovery of heavy metal ions and actinides/lanthanides from aqueous solutions by taking advantage of the fast processes of chemical sorption and magnetic separation. The selectivity of the target species over the competitive ions can be achieved by modifying the chelators/ligands functionalized on the MNP surface. However, the application of magnetic nanosorbents is still on the laboratory experiments scale. In addition, a lot of questions, such as the hydrodynamic behavior of magnetic nanosorbent materials in a continuous flow system, are not fully understood. More work is needed for the development of magnetic nanosorbents to be utilized at an industrial scale.

## Chapter 3: Synthesis and Characterization of Magnetic Nanosorbents

## 3.1 Three-step synthesis process of dMNP-DTPA nanosorbents

In this thesis, novel magnetic nanosorbents – double coated iron nanoparticles coupled with diethylene triamine pentaacetic acid (DTPA) chelators – have been synthesized according to Figure 3.1. The starting magnetic nanoparticles are the zero valent iron (ZVI) nanoparticles (referred to as Nanofer25) that were kindly provided by Nanoiron s.r.c. (Czech Republic), with an average particle size of ~50 nm and a size distribution from 20-100 nm. The product specification was summarized in Table 3.1.
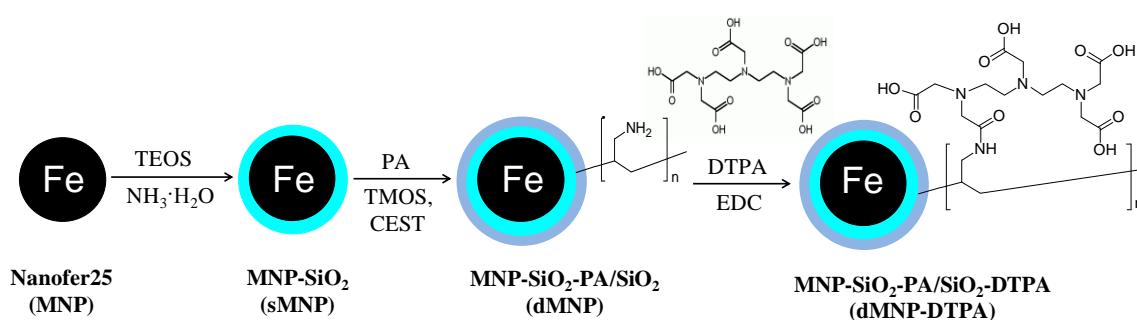


**Figure 3.1** Synthesis procedure of dMNP-DTPA nanosorbents.

**Table 3.1** Product specification of Nanofer25 from Nanoiron s.r.c.[118]

| | |
|---|---|
| Chemical composition of Fe(0) | Fe(core) FeO(shell) |
| Content of solid phase in dispersion by weight | 20% |
| Content Fe(0) in solid phase | $\approx 85\%$ |
| Other ingredients in solid phase | $Fe_3O_4$, FeO, C |
| Content of Fe(0) in dispersion by weight | 17% |
| Crystalline structure of Fe(0) | Alpha Fe |
| Particles morphology | spherical |
| Average particle size | d50 < 50nm |
| Particles specific surface area | >25$m^2$/g |
| Dispersion density | 1210 kg/$m^3$ |
| Fe(0) particles density | 7870 kg/$m^3$ |
| $Fe_3O_4$ density | 5700 kg/$m^3$ |

### 3.1.1 First silica coating

Since ZVI nanoparticles ($Fe^0$) synthesized at nanoscale are highly reactive, either subsequently oxidizing to $Fe_3O_4$ or easily dissolving in acid conditions, the magnetization of $Fe^0$ decreases in time or in harsh environments. Therefore, the chemically inert coating is necessary to maintain the stability of ZVI nanoparticles.

The oxidation and solubilization of ZVI nanoparticles can be addressed by coating the particles with a uniform silica layer using the sol-gel process modified from the Stöber method.[119,120] In general, the sol-gel process, as the name implies, involves a transition of a system from a liquid "sol" (mostly colloidal) into a solid "gel" phase. The starting materials used in the preparation of the "sol", called precursors, are usually metal organic compounds such as metal alkoxides. The sol-gel process is based on the hydrolysis and condensation of the precursors in solution. Further condensation, polymerization and heat treatment eventually result in a three dimensional silica network on the surface of magnetic nanoparticles.[121]

The silica coating can be optimized to enhance acid resistance by varying the concentration of the silane precursor tetraethoxysilane (TEOS) in the sol-gel reaction (Figure 3.1). As reported, [119] 10% of TEOS precursor was determined to be the optimal concentration to obtain a silica coating that was resistant to iron leaching in 1 M HCl with minimized loss of magnetization.
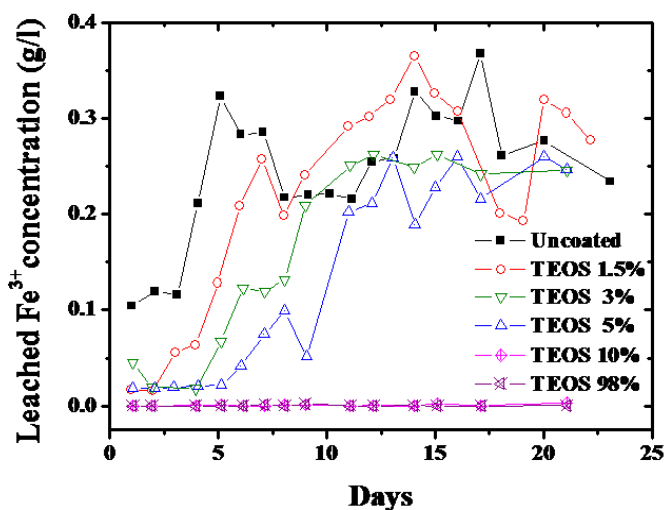
**Figure 3.2** Time dependence of iron leaching from the original and silica coated MNPs made with increased precursor TEOS concentration.[119]

The sol-gel silica coating experimental procedure was described as follows: 500 mg of Nanofer25 slurry was washed three times with absolute ethanol and transferred to a 100 mL three-necked flask, and then resuspended in ~20 mL absolute ethanol. After 15 min of incubation in an ultrasonication bath (Branson Ultrasonic Corp., Bransonic 3510) with vigorous overhead stirring, 7.8 mL of 10% TEOS (≥99%, Aldrich) in absolute ethanol and 16.7 mL of 30% ammonia were added slowly by peristaltic pump into the continuous mixing system. After an additional 1 hour of incubation, the suspension was allowed for ~8 hours of incubation with overhead stirring only to ensure the maximum hydrolysis of TEOS and the formation of the monosilicic acid necessary for condensation. After that step the coated particles were removed by magnetic decantation and washed three times with absolute ethanol. The washed particles were dried in a vacuum oven at 110 $^{\circ}$C for 4 hours, and stored in a desiccator.

### 3.1.2 Second silica/PA composite coating

In addition to the stability, magnetic nanosorbents for efficient removal or recovery of heavy metal ions from wastewater should have a large loading capacity for reactive functional groups. This can be achieved by introduction of a long-chain polymer coating containing amine groups, such as poly(allylamine) (PA) (see Figure 3.3). In our research, PA polymer with a molecular weight of 16,000 and ~180 primary amine groups per molecule was used. PA, highly cationic due to its high amine content, can initiate the precipitation of negatively charged silicic acid molecules to form silica.[122,123] Subsequently, the PA molecules are partially imbedded in the newly formed silica coating by controlling the pH of the reaction.
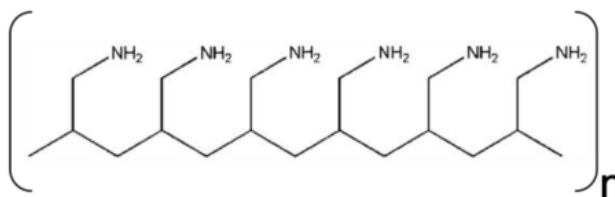


**Figure 3.3** Chemical structure of poly(allylamine) (PA).

Therefore, the second coating is a PA/silica composite coating. Briefly, 500 mg of silica coated Nanofer25 MNPs (sMNP) were first washed three times with HCl acidified DI water at pH ~3, then transferred in to a 100 mL three-necked flask and resuspended in 20 mL HCl acidified DI water (pH ~3). After 30 min of incubation in an ultrasonication bath with vigorous overhead mixing, 1% poly(allylamine) hydrochloride (molecular weight 16000, Aldrich) in dH$_2$O and silicic acid solution prepared freshly by diluting TMOS (tetramethoxysilane, 98%, Aldrich) to 10% with 0.1 M HCl, were alternately added in 5 mL aliquot by peristaltic pump into the continuous mixing system, until a total of 20 mL of each

solution was added. The initial pH was kept at pH ~3. After 1 hour of incubation, the reaction mixture was slowly titrated with 5% CEST (carboxyethylsilanetriol, sodium salt 25% in water, Gelest) to pH 9.2 over the course of 1 hour. The suspension was allowed for an additional 1 hour of incubation to maximize the reaction. The double coated particles were washed repeatedly and stored in HCl acidified DI water (pH ~3).

### 3.1.3 DTPA conjugation

Diethylene triamine pentaacetic acid (DTPA) was chosen as the chelator for the specific binding of metal ions onto the surface of magnetic nanosorbents. DTPA is a polyamino carboxylic acid consisting of a diethylenetriamine backbone modified with five carboxymethyl groups (Figure 3.4a). The molecule can be viewed as an expanded version of ethylenediaminetetraacetic acid (EDTA) which is very efficient at heavy metal extraction as discussed in Chapter 2. The conjugate base of DTPA also has a high affinity for metal cations. In contrast to EDTA, DTPA compound possesses 8 centers to form coordination bonds with metals (each atom of nitrogen counts as a center of coordination, as does each $COO^-$ group) (Figure 3.4b). Most metals, especially transition metals, have a limited coordination capacity, capable of forming less than 8 such bonds. Therefore, after forming a complex with a metal, the DTPA molecule still has spare "handles" which can be used to bind to other compounds or a substrate.[124]
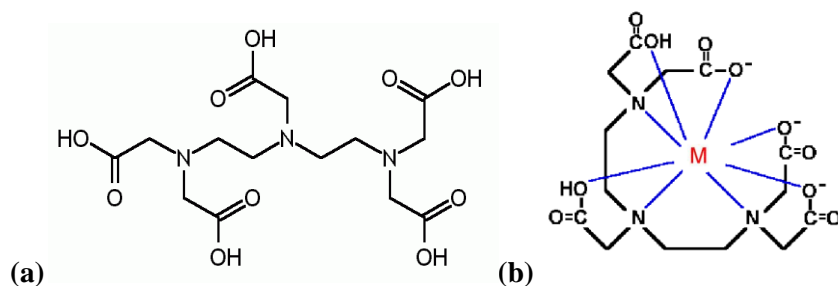
**Figure 3.4** (a) Chemical structure of DTPA; (b) Theoretical molecular structure of DTPA-metal complex (M=heavy metal ion).

DTPA molecules were covalently coupled to the primary amine groups on the second coating by carbodiimide activation.[125] 1-ethyl-3-(3-dimethylaminopropyl) carbodiimide (EDC, 98%, TCI America) was used to activate the carboxylic groups of DTPA to form an amine reactive intermediate. Specifically, 350 mg of double coated Nanofer25 particles (dMNP) were transferred into 0.1M 2-(N-morpholino)ethanesulfonic acid (MES, ≥99%, ULTROL) buffer at pH 5.5 and mixed with 280 mg of DTPA (2 mmol/g of dMNP) in $dH_2O$ at pH ~5. The mixture was agitated for 30 min before the addition of EDC. 136 mg of solid EDC (2 mmol/g of DTPA) were added in four equal portions at 1 hour intervals. At last, the nanosorbents were collected by magnetic separation and washed repeatedly with HCl acidified water pH 3.

## 3.2 Characterization of dMNP-DTPA nanosorbents

Dry powder samples were prepared for physical and chemical characterization unless otherwise specified. Aliquots of each sample were thoroughly washed 3 times with HCl acidified water pH 3, 2 times with DI water, and 2 times with absolute ethanol, and dried overnight in a 110 °C oven.

### 3.2.1 Vibrating Sample Magnetometer (VSM)

Magentic properties were characterized using a DMS 1660 VSM where each pre-weighted sample is placed inside an external magnetic field to get magnetized at room temperature. A hysteresis loop was acquired by applying a scanning magnetic field of 13500 Oe to -13500 Oe.

### 3.2.2 Transmission Electron Microscope (TEM)

TEM is a microscopy technique whereby an electron beam is transmitted through an ultra-thin sample, interacting with the sample and forming an image detected by a sensor such as a CCD camera. The particle shape, size distribution, faceting and crystallinity can be obtained using TEM.[126] Here, electron microscopy experiments were conducted on a JEOL 1200 TEM, operating at 120 kV. The samples were prepared by drying the solvent of the MNPs' dispersion onto a 200 mesh copper grid with a carbon coated Formvar film.

### 3.2.3 Elemental Analysis

Dry samples were sent to Midwest Microlabs, LLC (Indianapolis, IN) for determination of carbon (C), hydrogen (H), and nitrogen (N) content. In this CHN analysis, a sample is burned in an excess of oxygen at 990 $^{\circ}$C, and the combustion products – carbon dioxide, water, and nitric oxide – are collected by various traps. The masses of these combustion products can be used to calculate the CHN composition of the sample. In this thesis, the results of the elemental analysis were used to determine the loading density of DTPA on the surface of dMNPs.

### 3.2.4 Fourier Transform Infrared Spectroscopy (FTIR)

FTIR is used to obtain an infrared spectrum of absorption in a wide spectral range. It exploits the fact that molecules absorb specific frequencies that are characteristic of their structure. Specifically, IR radiation causes the excitation of vibrations (stretching or bending) of covalent bonds within a molecule. Absorption occurs when the frequency of the IR is the same as the vibrational frequency of a chemical bond. Therefore, FTIR is a very useful and powerful tool for identifying chemicals, especially types of functional groups, from polymers and coatings.

IR spectra of dry samples were obtained and analyzed on a Thermo-Nicolet Avatar 370 FTIR spectrometer (SmartPerformer, ZnSe crystal) operating in attenuated total reflectance (ATR) mode. A background scan of the ZnSe crystal was performed before each sample. Each spectrum was taken as an average of 64 sample scans at a resolution of 4 cm$^{-1}$. Moderate pressure was applied to the samples to ensure the good contact between samples and ZbSe crystal. The resultant spectra were baseline corrected. Special interest was focused on the signals assigned to the carboxylate group as well as the primary and secondary amine groups.

### 3.2.5 Dynamic Light Scattering (DLS)

DLS is a technique used commonly to determine the size distribution profile of small particles in suspension or polymers in solution.[127] In this technique, a monochromatic light, such as laser, is shined onto a solution containing particles in Brownian motion; a Doppler Shift happens when the light hits the moving particle. The change of the wavelength of the incoming light is related to the size of the particle. Therefore, DLS is possible to compute

the sphere size distribution and give a description of the particle's motion in the aqueous medium.[128]

The hydrodynamic diameters of particles with different surface functionalized structures in standard KCl solution (1 mM) were measured using a 90Plus Particle Size Analyzer (Brookhaven Instruments Co.). In a typical experiment, the stock suspension was usually diluted to test for multiple scattering effects.[129] Nine particle concentrations from 10 to 100 mg $L^{-1}$ were investigated here. After the addition of each sample, the suspension was sonicated for 2 min, and then ~4 mL of the well-mixed suspension was transferred into a plastic cuvette for DLS measurements at room temperature.

The zeta potential, the potential difference between the dispersion medium and the stationary layer of fluid attached to the dispersed particle, is a function of the surface charge which develops when a material is placed in solution. It can be characterized by electrophoretic light scatting that is based on DLS. The frequency shift of an incident laser beam depends on the dispersed particles mobility which is induced by an oscillating electric field. In this research, the particle mobility data were measured using a DLS instrument (Brookhaven Instruments Co.), and raw data from DLS were analyzed using a BIC PALS Zeta Potential Analyzer software to compute the zeta potential data as a function of pH. 0.1M HCl and 0.1M NaOH were used to adjust the pH to the desired value, and then a predetermined amount of the sample stock was introduced to obtain the desired particle concentration of 30 mg $L^{-1}$. After the addition of each sample, the suspension was sonicated for 10 seconds and then ~1.5 mL of the well-mixed suspension was transferred into a plastic cuvette for measurements. The electrode was slowly inserted into the cuvette to avoid any bubble.

**3.3 Characterization results and discussion**

The uncoated Nanofer25 MNPs have an average particle size of ~50 nm and a size distribution from 20-100 nm. After the second coating, due to the introduction of the polymer structure of PA, the size of dMNP in water obtained by DLS significantly increased by 60-70 folds compared to the uncoated coated MNPs (Figure 3.5), while the dry weight of dMNP only increased by 3.5-4 fold. Johnson *et al.* [130] reported that this swelling is caused by the adsorption of water. After DTPA coupling, the dMNP-DTPA nanosorbents kept the similar swelling structure.
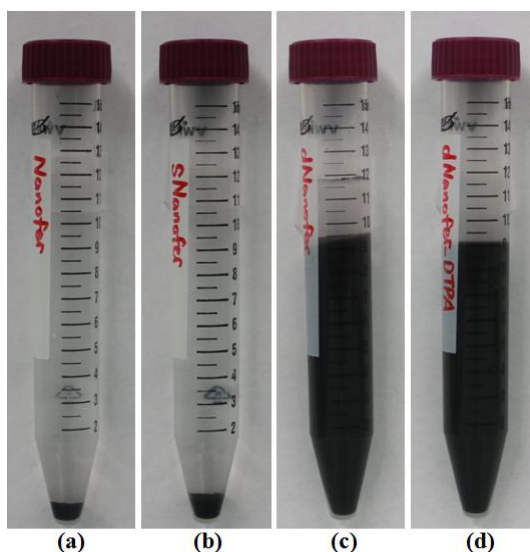


**Figure 3.5** Same amount of Nanofer25 MNPs before and after each coating: (a) MNP (uncoated), (b) sMNP (single silica coated), (c) dMNP (double coated), and (d) dMNP-DTPA (double coated MNP coupled with DTPA).

The speed at which the MNPs can be removed from the bulk solution is directly related to the magnetic properties. Saturation magnetization ($M_s$ in emu g$^{-1}$) is the maximum

induced magnetic moment that can be obtained in a magnetic field. It is an important parameter obtained from the hysteresis loop of a magnetic material. In general, the higher the $M_s$ value, the more readily the MNPs are collected by an external magnetic field. $M_s$ of the particles from MNP to dMNP-DTPA decreased with the increase of the non-magnetic coating materials on MNPs as shown in Figure 3.6. For the dMNP-DTPA nanosorbents $M_s$ was 21 emu g$^{-1}$, which corresponds to a ~75% reduction compared to the uncoated Nanofer25 MNPs. However, the magnetization of uncoated Nanofer25 MNPs was not stable, especially in acid, due to iron leaching into solution. With the chemically inert silica coating (sMNP), the particles could be stored in 0.1M HNO$_3$ for at least 3 weeks with less than 2% of iron leached (Figure 3.7). According to our previous study, the $M_s$ values above 13 emu g$^{-1}$ were sufficient for fast magnetic separation in less than 1 min.[130,131]
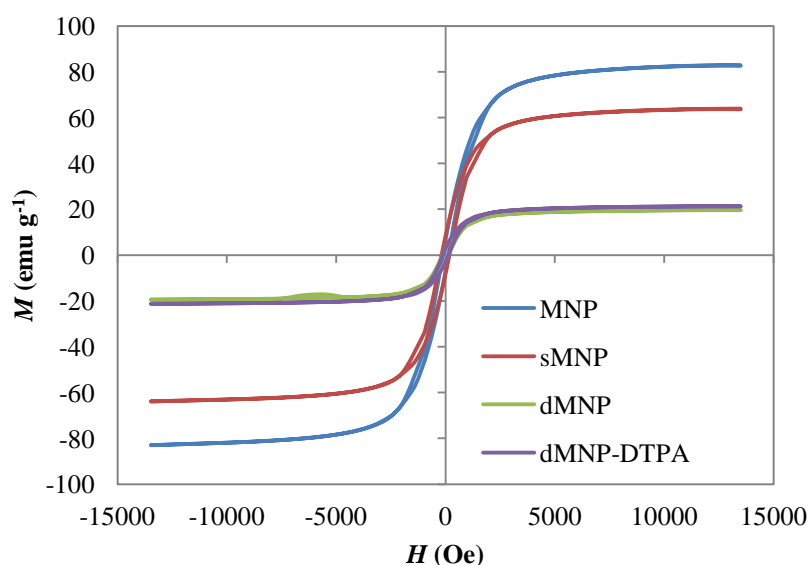


**Figure 3.6** Hysteresis loops of MNPs with different surface functionalities.
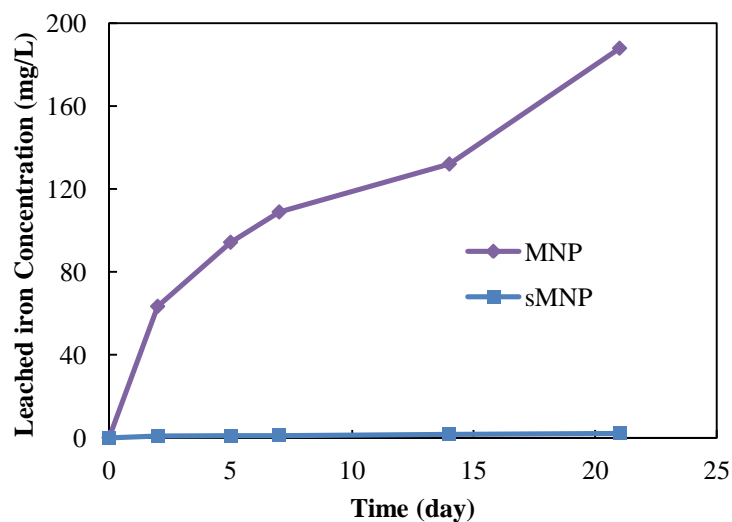
**Figure 3.7** Time dependence of iron leaching from MNP and sMNP in 0.1M HNO$_3$.

Increases in nitrogen (%N) and carbon (%C) contents measured by elemental analysis as shown in Table 3.2 gave the quantitative evidence for PA loading and DTPA attachment. The difference of %N of dMNP and dMNP-DTPA was used to estimate the efficiency of DTPA attachment. The increase of 0.39 mmol of %N indicated that the density of DTPA on the nanosorbent surface was ~130 μmol g$^{-1}$. The elemental analysis results listed in Table 3.3 also demonstrated the good stability of the loaded DTPA. After storage for three months in 1.0 M NaNO$_3$ at pH 3.0, there was more than 85% of DTPA remaining on the dMNP-DTPA surface of the MNPs.

**Table 3.2** Elemental analysis results after each synthesis step and increases in %N compared to the prior step.

| Sample Name | %C (wt) | %N (wt) | ΔN (mmol/g) |
|---|---|---|---|
| sMNP | 0.28 | 0 | |
| dMNP | 6.22 | 1.3 | 0.93 |
| dMNP-DTPA | 8.13 | 1.84 | 0.39 |

**Table 3.3** Elemental analysis results of DTPA loading and stability in 1M $NaNO_3$ pH 3.0.

| Incubation Time | DTPA ($\mu mol\ g^{-1}$) | % Remaining |
|:---:|:---:|:---:|
| Initial | 131 | |
| One week | 122 | 93.1% |
| Three months | 115 | 87.8% |

The IR spectra in Figure 3.8 provided additional confirmation of DTPA being bound to the surface of the MNPs. Broad peaks centered at 3100-3300 $cm^{-1}$ associated with N-H stretching from primary amine and secondary amide groups confirmed the co-precipitation of PA in the second coating. After baseline correction and normalization, clearly increased peak intensity in C=O stretching band at ~1710 $cm^{-1}$, amide I band at ~1640 $cm^{-1}$ from C=O stretching, as well as amide II band at ~1550 $cm^{-1}$ associated with N-H bending were observed, which offered the qualitative evidence for DTPA attachment. The peak at ~1400 $cm^{-1}$ was due in part to C-N stretching from secondary amide groups and symmetric stretching of carboxylates. A band at ~1300 $cm^{-1}$ was associated with the $CH_2$ wagging. The significantly intense peak starting at 1250 $cm^{-1}$ was assigned to the Si-O-Si stretching of the silica coating.
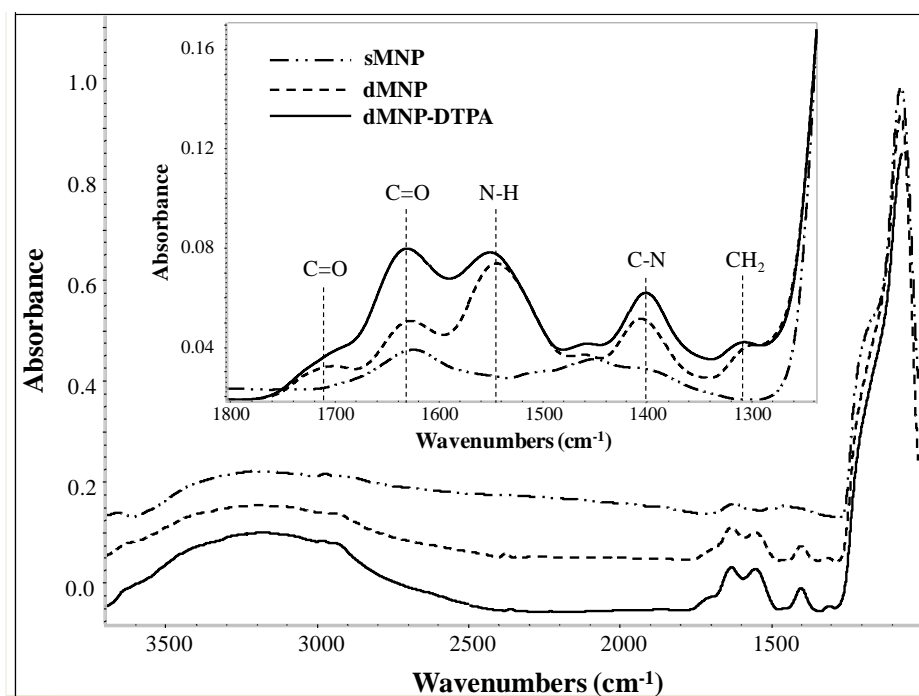
**Figure 3.8** ATR-FT-IR spectra of sMNP, dMNP and dMNP-DTPA.


Figure 3.9 showed representative microstructures of the samples. In addition, their

chemical compositions were confirmed by using energy dispersive X-ray spectroscopy

(EDS) technique. The TEM images clearly showed that the successive increase in thickness

of coating on MNPs by different surface functionalities. The thickness of the first silica

coating was ∼ 40 nm (Figure 3.9b). After second coating, the size of particles with polymer

structure (silica and polyamine) significantly increased to micro-scale (Figure 3.9c). The

first silica coating was still clearly recognizable after the second coating (Figure 3.9d). The

DTPA attachment did not have a significant effect on the particle size and surface structure

(Figure 3.9e and f). The TEM images also revealed that the first silica coating was not

coated on the individual iron/iron oxide MNPs. Instead, the MNPs agglomerated before the

surface coating. Another issue with the conventional TEM analysis is that it requires dry

samples. However, the size and surface structure of dMNP and dMNP-DTPA particles significantly changed after dry due to the water-absorbing polymer structure of polyallylamine on the second coating. Therefore, other imaging technique will be needed which allows doing the sample analysis in aqueous solution.
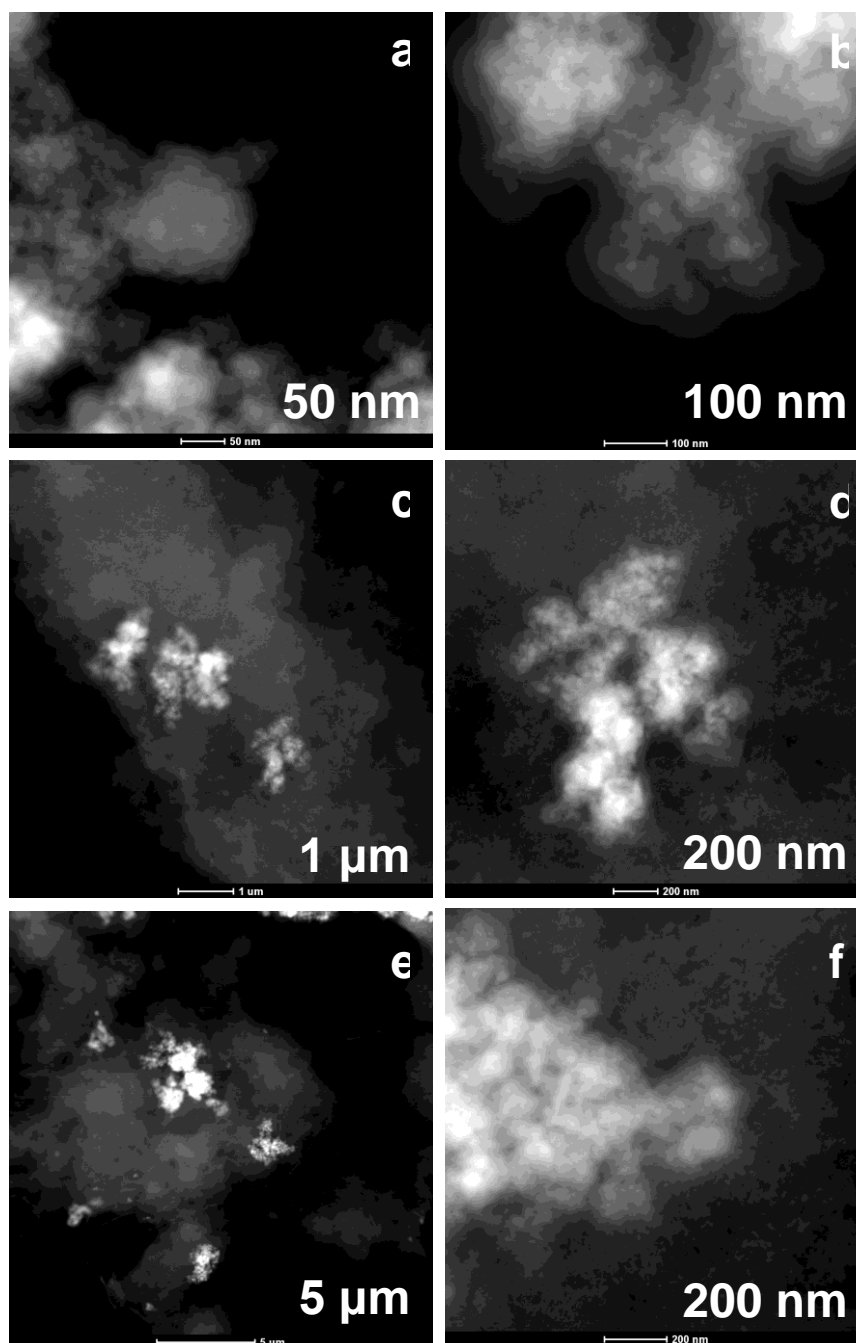
**Figure 3.9** TEM images of MNPs before and after surface functionalization with silica, co-precipitation of silica and polyallylamine, and complex nanosorbent of DTPA attached MNPs. (a) Uncoated MNP, (b) sMNP, (c-d) dMNP, and (e-f) dMNP-DTPA.

Zeta potential data of dMNP and dMNP-DTPA as a function of pH are shown in Figure 3.10. The standard method used to transfer mobility data to zeta potential data assumes smooth hard particles. Therefore, the polymer surface structure of dMNP and dMNP-DTPA gives rise to a large uncertainty to the absolute zeta potential data. However, the sign of the zeta potential and the position of the point of zero charge (PZC) should be correct.[132] In both cases, the data had positive values at low pH, passed through a PZC, and then turned to negative at high pH. The PZC for dMNP-DTPA was at pH ~5, indicating that when the pH was lower than 5, DTPA molecules were mostly protonated. This corresponded to the acid dissociation constant of DTPA (p$K_a$: 1.9, 2.9, 4.4, 8.7, 10.5).[133] The PZC for dMNP was at pH ~6.5. The zeta potential data suggested the surface charge of dMNP and dMNP-DTPA, which was highly related to their sorption power as discussed below.
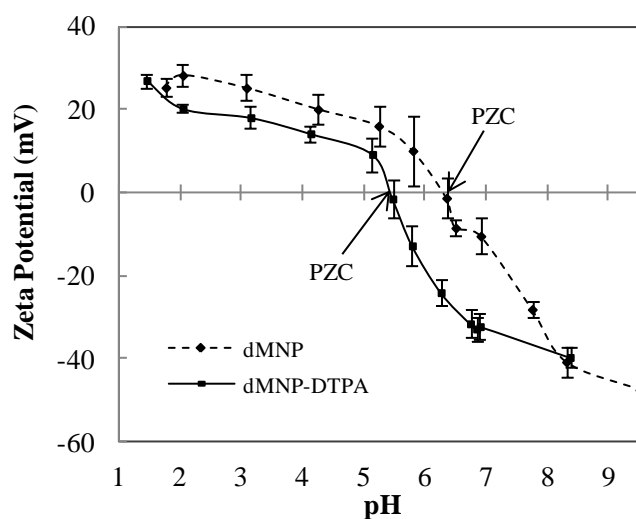


**Figure 3.10** Zeta potential vs. pH for dMNP and dMNP-DTPA at a particle concentration of 30 µg/mL.

**3.5 Summary**

The dMNP-DTPA nanosorbents were synthesized and characterized. Briefly, Nanofer25 MNPs were initially coated with silica using a modified sol-gel process to increase the particle stability in acidic conditions. In the second step, poly(allylamine) hydrochloride (PA) molecules were partially imbedded in a second silica layer formed from TMOS, via titrating the pH to 9.2 with alkaline 5% CEST. The long polymer chains introduced on the surface largely increased the loading density for chelators. In the third step, DTPA molecules were directly covalently coupled to the primary amine groups of dMNP by carbodiimide activation of carboxylic groups. According to the characterization results, the DTPA molecules were successfully attached to the MNPs' surface, with a loading density of 130 μmol/g. The surface functionalization significantly changed the particle size, magnetic properties, and stability in acidic conditions.

**Chapter 4: Kinetics, Thermodynamics, and Reusability of dMNP-DTPA for Heavy Metal Treatment**

**4.1 Introduction**

As a serious global environmental issue, heavy metal pollution has attracted increasing attention due to their persistency and high toxicity. In Idaho, there are six Superfund sites on the National Priorities, located in Shoshone, Power, Bannock, Butte, Clark, Jefferson, Bingham, Caribou, and Elmore Counties.[134] Five of them are experiencing heavy metal contamination in soil, sediments, groundwater, and surface water. Those heavy metals are mainly from former mining and smelting operations, ore and chemical processing plants, and laboratories.[134] Whether in the soil or aquatic environment, heavy metals can be transported by several processes over long distances, especially posing a high risk to the nearby environment and community. The dissolved concentration of cadmium (Cd) in groundwater samples from the Penn Mine site in central California ranged from 10 to 3700 $\mu$g L$^{-1}$.[135] In the northern Idaho, a century of mining and smelting operations in the Coeur d'Alene mining district in Silver Valley has contaminated the Coeur d'Alene River-Lake System, and resulted in the accumulation of significant amounts of lead, zinc, and other heavy metals in the sediments.[136,137] According to previous reports, the average concentrations of these metals in the Coeur d'Alene River sediments are: Pb, 3820 ppm; Zn, 2995 ppm; and As, 201 ppm.[138,139] The high concentrations of heavy metals in the sediments are a huge contamination source. Via leaching process, those heavy metals can be easily transported into the surface water and affect the water quality of the Coeur d'Alene River-Lake system.

Exposure to Cd, one of the most toxic heavy metals, may cause adverse health effects, such as renal dysfunction, bone lesion, lung fibrosis, or even cancer development.[140] Cd is usually regulated to concentrations of less than 0.1 mg $L^{-1}$ (ppm) for industrial discharges to protect human health and the environment. The maximum concentration in drinking water is extremely low, 5 μg $L^{-1}$ (ppb).[141]

Removing heavy metals from contaminated water to meet the regulation limits instituted by US federal and state governments is always a task with high priority. Heavy metals in wastewater have been traditionally treated by ion exchange,[61,63] adsorption,[66,142] chemical precipitation,[67,68] and membrane filtration.[69,143] Although these methods are widely used in practical exercises, there are some common limitations existing in industrial applications, such as high capital and energy costs, slow separation kinetics, prefiltration required to avoid clogging problem, and significant secondary waste generation.[55] Right now, the greater quantities of wastewater generation and the more stringent regulations for wastewater discharge call for a simple, fast, and cost-effective heavy metal treatment process to overcome the drawbacks existing in the traditional methods. Under such guidance, an alternative magnetic separation nanotechnology[96,144,145] has been investigated and developed in our laboratory recently.[43,85,106,130,131,146] The concept is to introduce metal chelators onto the surface of magnetic nanoparticles (MNPs), so that the magnetic nanosorbent complex with a magnetic core and a functionalized shell can be manipulated and recovered in a magnetic field produced by the separation system. The design of magnetic nanosorbents is under the guidance of the 3R's: reduce (the volume of primary and secondary waste), recycle (the concentrated target species), and reuse (the sorbent materials in a closed-cycle).

Based on this idea, the dMNP-DTPA nanosorbents, double coated iron nanoparticles (dMNP) coupled with diethylene triamine pentaacetic acid (DTPA), have been synthesized and used to remove heavy metal ions from contaminated water. Our previous batch sorption experiments have demonstrated that the dMNP-DTPA nanosorbents can be effectively used to remove Cd(II) and Pb(II) from aqueous solutions. Under the optimum conditions for the sorbent concentration at 500 mg/L, i.e. contact time more than 30 min, pH ~5, and initial metal concentration below 4 mg/L, the distribution coefficient ($K_d$) reached 18000 mL/g for cadmiun and 40000 mL/g for lead, which confirmed the sorption efficiency of dMNP-DTPA. In this study, possible sorption mechanisms were determined by evaluating the effect of contact time, initial metal concentration, and temperature on the Cd(II) sorption efficiency. More importantly, the stability and reusability of the magnetic nanosorbents for removing Cd(II) from wastewater was systemically investigated by performing Cd(II) sorption/desorption cycle experiments. Desorption, also known as stripping, of Cd(II) from dMNP-DTPA is a key process to realize the objectives of the 3R's. The successful achievement of the stripping process without adverse effects on the nanosorbents' sorption efficiency is important and necessary to reduce the inventory utilization of nanosorbents and, therefore, reduce the generation of secondary waste. The ability to reuse the magnetic nanosorbents for a longer time will greatly offset the relatively high synthesis cost of nanomaterials, making this magnetic separation method economical and cost-effective. In addition, thermodynamic study, the effect of temperature on Cd(II) sorption, was conducted to further probe the sorption mechanisms.

## 4.2 Experimental procedures

### 4.2.1 Sorption experiment

Batch sorption procedure was used to determine the effect of various operating conditions on the metal sorption process. For each experiment, 10 mL of Cd(II) solution with the desired concentration (1-9 mg $L^{-1}$) was treated with 5 mg of each sorbent material. The metal solutions were prepared by diluting standards (Cd standard for ICP, 1000 mg $L^{-1}$ in 2 vol.% $HNO_3$, Ultra Scientific) with 0.1 M acetate (sodium acetate, trihydrate, Mallinckrodt) buffer at pH 5.0. Each sample was first sonicated for 10 seconds to disperse the particles and then agitated at 160 rpm in a horizontal shaker at 25 $^oC$. After sorption, the particles were separated from the solution by magnetic field assisted decantation. The supernatant was removed for metal analysis using the atomic absorption spectrophotometer (AAS, Thermo S Series). The effects of initial metal concentration (1-9 mg $L^{-1}$), contact time (2 -1440 min) and temperature (25-57 $^oC$) were investigated. To determine the effect of a particular parameter, that parameter was varied while others were kept constant.

### 4.2.2 Desorption experiment

Desorption experiments were performed using distalled water, HCl, and $HNO_3$ as stripping agents. The effects of contact time and HCl concentration on desorption were studied by washing 5 mg of the Cd(II) loaded with 5 mL of different stripping agent. The mixture was agitated for 2 min at each washing step, magnetically separated, and the concentration of Cd(II) desorbed was checked in the supernatant by the AAS. The percentage of Cd(II) ions desorbed was calculated by the following equation:

$$\%\text{Desorption} = \frac{c_D V_D}{M_S} \times 100 \qquad (4\text{-}1)$$

where $c_D$ (mg L$^{-1}$) is the concentration of Cd(II) ions in the desorbed solution, $V_D$ (L) is the volume of the desorbed solution, and $M_S$ (mg) is the mass of adsorbed Cd(II) ions on the adsorbent.

## 4.3 Results and discussion

### 4.3.1 Cd(II) sorption on dMNP-DTPA

#### 4.3.1.1 Effect of contact time and sorption kinetics

A high sorption rate is an important requirement for a sorbent material to minimize the time to remove metal ions from wastewater. As shown in Figure 4.1 it took 30 min for dMNP-DTPA nanosorbents to reach the sorption equilibrium. In addition, by successfully coupling DTPA to dMNP, the $K_d$ value dramatically increased to 12000 mL g$^{-1}$. By contrast, the $K_d$ values of dMNP were only 100 mL g$^{-1}$ for Cd(II).
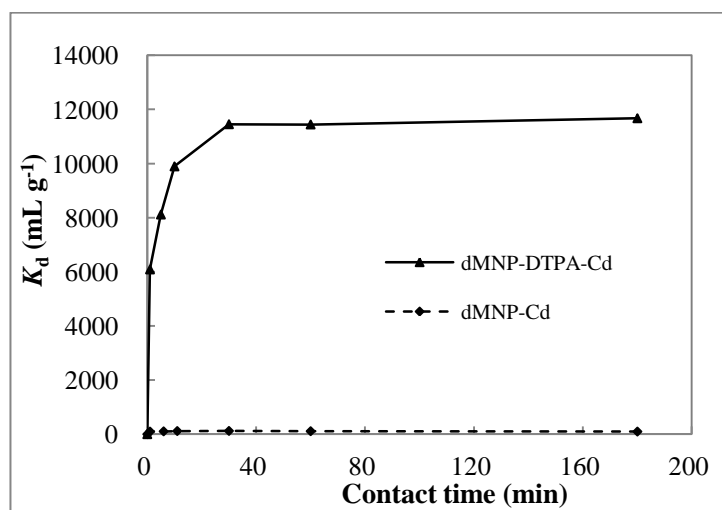


**Figure 4.1** Sorption kinetics of 4 mg L$^{-1}$ Cd(II) in pH 6.0 buffer on dMNP-DTPA and dMNP, respectively, at 25 $^{\circ}$C (Contact time: 0-180 min).

The sorption kinetics was determined by the pseudo-first order, pseudo-second-order and intraparticle diffusion model. The kinetics equation and parameters obtained are presented in Table 4.1. $Q_t$ and $Q_e$ is the amount (mg g$^{-1}$) of metal ions adsorbed at time $t$ and the equilibrium, respectively, and $k$ is the equilibrium rate constant of each model. From Table 4.1, the values of correlation coefficient, $R^2$, indicated that only the plot of pseudo-second-order model gave a straight line, which indicated the pseudo-second order model was the best fit to the experimental data. It suggested that the sorption rate was proportional to the cencentration of Cd(II) squared, and chemisorption might be the principal mechanism for the Cd(II) sorption on dMNP-DTPA.

**Table 4.1** Kinetic models and parameters of the Cd(II) sorption process.

| Kinetic models | Equation | Parameters | |
|---|---|---|---|
| **Pseudo-1$^{st}$ order** | $\log(Q_e - Q_t) = \log Q_e - k_1 t / 2.303$ | $Q_e$ (mg g$^{-1}$) | 1.101 |
| | | $k_1$ (min$^{-1}$) | $1.612 \times 10^{-3}$ |
| | | $R^2$ | 0.734 |
| **Pseudo-2$^{nd}$ order** | $\dfrac{t}{Q_t} = \dfrac{1}{k_2 Q_e^2} + \dfrac{1}{Q_e} t$ | $Q_e$ (mg g$^{-1}$) | 7.734 |
| | | $k_2$ (g mg$^{-1}$ min$^{-1}$) | 0.017 |
| | | $R^2$ | 0.999 |
| **Intra-particle diffusion** | $Q_t = k_d t^{1/2} + C$ | $k_d$ | 0.035 |
| | | $C$ | 6.508 |
| | | $R^2$ | 0.832 |

In the intra-particle diffusion model, instead of exhibiting a linear relationship, the data gave multi-linear plots as illustrated in Figure 4.2. This suggested two or more diffusion steps influenced the sorption process: the first straight portion ($R^2$=0.996) represented macro-pore diffusion and the second ($R^2$=0.953) depicted micro-pore diffusion. The $C$

values from both portions were not zero, indicating the existence of some boundary layer effect and that intra-particle diffusion was not the rate-determining step in the overall sorption process. Such diffusion phenomenon was observed by extending the contact time to 24 hours (Figure 4.3). We found that after the equilibrium reached (30 min) until 3 hours of contact, the metal concentration remained stable. However, from 3 to 24 hours, there was a slow decrease in the metal concentration: additional 10% of Cd(II) was slowly removed by dMNP-DTPA. This slow diffusion could be caused by the covalent crosslinking between PA and DTPA. With five carboxylic groups, each DTPA can react with multiple amine groups on the imbedded PA; this crosslinking could form a relatively tight network between PA and DTPA; when metal ions slowly diffuse into the network, they could be sequestered there and subsequently removed by magnetic separation. By contrast, the metal concentration in control dMNP groups remained stable in the whole period tested, since there was no crosslinking structure on the dMNP sample.
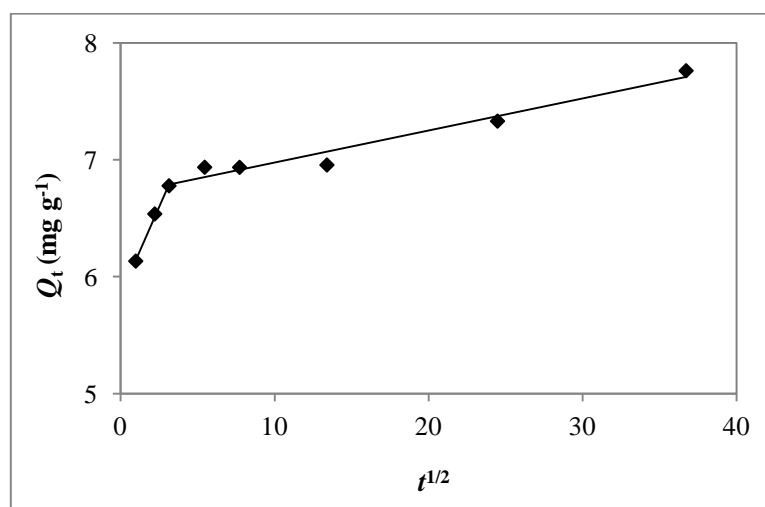


**Figure 4.2** Intra-particle diffusion plots for sorption of Cd(II) ions on dMNP-DTPA
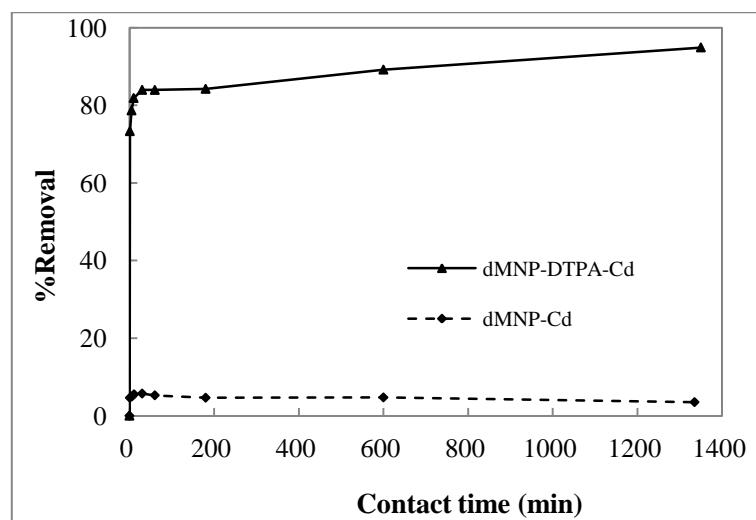
**Figure 4.3** Sorption Kinetics of 4 mg L$^{-1}$ Cd(II) in pH 6.0 buffer on dMNP-DTPA and dMNP, respectively, at 25 $^{\circ}$C (Contact time: 0-1440 min).

## 4.3.1.2 Effect of initial metal concentration and isotherm models

Figure 4.4 showed the influence of the initial metal ion concentration on the batch sorption of Cd(II) onto dMNP-DTPA and dMNP. More than 90% of Cd(II) ions were removed when the initial metal concentration was below 4 mg L$^{-1}$. Again, the sorption results demonstrated the excellent performance of dMNP-DTPA and the essential value of DTPA chelators for binding Cd(II) ions, as well as the successful attachment of DTPA to dMNP. As the initial concentration increased, decreases in the values of $K_d$ and removal percentage were observed due to the approach to the sorption saturation of the sorbent. As a result of the interference among metal ions, the fewer the unoccupied sorption sites, the more difficult it is for the metal ions to be adsorbed. This is a result of the increase in the driving force from the concentration gradient.[147]
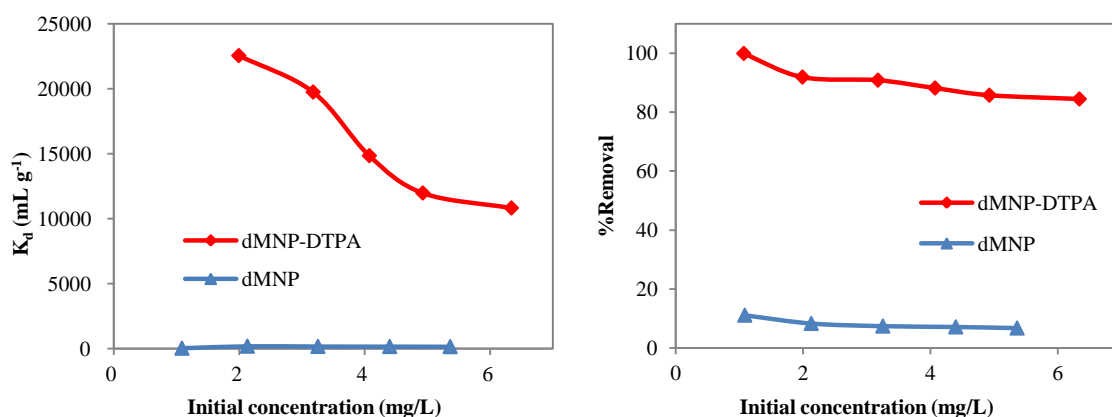
**Figure 4.4** Effect of initial concentration on the $K_d$ values (left) and the removal percentage (right)

The sorption data obtained by varying the initial metal concentration were analyzed by two common sorption models, the Langmuir isotherm and the Freundlich isotherm, as given by the following equations:

$$\text{Langmuir:} \qquad \frac{c_e}{Q_e} = \frac{1}{K_L Q_{max}} + \frac{1}{Q_{max}} c_e \qquad\qquad (4\text{-}3)$$

$$\text{Freundlich:} \qquad \log Q_e = \log K_F + \frac{1}{n} \log c_e \qquad\qquad (4\text{-}4)$$

where $Q_e$ is the sorption capacity (mg/g) at the equilibrium based on the dry weight of dMNP-DTPA, $Q_{max}$ is the maximum sorption capacity, $c_e$ is the equilibrium concentration of metal ions (mg L$^{-1}$) in solution, $K_L$ is the Langmuir constant (L mg$^{-1}$), $K_F$ and $n$ are the Freundlich constants indicating the maximum sorption capacity and the sorption intensity, respectively. The values of these parameters, calculated according to Eqn. (4-3) and (4-4), are listed in Table 4.2. By comparing the values of $R^2$, the sorption data fitted better to the Langmuir isotherm than to the Freundlich isotherm, suggesting the uniform distribution of sorption sites and the formation of monolayer of absorbed metal ions on the nanosorbent

surface. In addition, the information given by the Freundlich model did not conflict with that given by the Langmuir model. Specifically, the value of $n>1$ indicates a concave downward sorption isotherm, which is also the characteristic of the Langmuir sorption isotherm. The values of $n$ within the range of 2-10 represent good sorption.[148]

**Table 4.2** Isotherm parameters from the Langmuir model and the Freundlich model.

| Langmuir | | | Freundlich | | |
|---|---|---|---|---|---|
| $Q_{max}$ (mg/g) | $K_L$ | $R^2$ | $K_F$ (mg/g) | $n$ | $R^2$ |
| 13.64 | 2.51 | 0.991 | 9.03 | 2.40 | 0.906 |

Since the DTPA density on the dMNP-DTPA nanosorbents calculated from the elemental analysis data was 130 μmole $g^{-1}$, the theoretical $Q_{max}$ would be 14.6 mg $g^{-1}$ for Cd(II). This assumes that one DTPA molecule could only sequestrate one metal ion. The fact that the $Q_{max}$ calculated by the Langmuir isotherm (13.6 mg/g) was slightly smaller than the theoretical $Q_{max}$ could be explained by the fact that the crosslinking between DTPA and polyamine on dMNP reduced the metal sorption capacity of dMNP-DTPA by blocking some of the chelating carboxylic groups of DTPA on the sorbent surface.

**4.3.1.3 Thermodynamic studies**

The variation in the amount of Cd(II) ions adsorbed onto dMNP-DTPA as a function of temperature was shown in Figure 4.5. It was observed that the Cd(II) sorption increased slightly as the temperature increased from 298 to 330 K. This indicated that a high temperature favored the sorption process. The improved sorption capability with increasing temperature suggested that the Cd(II) sorption on dMNP-DTPA was an endothermic process. The endothermic process could be explained by the enlargement and/or activation

of the adsorbent surface at higher temperatures. This could also be due to the increased

mobility of heavy metal ions from the bulk solution towards the adsorbent surface (Cd(II)

ions gaining more kinetic energy to diffuse from the bulk phase to the solid phase with an

increase in solution temperature) and the enhanced accessibility to the adsorbent active

sites.[149,150] On the other hand, the results from the temperature effect experiments suggested

that the dMNP-DTPA nanosorbents possessed the excellent thermal stability (it has only

about 3% change between temperature of 298 and 330 K) so that they can be directly

applied in a waste stream from a higher temperature source without cooling it down.
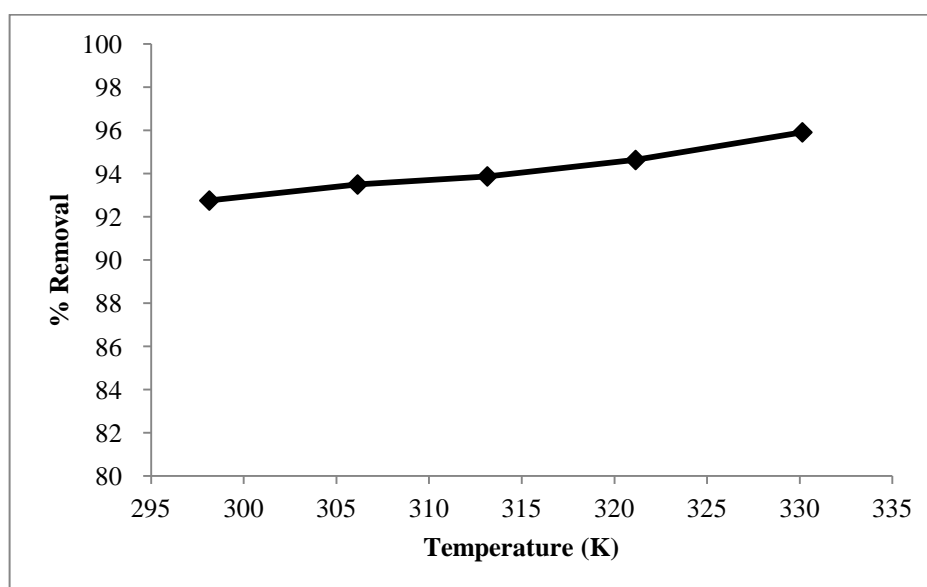


**Figure 4.5** . Effect of solution temperature on the Cd(II) sorption on dMNP-DTPA (initial concentration 5 ppm, pH 5.0, contact time 1 hour).

In order to evaluate the feasibility of the sorption process, thermodynamic

parameters such as the standard free energy ($\Delta G^0$), enthalpy change ($\Delta H^0$) and entropy

change ($\Delta S^0$) were estimated. The Gibb's free energy change of adsorption was calculated from the following equation:

$$\Delta G^0 = -RT \ln K_c \tag{4-5}$$

where $R$ is the ideal gas constant (8.314 J mol$^{-1}$ K$^{-1}$), $T$ (K) is the absolute temperature and $K_c$ is the thermodynamic equilibrium constant that is expressed as

$$K_c = c_a/c_e \tag{4-6}$$

where $c_a$ (mg L$^{-1}$) is the amount of metal ion adsorbed at equilibrium, and $c_e$ is the concentration of metal ion in solution at equilibrium. The Gibb's free energy is also related to enthalpy change ($\Delta H^0$) and entropy change ($\Delta S^0$) at constant temperature by the Van't Hoff equation as follows:

$$\ln K_c = -(\Delta G^0/RT) = -(\Delta H^0/RT) + \Delta S^0/R \tag{4-7}$$

The value of $\Delta H^0$ and $\Delta S^0$ were calculated from the slope and interception of the plot of $\ln K_c$ vs. $1/T$. The thermodynamic parameters were listed in Table 4.3. The negative values of $\Delta G^0$ at all temperatures indicated that the adsorption process was spontaneous in nature. The increase of the magnitude of free energy with the increase in temperature suggested that higher temperatures made the adsorption easier. It has been reported that $\Delta G^0$ values up to -20 kJ mol$^{-1}$ are consistent with electrostatic interaction between sorption sites and the metal ion, while $\Delta G^0$ values more negative than -40 kJ mol$^{-1}$ involve charge sharing or transfer from the adsorbent surface to the metal ion to form a coordinate bond.[151] The positive value of $\Delta H^0$ indicated an endothermic process which was supported by the increase sorption of Cd(II) with rise in temperature. Furthermore, positive values of $\Delta S^0$ shows an increase in randomness of adsorbate molecules on the solid surface than in solution, which implies the interaction between Cd(II) ion and dMNP-DTPA nanosorbents during the

sorption process. Also, the magnitude of $\Delta S^0$ reveals whether the adsorption reaction involves an associative or dissociative mechanism. If the value of $\Delta S^0$ larger than -10 J mol$^{-1}$ K$^{-1}$, it means that the adsorption conforms to a dissociative mechanism.[152] The values of $\Delta S^0$ (Table 4.3) obtained showed that the sorption of Cd(II) ions on dMNP-DTPA involves a dissociative sorption mechanism (liberation of water molecules from the solvated Cd(II) ions before sorption). The necessity of a large amount of heat to remove the Cd(II) ions from the solution makes the sorption process endothermic.

**Table 4.3** Cd(II) sorption thermodynamic parameter.

| Temperature (K) | 298.15 | 306.15 | 313.15 | 321.15 | 330.15 |
|---|---|---|---|---|---|
| $K_c$ | 12.80 | 14.38 | 15.31 | 17.62 | 23.45 |
| $\Delta G^0$ (kJ mol$^{-1}$) | -6.32 | -6.78 | -7.10 | -7.66 | -8.66 |
| $\Delta H^0$ (kJ mol$^{-1}$) | | | 14.69 | | |
| $\Delta S^0$ (J mol$^{-1}$ K$^{-1}$) | | | 70.12 | | |
| $R^2$ | | | 0.9309 | | |

### 4.3.1 Cd(II) desorption and reusability of dMNP-DTPA

An effective and excellent nanosorbent for the removal of metal ions should not only have a good sorption capacity but also a good desorption ability for a high reusability. Therefore, it was necessary to investigate the desorption of Cd(II) ions from dMNP-DTPA. Dilute acids or deionized water (DW) were often used to effectively separate the metal ions from the functional groups on the particle surface.[103,105,153,154] As a result, HNO$_3$ and HCl were chosen as the stripping agents for this study.

The desorption kinetics was firstly conducted to determine the possibility to remove the Cd(II) ions from the dMNP-DTPA nanosorbents and the rate of metal desorption. The

results in Figure 4.6 showed that both 0.1 M $HNO_3$ and 1 M HCl can be used as an efficient stripping agent. The stripping reaction was fast, recovering over 99% of Cd(II) back into solution in less than 5 min of contact time. Therefore, a short-time multi-step washing process were developed by shaking the Cd(II) loaded particles twice in 5 mL of the stripping agent for 2 min, and then one time in 5 mL of DW for 1 min.
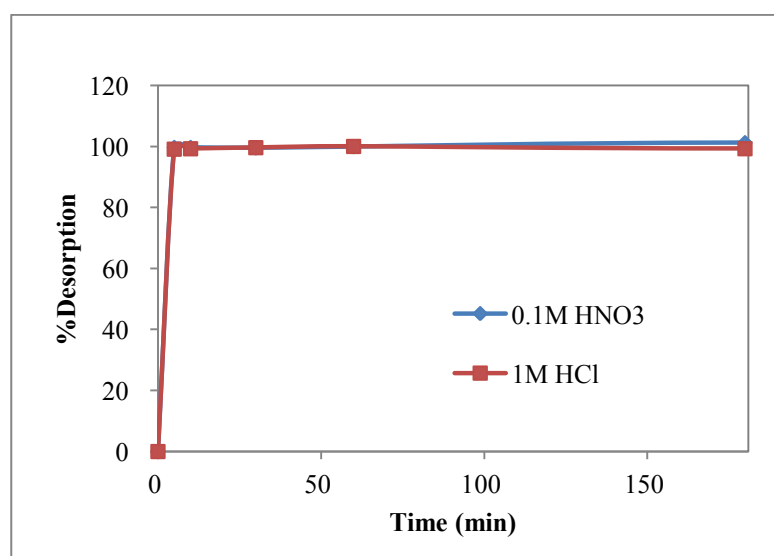


**Figure 4.6** The desorption percentage of Cd(II) from dMNP-DTPA-Cd complex into the stripping agent as a function of contact time

The possibility and efficiency to reuse the dMNP-DPTA nanosorbents were investigated by performing the sorption/stripping cycle tests. For each cycle, 10 mg of dMNP-DTPA particles were used to treat 10 mL of 4 ppm Cd(II) solution at pH 5 acetate buffer with 1 hour contact time at 25 $^o$C. After sorption, the supernatant was removed for Cd(II) analysis to calculate the sorption efficiency, while the dMNP-DTPA-Cd complex particles went to multi-step stripping process for the Cd(II) desorption. The same amount of regenerated dMNP-DTPA nanosorbents were reused for another sorption cycle. As shown in

Figure 4.7 and Figure 4.8, generally, no significant decrease in sorption capacity was observed during 15 sorption/stripping cycles for both cases. Over 90% of absorbed Cd(II) was back-extracted in solution by the first acid stripping step, and there was a negligible amount of Cd(II) in the third time DW washing. Overall, more than 95% of adsorbed Cd(II) was recovered back into the solution using either 0.1 M $HNO_3$ or 1 M HCl. These results indicated the resident of Cd(II) ions on dMNP-DTPA (irreversible binding) was not significant. There was no significant difference in stripping effectiveness between $HNO_3$ and HCl. However, $HNO_3$, as a stronger oxidizer, exhibited more damage to the dMNP-DTPA nanosorbents: as illustrated in Figure 4.9, the dMNP-DTPA nanosorbents washed with $HNO_3$ started to decay in terms of percentage removal after 13 sorption/stripping cycles, whereas nanosorbents washed with HCl were able to maintain nearly the 100% sorption for at least 15 cycles. For this reason, HCl would be a better stripping agent choice. Several studies have also shown HCl to be more effective in desorbing heavy metals from their loaded adsorbents when compared to other stripping agents such as $HNO_3$, $H_2SO_4$, and NaOH.[155,156] As a result HCl was used as the stripping agent in the following study.

**Sorption/Stripping Cycles with 0.1 M HNO$_3$**
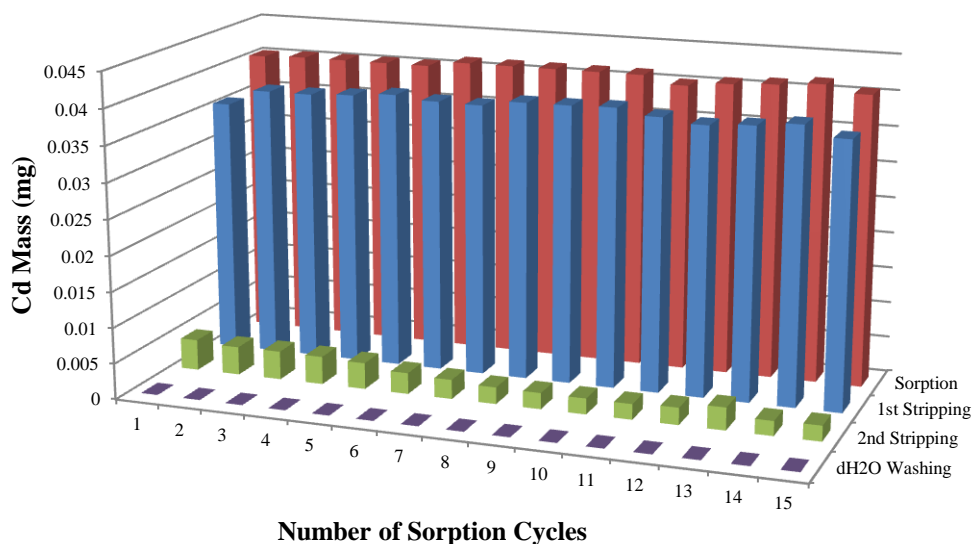


**Figure 4.7** Mass of adsorbed and desorbed Cd(II) during 15 sorption/stripping cycles with dMNP-DTPA using 0.1 M HNO$_3$.

**Sorption Cycle Test Stripping with 1M HCl**
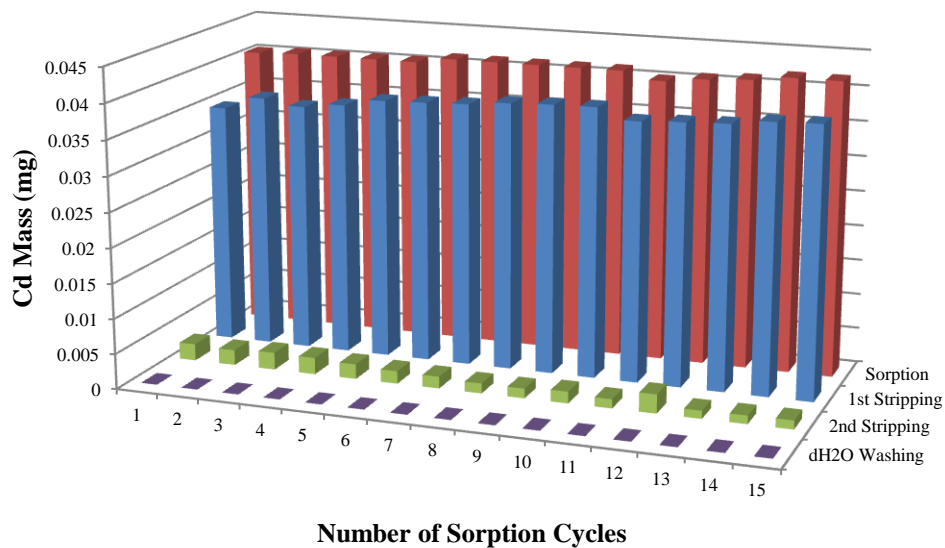


**Figure 4.8** Mass of adsorbed and desorbed Cd(II) during 15 sorption/stripping cycles with dMNP-DTPA using 1 M HCl.
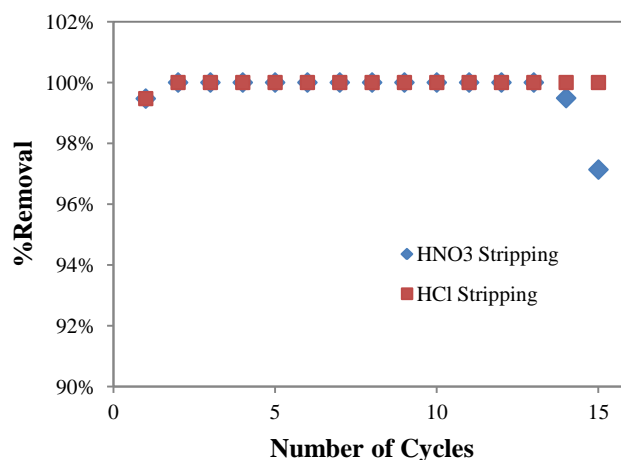
**Figure 4.9** Percentage removal of Cd(II) ions during 15 sorption/stripping cycles.

In order to evaluate the loss of chelator during the HCl desorption process, the fresh and regenerated dMNP-DTPA nanosorbents were checked for the change in the elemental analysis and the maximum sorption capacity ($Q_{max}$). The nitrogen (%N) and carbon (%C) contents measured by the elemental analysis for particles with different surface functionalities were listed in Table 4.4. The difference of %N between dMNP and dMNP-DTPA was used to estimate the DTPA density (mmol g$^{-1}$) on the nanosorbent surface. For the regenerated dMNP-DTPA nanosorbents, the decrease in %N (~0.04 mmol g$^{-}$1) indicated that there was ~30% of DTPA lost after the nanosorbents went through the first time of the desorption process.

**Table 4.4** Elemental analysis results after each synthesis step and increases in %N compared to dMNP.

| Sample Name | %C (wt) | %N (wt) | $\Delta$N (mmol g$^{-1}$) | DTPA (mmol g$^{-1}$) |
|---|---|---|---|---|
| MNP | 0.15 | NA | | |
| sMNP | 0.58 | 0.27 | | |
| dMNP | 7.65 | 1.50 | | |
| dMNP-DTPA (Fresh) | 9.41 | 2.04 | 0.386 | 0.129 |
| dMNP-DTPA (Regenerated) | 8.61 | 1.87 | 0.264 | 0.088 |

The Cd(II) sorption isotherms on fresh and regenerated dMNP-DTPA were compared in Figure 4.10. In the inset, the plot of $c_e/Q_e$ as a function of $c_e$ yielded a straight line for both cases. The linear fit correlation ($R^2 > 0.999$) suggested that, after desorption process, re-sorption of Cd(II) on the regenerated dMNP-DTPA nanosorbents still obeyed the Langmuir isotherm, forming a single monolayer on the surface. From the slope, the values of $Q_{max}$ for the regenerated dMNP-DTPA nanosorbents were calculated to be 10.06 mg g$^{-1}$, which dropped by ~26% compared to the fresh dMNP-DTPA nanosorbents. The decrease in the maximum sorption capacity was consistent with the loss of DTPA from the elemental analysis results, assuming the complexing reaction radio between DTPA and Cd(II) was 1:1. Although there was a ~26-30% of DTPA lost during the initial desorption process, the results from the sorption/desorption cycle experiment demonstrated that the sorption capacity decay rate (or the loss of DTPA) was much lower in the following stripping steps, as shown in Figure 4.11. If the decay rate remained constant, the HNO$_3$ regenerated dMNP-DTPA could be reused for another 3 cycles with more than 80% of Cd being effectively removed from the solution. With a lower decay rate, the HCl regenerated dMNP-DTPA could be reused for a longer time. Before the percentage removal of Cd(II) started to

decrease in the 14th cycle for the regenerated dMNP-DTPA (Figure 4.9), available

unsaturated sorption sites compensated the loss of DTPA during the sorption/desorption
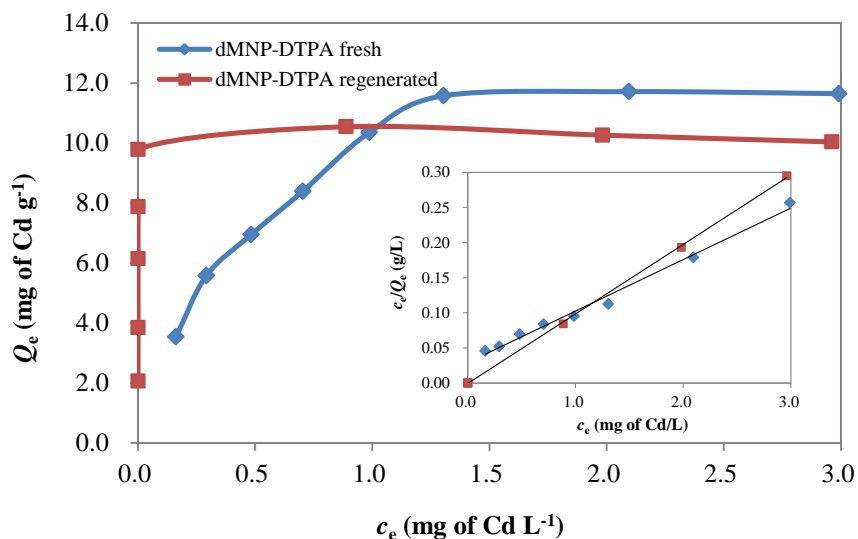
cycles.



**Figure 4.10** Equilibrium sorption isotherm of Cd(II) ions on dMNP-DTPA (pH 5.0 acetate buffer, 25 $^o$C). The inset illustrates the linear dependence of $c_e/Q_e$ on $c_e$.
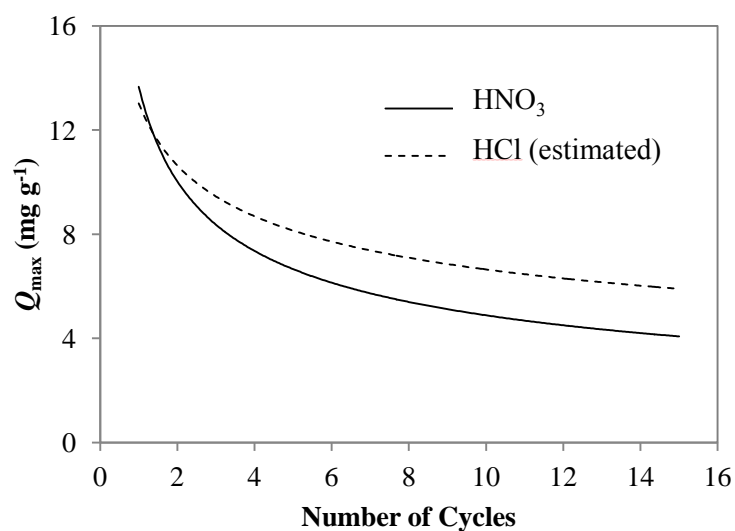


**Figure 4.11** Sorption capacity decay for dMNP-DTPA during the 15 sorption/desorption cycles.

The effect of DW and different concentration of HCl (0.05-1.0 M) on the desorption rate of Cd(II) from its loaded dMNP-DTPA nanosorbents were shown in Figure 4.12. This study was important because it helped elucidate the optimum concentration of the stripping agent to be applied during the stripping process. As observed, DW had very little stripping power, and there was no significant difference in desorption effectiveness among different concentrations of HCl. From the safety point of view, a lower acid concentration should be chosen, which will also cause less environmental issue during further metal treatment or disposal.
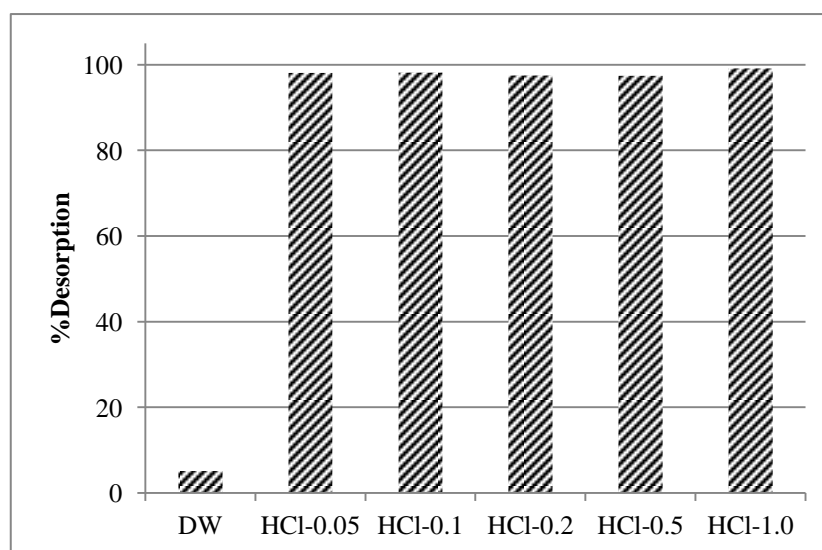


**Figure 4.12** Effect of HCl concentration on desorption

**4.4 Summary**

The dMNP-DTPA nanosorbents investigated in this study showed good potential for the removal of Cd(II) from contaminated water. The sorption equilibrium reached after 30 min of contact time. The sorption process was best described by the pseudo-second-order kinetics model, although intra-particle diffusion may also exist but not as a controlling factor.

The sorption isotherm was well fit by the Langmuir equation. Thermodynamic study suggested the endothermic process as increase in percentage removal of Cd(II) with temperature. The dMNP-DTPA nanosorbents remained the thermal stability with a 32 K of temperature increase. Thermodynamic parameters also indicated a spontaneous sorption process, a dissociative mechanism. The Cd(II) sorption on dMNP-DTPA was hightly reversible so that desorption could be achieved using acid washing to protonate the chelating functional groups of DTPA at low pH. The results from this study demonstrated that over 95% of absorbed Cd(II) ions were back-extracted to the stripping agent solution in 2 min. Despite the loss of DTPA during the stripping process, the dMNP-DTPA magnetic nanosorbents could maintain its high sorption efficiency and have an excellent reusability for more than 15 sorption/desorption cycles.

**Chapter 5: Lanthanide Removal Characteristics from Aqueous Solution by DTPA-Functionalized Magnetic Nanosorbents**

**5.1 Introduction**

Dissolved used nuclear fuel mixtures contain U, Pu, trivalent minor actinides and lanthanides and other fission products, covering a total of about 1/3 of the periodic table. The lanthanides plus yttrium represent about 40% of the mass of the fission products.[157] It is widely noted that in a given oxidation state, actinides and lanthanides behave similarly. Both of them have the most common oxidation state of +3 in aqueous solutions, and their chemistry is largely determined by the ionic radius, which decreases steadily across the series. However, all the actinides are radioactive while all the lanthanides (except promethium) are non-radioactive. Therefore, in this study, the trivalent lanthanides were chosen as the non-radioactive surrogates to help us to obtain some fundamental understanding on the actinide separation without generating any radioactive waste and safety concern.

The lanthanide (Ln) series from lanthanum through lutetium, along with the chemically similar elements scandium and yttrium, are collectively known as the rare earth elements (REEs). During the last few decades, owing to their unique electronic, magnetic, optical, and catalytic properties, REEs have been increasingly used in renewable energy and energy-efficient technologies, from electric car batteries and solar panels to high-performance magnets.[158,159] Clean energy development recently will further boost the demand for such technological materials. China now is the world's dominant producer of REEs, accounting for more than 95% of global REE production.[160] Because of such a quasi-monopoly on production, the REE export reduction introduced by China in 2009 caused

anxiety among many world economies.[161] Over the past 15 years, the United States has become 100% reliant on imports of REEs because of lower-cost operations.[162] Because they are essential to the clean energy economy and are at risk for supply disruptions, REEs are addressed as the key materials in the U.S. Department of Energy (DOE) Critical Materials Strategy.[163] Thus, the separating and recycling of REEs are of great importance to diversify the sources of REEs, to advance the efficient use of REEs recourses, and to manage the supply risk.[164,165]

The increased demand for lanthanides also leads to the increased public exposure to the lanthanides, both from various commercial products and from production waste streams. Increased mining activity has resulted in increased REE releases and mobility in environment.[166–168] In areas with high levels of REE, elevated levels are found in humans[168,169] and other organisms.[170] Recent toxicology studies of the rare earth chlorides have shown that they tend to have similar toxicities to the $CdCl_2$.[171] Therefore, removal of lanthanides from contaminated water is of great environmental and public health importance as well.

REEs extraction from aqueous solution is an efficient way to recover REEs from their wastes by dissolving them into a solution.[172] Current processes, such as solvent extraction, need repetitive process steps and involve great quantities of harmful or expensive reagents such as strong acids, organic solvents and extractants.[173–175] The development of new separation methods with high efficiency and low cost and that are more environmentally friendly will reduce costs and environmental impacts, allowing the REEs to be processed more widely and increasing the amounts that are recovered through recycling. Recently, magnetic sorbent nanotechnology has been developed to extract metallic cations

from aqueous solutions.[176–181] The concept introduces chelators onto the surface of magnetic

nanoparticles so that the magnetic sorbent complex is composed of a magnetic core and a

functionalized shell. Compared to traditional sorbent materials and separation methods such

as centrifugation and filtration, magnetic nanosorbents exhibit special superiority due to

convenient separation by an external magnetic field that requires less time, space,

maintenance, and operating cost.[12,13] In addition, the high surface area to volume ratio of

nanoparticles offers a larger loading density, which further contributes to the high sorption

efficiency.

In aqueous solution, the complexing reaction between Ln(III) and

diethylenetriamine-pentaacetic acid (DTPA), an octadentate aminopolycarboxylate

complexing agent, has been well understood.[182–186] However, there are few studies[117,187]

focusing on the Ln(III) complexation with immobilized DTPA, which contains at least one

fewer chelating carboxylic acid than DTPA. In addition, when attached to a surface, the

surface structure formed by the immobilized coordination groups can greatly affect the

sorption behavior toward different metal ions. In this paper, our lab-made magnetic

nanosorbents, double (silica and polyamine) coated magnetic nanoparticles coupled with

DTPA (dMNP-DTPA), were used to investigate the kinetics and selective recovery of

Ln(III) from aqueous solutions. Compared to other studies,[117,188] an excellent selectivity

between light Ln (La-Nd) and heavy Ln (Sm-Ho) were achieved using the dMNP-DTPA

nanosorbents. The similarity in physical and chemical properties of lanthanides make the

separation of individual elements very difficult. Therefore, in practical separation processes,

lanthanides are traditionally first separated into light-Ln and heavy-Ln groups so that further

separation and purification can be conducted.[175,189,190] Moreover, a high separation factor

will significantly increase the separation efficiency by reducing the number of repetitive

extraction process steps that are needed to isolate the individual Ln elements.

## 5.2 Batch Ln(III) sorption experiments

Batch sorption experiments were carried out using the dMNP-DTPA nanosorbents in

aqueous solution at a particle concentration of 500 mg L$^{-1}$. Ten lanthanides were chosen for

these studies to determine sorption trends across the lanthanide series: La$^{3+}$, Ce$^{3+}$, Pr$^{3+}$, Nd$^{3+}$,

Sm$^{3+}$, Eu$^{3+}$, Gd$^{3+}$, Tb$^{3+}$, Dy$^{3+}$ and Ho$^{3+}$. The solution was prepared by diluting trivalent

lanthanide nitrate stocks to 1.5 mg L$^{-1}$ at pH 3.0 with 0.1 M acetate buffer solutions at the

desired pH. After adding the dMNP-DTPA nanosorbents to the solution, the mixtures were

first sonicated for 5 seconds to disperse the particles and then agitated in a horizontal shaker

for desired period of time at room temperature. After sorption, the particles were separated

from the solution by magnetic field assisted decantation. The Ln(III) concentrations were

determined by inductively couple plasma mass spectrometry (ICP-MS). All batch

experiments were performed in triplicate, and the average values were reported.

## 5.3 Results and Discussion

## 5.3.1 pH effect

It is well-known that the solution pH is an important operational parameter that

controls the metal sorption process either by changing the overall surface charge of the

sorbent or by affecting the solution chemistry of metal ions (i.e. solubility, hydrolysis, redox

reactions, polymerization, and coordination). Figure 5.1 shows the sorption efficiency of the

Ln(III) by dMNP-DTPA under different pH conditions. For the total amount of all Ln(III)

adsorbed on dMNP-DTPA (inset of Figure 5.1), the Ln(III) sorption capacity increased with

increasing the solution pH from 1.0 to 4.0. This sorption behavior could be explained by the pH effect on the overall surface charge of dMNP-DTPA nanosorbents and proton-competitive sorption. According to the zeta potential measurement in Figure 3.10, when the pH value was low, the functional groups, such as carboxylic acid groups of DTPA, were more positively charged because protons ($H^+$) and metal ions competed for the same binding sites.[179] The proton-competitive sorption resulted in a higher electrostatic repulsion between the sorbent surface and Ln(III) ions. Therefore, dMNP-DTPA showed the lower sorption efficiency at lower pH values. When the solution pH increased, the sorbent surface became less positively charged, suggesting that the functional groups were more reactive to adsorb Ln(III). According to the acid dissociation constants of DTPA ($pK_a$: 1.9, 2.9, 4.4, 8.7, and 10.5),[133] when pH was below 1.0, the DTPA molecules were highly protonated, resulting in the very low sorption capacity at pH 1.0. However, there was a significant increase in sorption efficiency (~10 times in $K_d$ values) when pH values increased to 2.0. Such a low working pH value (to pH 2.0) was seldom reported in other similar studies in which the sorption efficiency of the proposed magnetic nanosorbent materials significantly decreased when the pH values were lower than 4.0, and there was almost no sorption when the pH values were lower than 3.0.[117]
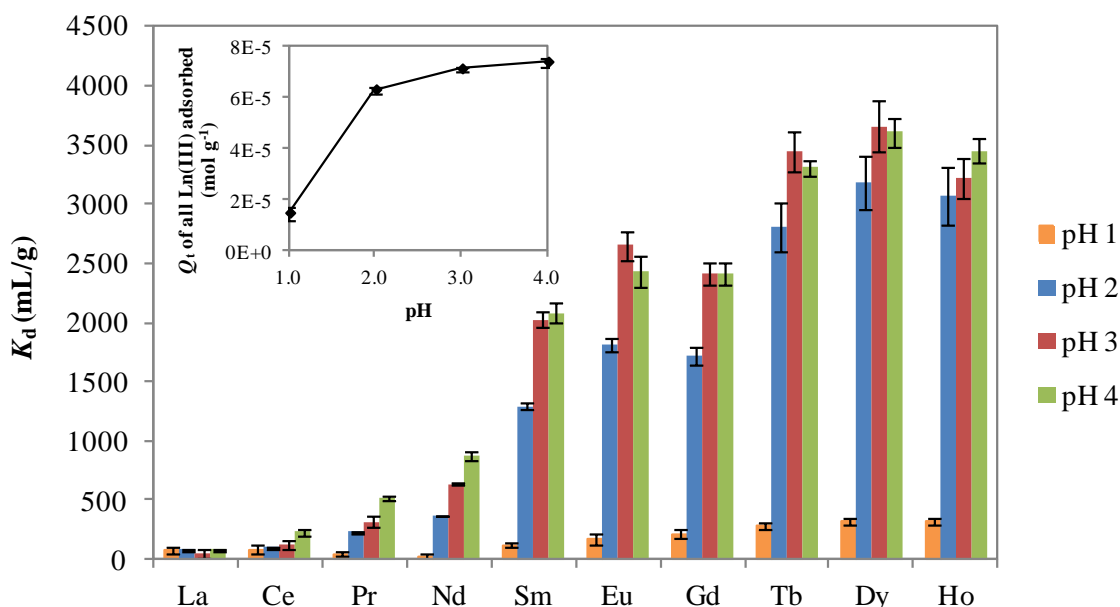
**Figure 5.1** pH effect on Ln(III) sorption on dMNP-DTPA after 180 min (Inset: pH effect on the total amount of all Ln(III) absorbed on dMNP-DTPA, and all date were obtained at equilibrium).

In addition, Figure 5.1 also showed the order of affinity to dMNP-DTPA across the Ln series. The Kd values increased as the atomic number increased, suggesting the nanosorbents have a higher sorption power to heavy Ln. The order of affinity among the metal ions perfectly followed the corresponding stability constants between Ln(III) and nonimmobilized DTPA as shown in Figure 5.6. This could originate from the lanthanide contraction, i.e. the greater than expected decrease in the ionic radii of the trivalent cations across the lanthanide series (Figure 5.2). This contraction is a consequence of the incomplete shielding of the outer electrons by the 4f subshell, causing the 5s and 5p electrons to experience a larger effective nuclear charge (nuclear attractive force). The smaller the ionic radii, the better the arms of DTPA can enfold the respective ion, resulting in the higher probability of complex formation and stronger coordination. Besides, it was easier for heavy

Ln with a smaller ionic radius to penetrate the (multi)layers on the dMNP-DTPA surface formed by the crosslinking reaction between DTPA and PA molecules. With five carboxylic groups, each DTPA can react with one, at least, or multiple amine groups on the imbedded PA; this crosslinking can form a relatively dense network between PA and DTPA. This surface structure effect contributed to the fact that more heavy-Ln ions than light-Ln ions were adsorbed on nanosorbents.[117] The loss of carboxylic acids (i.e. the chelating arms) of DTPA in the crosslinking also partially explained the difference between the DTPA density (~130 $\mu$mol g$^{-1}$) from the elemental analysis and the total maximum Ln(III) uptake (~75 $\mu$mol g$^{-1}$) from the batch sorption experiment as shown in the inset of Figure 5.1.
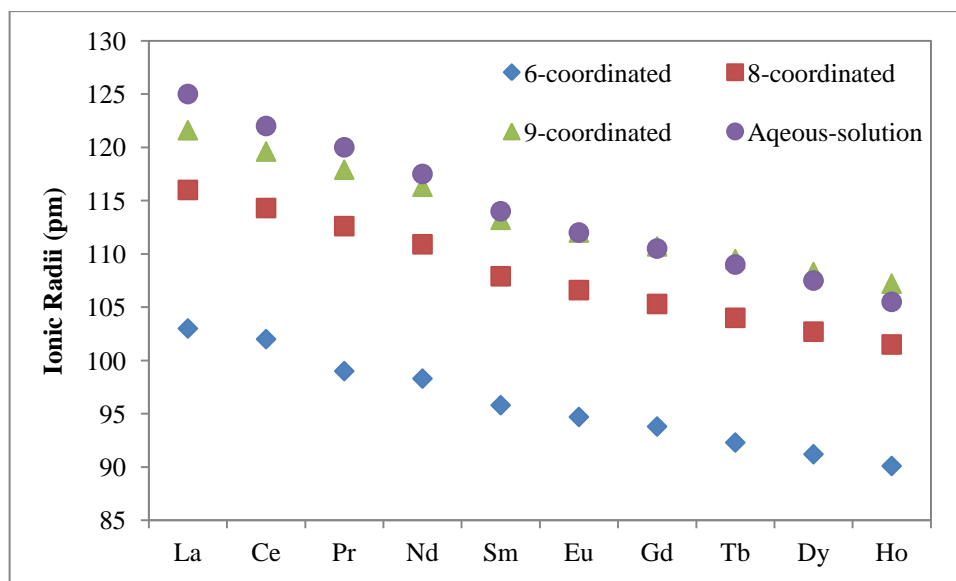


**Figure 5.2** Crystal ionic radii (pm) of Ln(III) for 6-fold, 8-fold and 9-fold coordination and ionic radii of Ln(III) in aqueous solution (data from ref.[191–193]).

### 5.3.2 Selective separation of Ln elements

It was observed that the selectivity between the adjacent Ln elements was low due to the similarity in ionic radius of these elements. For example, at pH 3.0, the separation factors for Pr/Ce, Gd/Eu, and Dy/Tb are 2.6, 0.9, and 1.1, respectively. However, excellent selectivity was observed between heavy Ln (Sm-Ho) and light Ln (La-Nd). As shown in Figure 5.3a, the separation of Ln elements were best carried out between pH 2.0 and 3.0 to ensure the extraction of Ln(III) with maximal selectivity between Sm-Ho and La-Nd groups. In addition, as shown in Figure 5.3b, the separation factor significantly increased as two Ln elements are farther away from each other in the element table, i.e. with more difference in ionic radius. The separation factors (SF) attained by dMNP-DTPA nanosorbents in the inset table in Figure 5.3b were significantly higher (up to 10 times) than that reported by other studies (2-5 by Fe$_3$O$_4$-TMS-EDTA[117] and 1-10 by Cyanex 925[188]). The improvement in separation factors clearly indicated that heavy Ln can be separated from light Ln in a fewer number of stages.
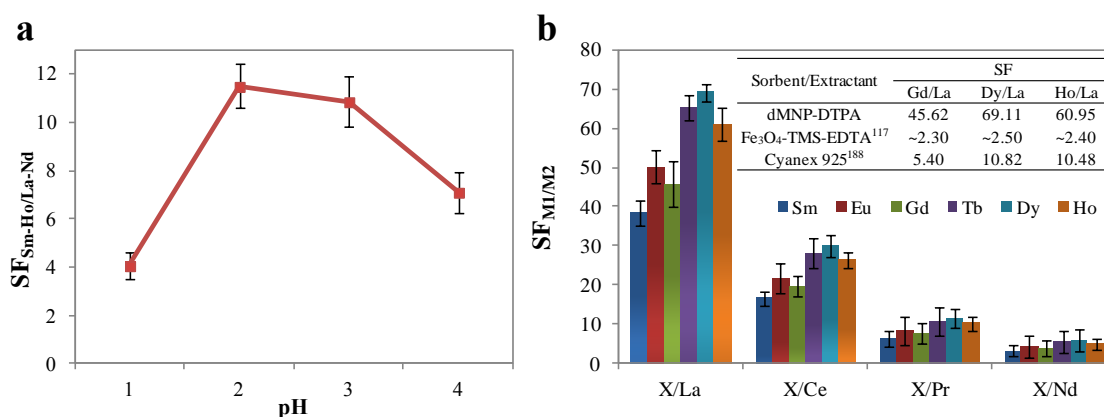


**Figure 5.3** Selectivity between heavy Ln and light Ln. a, Separation factor between heavy-Ln group (Sm-Ho) and light-Ln group (La-Nd) at different pH values. b, Separation factor of each heavy-Ln/light-Ln pair at pH 3.0.

### 5.3.3 Sorption kinetics

Fast sorption is one of the most important requirements for nanosobent material design to ensure efficiency and economy with existing processes. The kinetics of Ln(III) sorption were investigated by monitoring the amount of each Ln(III) adsorbed on dMNP-DTPA nanosorbents with time in pH 3.0 acetate buffer at room temperature (21 ℃ ±1 ℃) as shown in Figure 5.4. In general, the sorption kinetics included a rapid removal phase followed by a slower sorption phase until the equilibrium was established. Moreover, for light Ln (La-Nd), a clear desorption phenomenon was observed as the contact time increased. On the contrary, the adsorbed amount of heavy Ln (Sm-Ho) on the dMNP-DTPA nanosorbent surface increased with the contact time. However, the system reached the maximum uptake after approximately 30 min of mixing to give a total amount of Ln(III) ions adsorbed on the nanosorbent surface as $Q_t$ in mol g$^{-1}$. This may indicate, after 30 min, the amount of newly adsorbed heavy Ln (Sm-Ho) was equal to the amount of desorbed light Ln (La-Nd). In other words, the available active sorption sites on nanosorbents reached their saturation in 30 min; afterward, the free heavy-Ln ions in aqueous solution started to displace the adsorbed light Ln on the nanosorbent surface. Such displacement phenomena were also observed under other pH conditions (at pH 2.0 and pH 4.0 in Figure 5.5). The initial decrease in $Q_t$ in mol g$^{-1}$ for the total Ln between 10 and 15 min, as shown in Figure 5.4, was not observed under other pH conditions and was not fully understand. Additional study will be needed in the future.
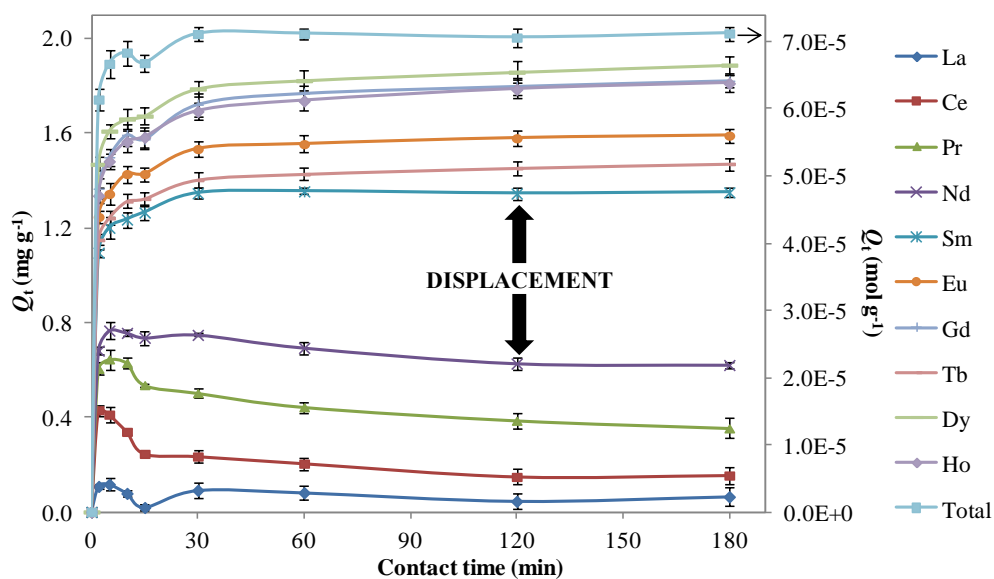
**Figure 5.4** The adsorbed amount (in mg $g^{-1}$) of each Ln(III) on dMNP-DTPA nanosorbents at different time (pH 3.0 acetate buffer, room temperature) and displacement phenomena between light Ln (La-Nd) and heavy Ln (Sm-Ho).
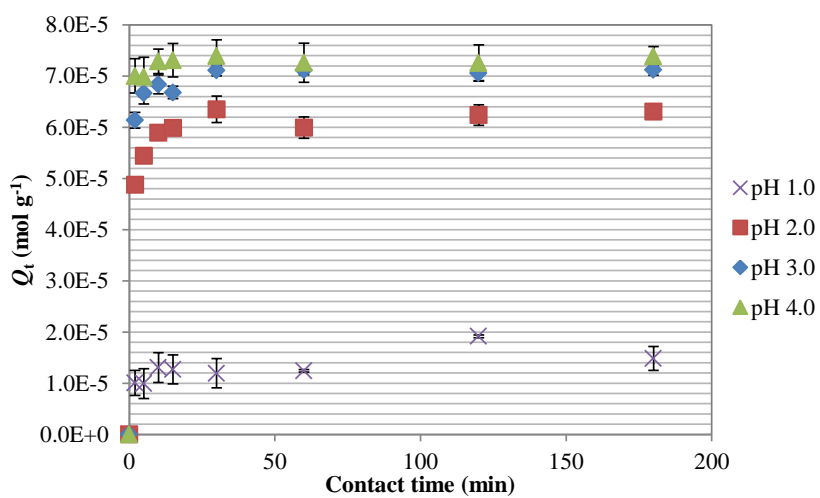


**Figure 5.5** The total adsorbed amount (in mol $g^{-1}$) of all Ln(III) on dMNP-DTPA nanosorbents at different time (pH 3.0 acetate buffer, room temperature).

In our previous kinetics study with a single metal element (Cd, Pb, or Ce), no

desorption behavior was observed within 24 h of contact time.[131,194] Because these kinetics study experiments were conducted with all the Ln(III) series coexisting and competing for the same binding sites, the displacement phenomena had to do with the affinity of each Ln(III) to DTPA on the nanosorbent surface, which correlated to the stability constants between the Ln(III) and DTPA, as depicted in Figure 5.6. Despite the different values for the respective Ln(III) under different experiment conditions, the data from the two previous studies[186,195] demonstrated that the DTPA-Ln complex stability increased steadily from La to Sm and then remained relatively constant for the heavy Ln in the series. Once attached to the particle surface, each immobilized DTPA molecule contains at least one fewer chelating carboxylic acid. Therefore, the stability constants for the EDTA-Ln complex were compared in Figure 5.6 as well. Different from the plateaus that was reached for the heavy Ln (Eu-Ho) with DTPA, the EDTA-Ln stability increased steadily across the whole series. A metal ion in aqueous solution is a cation of chemical formula $[M(H_2O)_n]^{Z+}$, and n is the solvation number. Ln aqua ions have a solvation number of 8 and 9 and the hydration/coordination number drops smoothly from 9 to 8 around gadolinium (in the middle of the series).[196] The metal chelate formation involves the replacement of water molecules by a chelator (in our case, the DTPA molecule). The change from increasing complex stability to flattening of the stability curve coincides with the point at which the hydration numbers of Ln aqua ions change from 9 to 8, suggesting that the flattening of the curve relates to the decreased entropic stabilization of the complexes between DTPA (fewer water molecules released by the hydrated cation and the free ligand on complex formation).[186] The metal complexation reactions for Ln(III) ions with DTPA have been reported to proceed as both the $\beta_{101}$ reaction and the $\beta_{111}$ reaction as shown in the following equations: [197]

$$Ln^{3+} + DTPA^{5-} \underset{}{\overset{\beta_{101}}{\rightleftharpoons}} [Ln\text{-}DTPA]^{2-}$$

$$Ln^{3+} + H^+ + DTPA^{5-} \underset{}{\overset{\beta_{111}}{\rightleftharpoons}} [Ln\text{-}HDTPA]^-$$
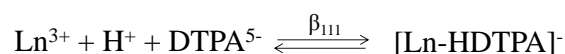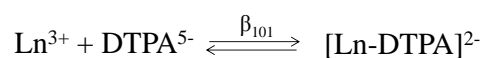
Given that $H_3DTPA^{2-}$ is the predominant free ligand species presenting in the pH range of 3.2-4.2, the reaction should be:

$$Ln^{3+} + H_3(DTPA)^{2-} \underset{k_{diss}}{\overset{k_{form}}{\rightleftharpoons}} [Ln\text{-}DTPA]^{2-} + 3H^+$$
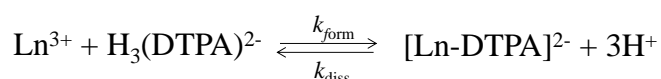
where $k_{form}$ and $k_{diss}$ are the rate constants for the complex formation and dissociation, respectively. In the beginning, abundant sorption sites provide nearly equal availabilities to all the Ln(III) ions. Therefore, the reaction mainly occurs to the right direction, forming Ln-DTPA complex as illustrated in Figure 5.7(a-b). When the sorption approaches saturation, the sorption sites become limited and complexation reactions for Ln(III) with DTPA reach equilibrium. At equilibrium, the Ln-DTPA complex formation and dissociation take place at the same time or rate. This is when the displacement happens. Heavy Ln with larger stability constants in solution have a higher affinity to DTPA. Their presence will break the equilibrium between DTPA and the light Ln with much smaller stability constants and displace them on the limited sorption sites, as illustrated in Figure 5.7(b-c), resulting in the increased $Q_t$ for the group of Sm-Ho and the decreased $Q_t$ for the group of La-Nd with time. The displacement phenomena further improved the separation factors between heavy Ln and light Ln.
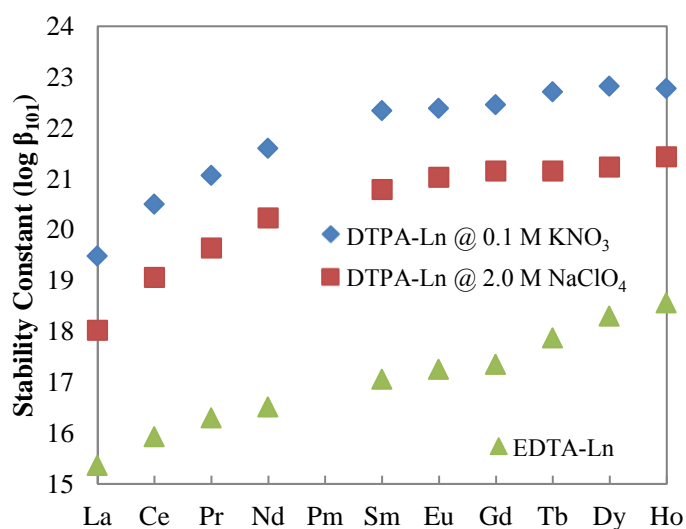
**Figure 5.6** Literature stability constants (log $\beta_{101}$) for the Ln(III) with non-immobilized DTPA (under different ionic strength solutions) and EDTA (data from ref.[186,195,198]).
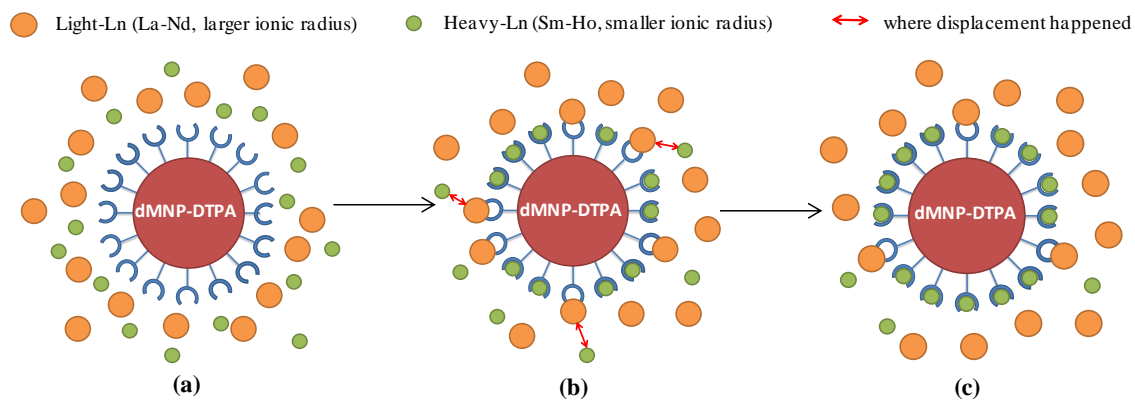


**Figure 5.7** Simple illustration of Ln(III) sorption and displacement between light Ln and heavy Ln: a. before sorption; b. initial sorption; c. after displacement.

## 5.3.4 Kinetic modeling of Ln(III) sorption process

In order to determine the controlling mechanism of the sorption process, different kinetic models were used to assess the experimental data at pH 3.0, including Lagergren

pseudo-first-order, pseudo-second-order, Elovich, intra-particle diffusion and liquid-film diffusion kinetic models. Pseudo-first-order equation, pseudo-second-order equation, and Elovich's equation all belong to sorption reaction models originating from chemical reaction kinetics. They are based on the whole process of sorption without considering the diffusion steps. However, the solute transport from the solution phase to the sorbent particles occurs in three consecutive steps: (1) diffusion across the liquid film surrounding the adsorbent particles, i.e., external diffusion or film diffusion; (2) diffusion in the liquid contained in the pores and/or along the pore walls, which is so-called internal diffusion or intra-particle diffusion; and (3) sorption and desorption between the sorbate and active sites, i.e., mass action. For physical sorption, mass action is a very rapid process and can be negligible for kinetic study. Thus, the kinetic process of sorption is always controlled by liquid film diffusion or intra-particle diffusion, i.e., one of the processes should be the rate-limiting step.[199] In general, a sorption process is diffusion controlled if the sorption rate is dependent on the rate at which components diffuse toward one another.[9]

The corresponding equations[200–204] for each kinetic model are presented in Table 5.1, where $Q_t$ and $Q_e$ is the amount of metal ions adsorbed at time $t$ and equilibrium (e) in mg g$^{-1}$, respectively, and $k$ is the rate constant. In Elovich model, $\alpha$ (in g mg$^{-1}$ min$^{-2}$) represents the initial sorption rate and $\beta$ (in mg g$^{-1}$ min$^{-1}$) is the desorption constant.

**Table 5.1** Mathematical equations for Ln(III) sorption kinetics.

| # | Kinetic model | Linear equation | Plot |
|---|---|---|---|
| I | Lagergren pseudo-first-order | $\ln(Q_e - Q_t) = \ln Q_e - k_1 t$ | $\ln(Q_e - Q_t)$ vs. $t$ |
| II | Pseudo-second-order | $\dfrac{t}{Q_t} = \dfrac{1}{k_2 Q_e^2} + \dfrac{1}{Q_e} t$ | $t/Q_t$ vs. $t$ |
| III | Elovich | $Q_t = b \ln(ab) + b \ln t$ | $Q_t$ vs. $\ln t$ |
| IV | Intra-particle diffusion | $Q_t = k_{id} t^{1/2} + C$ | $Q_t$ vs. $t^{1/2}$ |
| V | Liquid−film diffusion | $\ln(1 - \dfrac{Q_t}{Q_e}) = -k_{fd} t$ | $\ln(1 - \dfrac{Q_t}{Q_e})$ vs. $t$ |

*I. Pseudo-first-order kinetics model*: Becasue the $Q_t$ values decreased with time for the light Ln, the first-order mechanism suffered from inadequacies when applied to La-Nd sorption. Therefore, only sorption data for Sm-Ho were analysed using this model. The $Q_e$ (calc.) and $k_1$ values presented in Table 5.2 were calculated from the intercepts and slopes of Figure 5.8. The correlation coefficients ($R^2$) were in the range of 0.6544-0.7327, and the experimental $Q_e$ values significantly differed from the corresponding calculated $Q_e$ values, indicating that the binding kinetics is not the pseudo-first-order.

**Figure 5.8** Lagergren plots for sorption of Ln(III) ions on dMNP-DTPA (pH 3.0 acetate buffer, room temperature).

**Table 5.2** Pseudo-first-order kinetic parameters for Ln(III) sorption on dMNP-DTPA.

| Element | $Q_e$ (exp.) (mg L$^{-1}$) | $Q_e$ (calc.) (mg L$^{-1}$) | $k_1$ (min$^{-1}$) | $R^2$ |
|---|---|---|---|---|
| La | 0.091 | NA | NA | NA |
| Ce | 0.234 | NA | NA | NA |
| Pr | 0.502 | NA | NA | NA |
| Nd | 0.748 | NA | NA | NA |
| Sm | 1.346 | 0.564 | 0.152 | 0.6966 |
| Eu | 1.533 | 0.645 | 0.150 | 0.6867 |
| Gd | 1.721 | 0.737 | 0.139 | 0.6544 |
| Tb | 1.402 | 0.589 | 0.161 | 0.7195 |
| Dy | 1.787 | 0.708 | 0.149 | 0.6580 |
| Ho | 1.692 | 0.759 | 0.155 | 0.7327 |

*II. Pseudo-second-order kinetics model*: Figure 5.9 shows the plots of $t/Q_t$ vs. $t$ for all lanthanides under study and, with the exception of La, all data resulted in straight lines with an $R^2 > 0.99$. A relatively large deviation of La data resulted from the poor sorption rate

of La that were only 1.77-4.62% within the time period under examination. The calculated

$Q_e$ values were in excellent agreement with the experimental data (Table 5.3). Therefore, the

Ln(III) sorption reaction could be interpreted more favorably by pseudo-second-order

kinetic modeling. These results suggest that the uptake of Ln(III) ions on the surface of

dMNP-DTPA is a chemisorptions based process, involving valence forces through sharing

or exchange of electrons between sorbent and sorbate.[201] In other words, Ln(III) sorption on

dMNP-DTPA occurred either via chemical sorption by forming covalent bonds or via ion

exchange by forming ionic bonds.
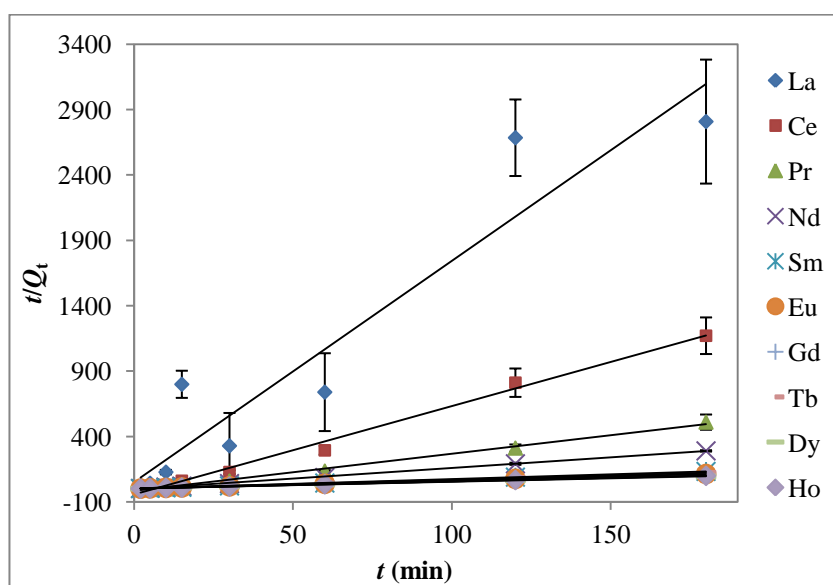


**Figure 5.9** Pseudo-second-order plots for sorption of Ln(III) ions on dMNP-DTPA (pH 3.0 acetate buffer, room temperature).

**Table 5.3** Pseudo-second-order kinetic parameters for Ln(III) sorption on dMNP-DTPA.

| Element | $Q_e$ (exp.) (mg $L^{-1}$) | $Q_e$ (calc.) (mg $L^{-1}$) | $k_2$ (g $mg^{-1}$ $min^{-1}$) | $R^2$ |
|---|---|---|---|---|
| La | 0.091 | 0.059 | 5.561 | 0.9060 |
| Ce | 0.234 | 0.148 | -1.085 | 0.9932 |
| Pr | 0.502 | 0.353 | -0.524 | 0.9953 |
| Nd | 0.748 | 0.616 | -0.627 | 0.9988 |
| Sm | 1.346 | 1.355 | 1.214 | 1 |
| Eu | 1.533 | 1.597 | 0.513 | 1 |
| Gd | 1.721 | 1.831 | 0.337 | 0.9999 |
| Tb | 1.402 | 1.475 | 0.508 | 0.9999 |
| Dy | 1.787 | 1.894 | 0.355 | 0.9999 |
| Ho | 1.692 | 1.820 | 0.309 | 0.9999 |

*III. Elovich kinetics model*: The Elovich equation has been widely used to interpret the sorption kinetics and successfully describe the predominantly chemical sorption on highly heterogeneous sorbents.[205] The relationships between $Q_t$ and $\ln t$ for Ln(III) sorption on dMNP-DTPA were illustrated in Figure 5.10. For La-Nd, the negative $\alpha$ and $\beta$ values in Table 5.4 were the results of the desorption of corresponding Ln(III) ions from dMNP-DTPA; and $R^2$ values were very low for La and Nd cases. Therefore, the sorption system for La-Nd might not follow the Elovich model. For the other cases, the Elovich model described the sorption process better than the pseudo-first-order kinetics model, but not as well as the pseudo-second-order kinetics model. The large values of $\alpha$ represented the initial rate of sorption that depend significantly on the amount of sorbent available in the working system. The sorption rate could be enhanced many times by increasing the applied amount of nanosorbents due to providing a large surface area for solute-sorbent interactions. Although Elovich equation was useful in describing the chemical sorption on heterogeneous systems, no definite mechanism for Ln(III)-nanosorbents interaction could be suggested.

Thus, it was predicted that Ln(III) (especially Sm-Ho) ions were held strongly to the

nanosorbent surface by chemisorptive bonds.[205]



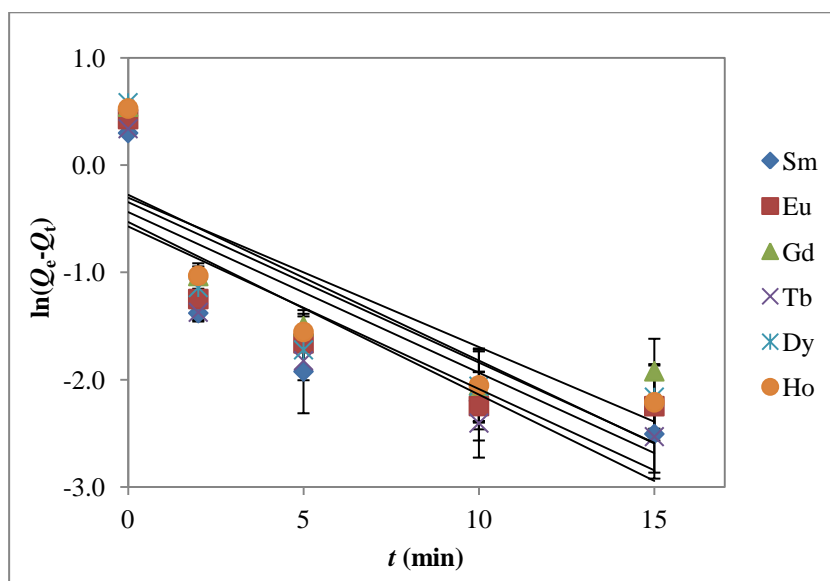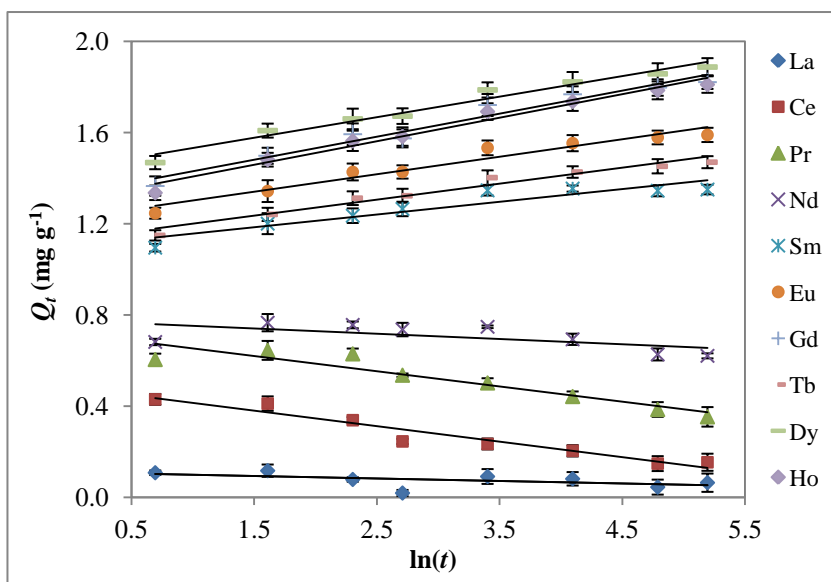**Figure 5.10** Elovich plots for sorption of Ln(III) ions on dMNP-DTPA (pH 3.0 acetate buffer, room temperature).

**Table 5.4** Elovich kinetic parameters for Ln(III) sorption on dMNP-DTPA.

| *Element* | $Q_e$ *(exp.) (mg L$^{-1}$)* | $Q_e$ *(calc.) (mg L$^{-1}$)* | *α (g mg$^{-1}$ min$^{-2}$)* | *β (mg g$^{-1}$ min$^{-1}$)* | *R$^2$* |
|---|---|---|---|---|---|
| La | 0.091 | 0.072 | -3.90E-03 | -0.011 | 0.2718 |
| Ce | 0.234 | 0.250 | -1.25E-02 | -0.068 | 0.9361 |
| Pr | 0.502 | 0.492 | -3.18E-04 | -0.067 | 0.8787 |
| Nd | 0.748 | 0.696 | -1.16E-13 | -0.023 | 0.395 |
| Sm | 1.346 | 1.291 | 6.63E+09 | 0.056 | 0.8665 |
| Eu | 1.533 | 1.486 | 1.09E+08 | 0.077 | 0.9486 |
| Gd | 1.721 | 1.673 | 4.97E+06 | 0.101 | 0.9607 |
| Tb | 1.402 | 1.368 | 1.34E+08 | 0.070 | 0.9622 |
| Dy | 1.787 | 1.748 | 9.60E+07 | 0.090 | 0.9691 |
| Ho | 1.692 | 1.655 | 2.96E+06 | 0.103 | 0.9749 |

*IV. Intra-particle diffusion model*: Intra-particle diffusion is a process involving solute transport from the bulk solution to the solid phase. In a well-stirred batch sorption system, the intra-particle diffusion model has been used to describe the sorption process occurring on a porous sorbent.[205–207] In this model, $k_{id}$ (in mg g$^{-1}$ min$^{-1/2}$) is the intra-particle diffusion rate constant and $C$ (in mg g$^{-1}$) is a constant indicating the thickness of the boundary layer. Generally, the higher the $C$ value, the greater the boundary layer effect is. If the plot of $Q_t$ vs. $t^{1/2}$ exhibits a linear relationship, the sorption process is controlled by intra-particle diffusion only. However, if the data give multi-linear plots as illustrated in Figure 5.11, then two or more steps influence the sorption process: the first straight portion represents macro-pore diffusion and the second depicts micro-pore diffusion.[205,207] The slope ($k_{id}$) of these plots is defined as a rate parameter, characteristic of the rate of sorption in the region where intra-particle diffusion is rate controlling. For La-Nd, the $k_{id}$ values (Table 5.5) for both portions were negative as a result of the displacement effect between light and heavy Ln ions. For Sm-Ho, the $k_{id}$ values for the first linear portion were at least 5 times larger than the $k_{id}$ values for the second portion. For both portions, the $k_{id}$ values increased with the atomic number, which might be due to the fact that the ionic radius decreased with the atomic number, and smaller ions were easier to diffuse. Moreover, the plots for the initial period showed curvature (lower $R^2$ values), usually attributed to boundary layer diffusion effects or external mass transfer effects. The intercepts ($C$ values) provide the measure of the boundary layer thickness. If the $C$ values are not zero, the pore diffusion is not the sole rate-controlling step. Significantly, the $C$ values from both portions were not zero, indicating that intra-particle diffusion might not be the controlling factor in determining the kinetics of the Ln(III) sorption process.[205]
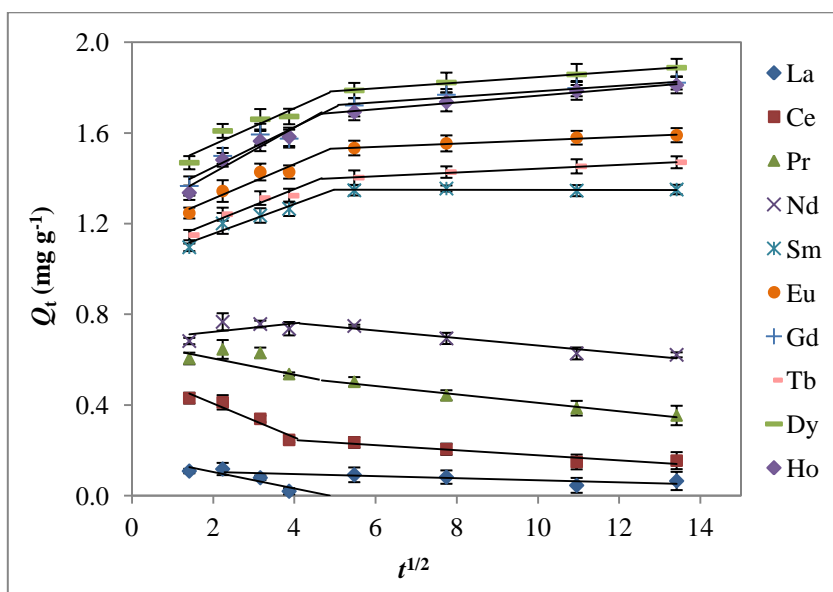
**Figure 5.11** Intra-particle diffusion plots for sorption of Ln(III) ions on dMNP-DTPA (pH 3.0 acetate buffer, room temperature).

**Table 5.5** Intra-particle diffusion kinetic parameters for Ln(III) sorption on dMNP-DTPA.

| Time Range | 0-15 min | | | 30-180 min | | |
|---|---|---|---|---|---|---|
| Element | $k_{id}$ | C | $R^2$ | $k_{id}$ | C | $R^2$ |
| La | -0.036 | 0.177 | 0.7736 | -0.005 | 0.113 | 0.5929 |
| Ce | -0.075 | 0.556 | 0.9183 | -0.011 | 0.289 | 0.8820 |
| Pr | -0.026 | 0.671 | 0.3221 | -0.019 | 0.595 | 0.9810 |
| Nd | 0.019 | 0.684 | 0.2871 | -0.017 | 0.828 | 0.9296 |
| Sm | 0.066 | 1.023 | 0.9061 | 0.000 | 1.349 | 0.0011 |
| Eu | 0.077 | 1.157 | 0.9073 | 0.007 | 1.496 | 0.9840 |
| Gd | 0.088 | 1.272 | 0.8409 | 0.012 | 1.663 | 0.9615 |
| Tb | 0.072 | 1.064 | 0.9296 | 0.008 | 1.359 | 0.9929 |
| Dy | 0.080 | 1.387 | 0.8537 | 0.012 | 1.722 | 0.9957 |
| Ho | 0.100 | 1.224 | 0.9107 | 0.015 | 1.615 | 0.9859 |

*V. Liquid-film diffusion model*: A linear plot of $\ln(1 - \frac{Q_t}{Q_e})$ versus t with a zero intercept would suggest that the kinetics of the sorption process is controlled by diffusion

through the liquid film surrounding the solid sorbents. Due to the decrease in some $Q_t$ values with time, the liquid film diffusion model suffered from the same inadequacies when applied to La-Nd sorption as that in the pseudo-first-order model. Therefore, only experimental data for Sm-Ho were plotted and calculated accordingly as shown in Figure 5.12 and

Table 5.6. The $R^2$ values were in the range of 0.6544-0.7327, indicating the significant curvature of the plots. The non-zero intercepts showed that the predictions of the liquid film diffusion model would have very limited applicability in Ln(III) sorption on dMNP-DTPA.
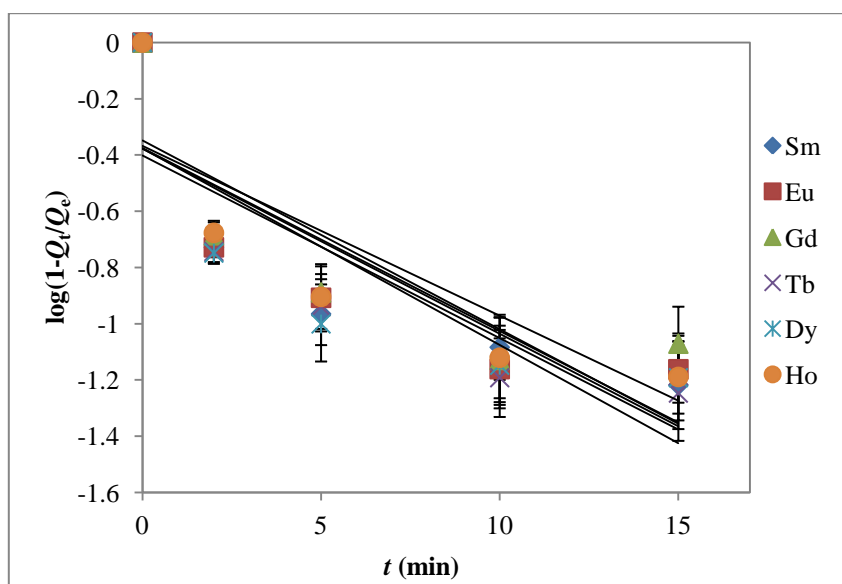


**Figure 5.12** Liquid film diffusion plots for sorption of Ln(III) ions on dMNP-DTPA (pH 3.0 acetate buffer, room temperature).

**Table 5.6** Liquid film diffusion kinetic parameters for Ln(III) sorption on dMNP-DTPA.

| Element | Qe (exp.) (mg L$^{-1}$) | Qe (calc.) (mg L$^{-1}$) | K$_{fd}$ (min$^{-1}$) | R$^2$ |
|---------|---------|---------|---------|---------|
| La | 0.091 | NA | NA | NA |
| Ce | 0.234 | NA | NA | NA |
| Pr | 0.502 | NA | NA | NA |
| Nd | 0.748 | NA | NA | NA |
| Sm | 1.346 | 1.332 | 0.152 | 0.6966 |
| Eu | 1.533 | 1.516 | 0.150 | 0.6867 |
| Gd | 1.721 | 1.695 | 0.139 | 0.6544 |
| Tb | 1.402 | 1.391 | 0.161 | 0.7195 |
| Dy | 1.787 | 1.767 | 0.149 | 0.6580 |
| Ho | 1.692 | 1.676 | 0.155 | 0.7327 |

## 5.4 Conclusions

As a simple, fast, and versatile technique, dMNP-DTPA nanosorbents showed a promising application for highly selective lanthanide extraction. The separation factor between heavy-Ln and light-Ln groups reached its maximum when the pH value was 2.0-3.0 and up to 10 times larger than other methods. The sorption process reached the maximum uptake after 30 min of contact. Displacement phenomena were subsequently observed between the heavy and light Ln ions that were coexisting in solution, causing the increase in sorption capacity of the heavy Ln on dMNP-DTPA surface with time. Further investigation on one representative element from heavy and light Ln groups is needed to better understand the displacement phenomena and compare the different sorption behavior between the heavy and light Ln. The order of affinity of Ln(III) to dMNP-DTPA perfectly followed the corresponding stability constants between Ln(III) and nonimmobilized DTPA. Displacement phenomena and lanthanide contraction, as well as the dense multilayer surface structure of dMNP-DTPA significantly improved the separation factors of heavy-Ln/light-Ln pairs. The

kinetics of Ln(III) interaction with our lab-made dMNP-DTPA nanosorbents does not appear to be straightforward. The pseudo-second-order (i.e., chemisorption) mechanism is the more reliable sorption kinetics model and intra-particle diffusion may be participating in ruling the diffusion of Ln(III) ions.

**Chapter 6: Computational Study on Continuous Magnetic Separation System Design**

**6.1 Introduction**

To design effective and efficient magnetic separation system for metal extraction from wastewater is challenging as it involves multi-phase flow with phase interactions, nonlinear two-way coupling between the fluid and MNPs, unsteady and turbulent effects, and various types of forces acting on the MNPs. Most previous studies either ignored these important physics or used simple analytical models or empirical formulas with inaccurate assumptions and approximations to analyse the separation process. As a result, these methods cannot be used to predict solid particle distributions, and information on the removal efficiency cannot be obtained. Additionally, these methods cannot be applied to design the whole separation system that consists of additional pipes, pipe fittings, and pumps, etc.

This study uses both experimental measurements and computational simulations for designing magnetic separation system. Experimental data are used to validate the simulation tools. The simulation tools, once validated, can be used to perform parametric studies and optimization. The simulation tool to be applied in this study is Computational Fluid Dynamics (CFD), which has been proved to be a promising tool for simulation based designs during the past decades and broadly influenced all science and engineering disciplines. CFD will not completely replace the analytical methods and experimental measurements but provide the 3$^{rd}$ approach to interpret flow physics, design fluid systems, and help understand physical fluid phenomena that are difficult or impossible for experiments and theory.

Recently, the use of CFD as a tool in wastewater treatment has been significantly increased. Mollinedo-Ponce-de-Leốn et al.[208] used a CFD model to design an electrochemical reactor used to remove high concentration of hexavalent chromium (Cr (VI)) that is a hazardous substance found in wastewater generated by the electroplating industry. The CFD model was used to evaluate effect of the angular velocity of a rotating electrodes array that is a crucial factor for the reactor performance. Stamou et al.[209] used a CFD model to design the secondary settling tanks of Psyttalia Wastewater Treatment Plant in Athens, Europe's largest sewage treatment facility, including examination of the performance of the tanks for various design conditions. Xu et al.[210] used CFD simulations prior to build the lab-scale equipment to save time, economic cost, and manpower for a new type oxidation ditch based on airlift circulation. The accuracy of CFD simulations for wastewater treatment can be ensured with validation using experimental data. Other examples are provided by the following references.[211–214] Once a CFD model is validated, it can be used to optimize a wastewater separation system using parametric studies or optimization theory.

More recently, CFD has been used in simulation of magnetic separations in fluid flow for simple geometries. Khashan et al.[215–217] used CFD to simulate the separation of labelled biospecies from a native fluid flowing through a planar two-dimensional microchannel under a magnetic field. The magnetic–fluidic interactions and interplay between the magnetophoretic mass transfer and molecular diffusion for different throughputs are analyzed. It was shown that the axial magnetic forces, created from a dipole-like magnetic field, is playing a major role in the vortex formation, and this complements the downward vertical force in confining the particles to a small region near

the point with the highest magnetic strength. These studies were restricted to low speed (laminar) flows and didn't consider the effect of turbulence, which is important for developing real-scale dynamic separation system for wastewater. The CFD models in this study are not validated using experimental data.

In this study, a new separation device that can be operated under continuous flow condition has been proposed. To better understand the hydrodynamic behavior of magnetic nanosorbent materials in a continuous flow system, a general framework to conduct CFD for both static and dynamic magnetic separation simulations have been developed and validated using previous studies and/or experimental measurements. The framework was built on top of the most popular commercial CFD software platform ANSYS FLUENT 14.0 using an Eulerian approach, which can be used for both two-phase (fluid and magnetic particles) and multiphase (fluid, magnetic particles, and non-magnetic particles). The framework includes user defined functions (UDFs) written in $C^{++}$ that is used to modify the existing governing equations, detailed step-by-step instructions to set up and run the simulations, and guidelines to set up all environmental variables. The framework can be used to design future dynamic separation system, analyze fluid and particle interactions, and elucidate physics for magnetic separations.

## 6.2 Continuous magnetic separation system

Currently one of the important problems that hinder the practical applications of magnetic separation in industries is the continuous removal of the magnetically captured particles from the mixture flow. It is considered that the continuous separation process can be achieved by properly manipulating the direction and magnitude of magnetic force and

drag force acting on the magnetic particles. Therefore, the open gradient magnetic

separation channel using quadrupole magnetic field was proposed in this study. Quadrupole

magnet creates a magnetic field whose magnitude grows rapidly with the radial distance

from its longitudinal axis. As shown in Figure 6.1, in the separation channel, the magnetic

field gradient only exits in $r$-axis and is normal to the flow of the particles, so that during the

movement of the magnetic particles from the inlet to the outlet, the magnetic force acting on

the particle drives the particle moving perpendicular to the flow and reach to particle outlet,

while the non-magnetic liquid mostly goes straight and leaves the channel from water outlet.
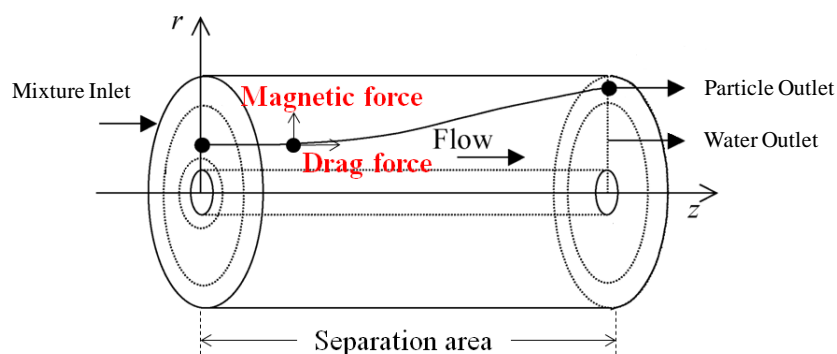


**Figure 6.1** The magnetic separation device with a quadrupole magnetic field.

The schematic design of a separation system is shown in Figure 6.2. It consists of a

cylindrical glass tube with an inlet and two separated outlets, one for concentrated particle

slurry and one for water, a quadrupole magnetic system required to produce a magnetic field

only in the radial direction, a mini pump with a variable rate flow meter to pump and control

the flow rate of feeding solution, a mixing system to maintain the even dispersion of particle

in initial solution, and a piston reciprocal pump to help removing the particle slurry from

particle outlet. A known volume and concentration of colloidal solution will be allowed to

flow through the quadrupole magnetic field in the glass tube. The magnetic force acting on the particle will drive the particle moving perpendicular to the flow and reach to particle outlet, while the non-magnetic liquid mostly goes straight and leaves the channel from water outlet. The difference in particle concentration between solution injected in the inlet and solution extracted from the water outlet will give an estimate of the magnetic separation efficiency.

In the presence of the quadrupole magnetic field, the fundamental forces acting on a MNP in solution are magnetic force ($\vec{F}_m$) and hydrodynamic drag force ($\vec{F}_d$). The gravitational force is only considered for large and dense particles. In our case, the gravity is weak so that it is neglected along with buoyant force. The theoretical calculations predicated that the transport of particles with diameter less than 40 nm is dominated by Brownian motion. But in many applications, the diffusive force from Brownian motion can be neglected if the applied forces (magnetic force, for instance) on the particle dominate. Therefore, Brown motion is neglected for MNPs greater than 40 nm. In addition, since we consider MNPs have a low concentration in the system, the interparticle effects (magnetic dipole-dipole interaction) are neglected as well. According to Eqn. 1-1 and Eqn. 1-2, the $\vec{F}_m$ is a function of particle size and magnetic susceptibility, and the $\vec{F}_d$ is a function of particle radius and flow velocity. Therefore, the trajectory of magnetic particles depends on the particle size, magnetic susceptibility, and flow velocity, which was also reported by Fukui *et al.*[218,219] With the help of CFD simulations, the effect of those parameters on the magnetic separation efficiency can be easily demonstrated and optimized.
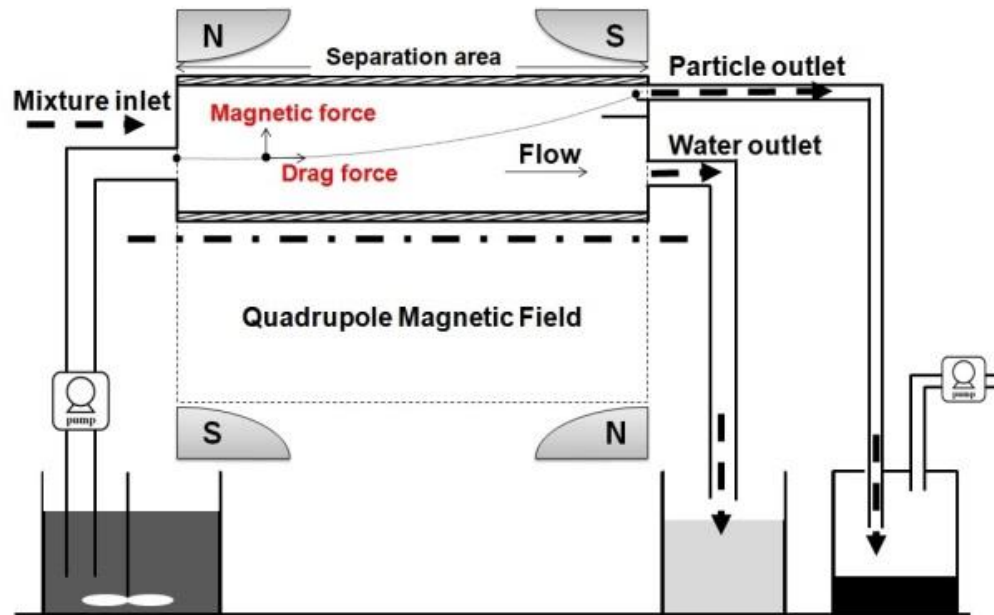
**Figure 6.2** Schematic diagram of the experimental set up of continuous flow separation system with a quadrupole magnetic field.



*(a)* $r_p = 5$ μm,     *(b)* $r_p = 5$ μm,     *(c)* $r_p = 5$ μm,

$\chi_p = 10^{-3}$           $\chi_p = 10^{-2}$           $\chi_p = 10^{-1}$

$v = 0.1$ m/s       $v = 0.1$ m/s       $v = 0.1$ m/s
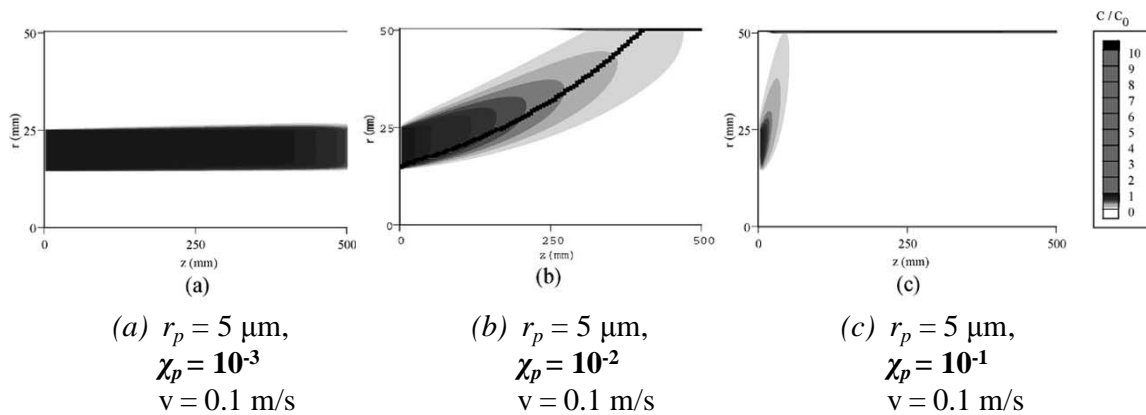
**Figure 6.3** Particle concentration profiles in a quadrupole magnetic system with different conditions.

**6.3 Verification of framework in FLUENT**

**6.3.1 2D unsteady two-phase flow[217]**

    (1) Geometry and flow conditions

A mixture of liquid water loaded with magnetic particles (volume fraction of 0.03 at inlet) flows through two parallel plates. The channel has a height $h = 1$ mm and a length $L = 1$ cm. The domain is meshed with a structured mesh consisting of 64,000 hexahedral cells. The granular particles have a diameter of 0.5 μm and magnetic volumetric susceptibility of 1. An unsteady state simulation was carried out for this laminar, incompressible fluid with a fully developed velocity at the inlet (mean velocity of 100 μm/s). A zero gauge pressure was specified at the outlet. The magnetic source is located at 1mm below the midway-point of the lower plate (reference point), and generated a maximum induction equal to 10 mT at that point.

    (2) Key governing equations

In addition to the Navier-Stokes Equations governing the Newtonian fluid flow, the governing equation for the magnetic force is given by

$$\vec{F}_{mag} = \frac{1}{2}\mu_0 \chi V_P \nabla \vec{H}^2 \qquad (6\text{-}1)$$

where, $\mu_0$ is the magnetic permeability, $\chi$ is the magnetic susceptibility, and $V_P$ is the volume of the magnetic particles. Since the CFD model utilized in FLUENT is an Eulerian model rather than a Lagrangian model, $V_p$ is replaced by the sum of volume fractions ($\alpha_s$) of the particles to form Eqn. 6-2. This source term was added to the momentum equation for the particles through the compiled UDF.

$$\vec{F}_{mag} = \frac{1}{2}\mu_0 \chi \alpha_s \nabla \vec{H}^2 \qquad (6\text{-}2)$$

(3) Selected Results

By hooking the compiled UDF into the FLUENT solver, the same magnetic field distribution was obtained as that was reported by Khashan *et al.*[217] As shown in Figure 6.4, the magnetic field and the gradient are highest near the reference point, where the solid phase experiences the maximum magnetic force. The magnetic force is attracting the incoming particles downward toward the reference point. It is observed that maximum particle concentration (volume fraction) is located at the reference point (Figure 6.5). As time increases more particles are accumulated and concentrated near the reference point, and consequently, they behave as an obstacle in the flow. As a result, the flow separates and a vortex is formed at the downstream next to the region with the high concentrations. Similar results were also reported by Khashan *et al.*[217] The vortex formation can be also attributed to the adverse migration of particles as driven by the magnetic force in the opposite direction than the flow.
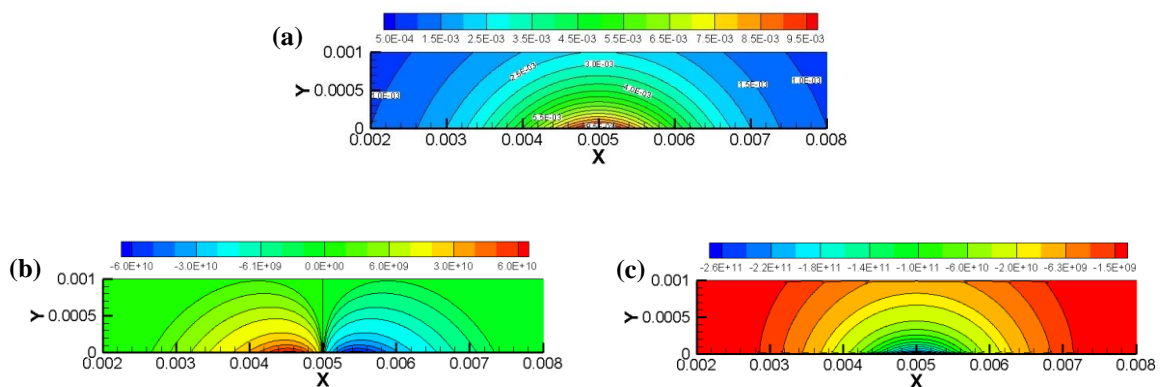


**Figure 6.4** Contour of magnetic field in the 2D planar channel: (a) magnetic induction $B(x, y)$, (b) $\nabla H^2(x)$, and (c) $\nabla H^2(y)$.
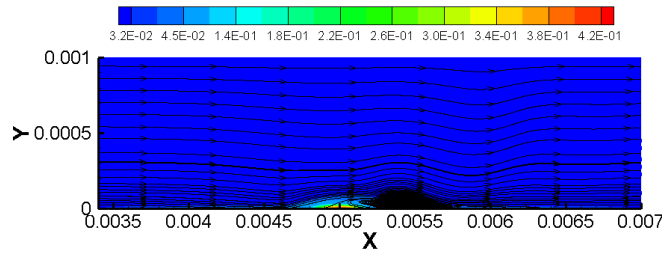
**Figure 6.5** Streamline and contour of the magnetic particle concentration at t=61s.

**6.3.2 3D unsteady tri-phase flow[220]**

(1) Geometry and Flow Conditions

A three-phase fluid, consisting of liquid water, magnetic particles ($\alpha_s = 0.04$), and non-magnetic particles ($\alpha_s = 0.045$), is flowing through two grooved plates with a series of prisms. The plates are magnetized by an applied magnetic field ($\vec{H}_0$), and each prism behaviors as a string of magnetic dipoles generating a magnetic field ($\vec{H}_{p,n}$). The length and height of the plate is $0.1995 \times 0.2$ m, and the distance between the two plates is 0.005 m. The granular particles had a diameter of 0.5 μm and magnetic volumetric susceptibility of 1. The laminar, incompressible fluid entered the plates with a linear velocity of 0.25 m/s at the inlet. A zero gauge pressure was specified at the outlet.

(2) Governing equations

In addition to the Navier-Stokes Equations governing the Newtonian fluid flow, the particles experienced the magnetic force from multiple magnetic sources. Therefore, the equation for magnetic source term became:

$$\vec{F}_{mag} = \frac{1}{2}\mu_0 \chi \alpha_s \nabla (\vec{H}_0 + \sum_{i=1}^{n} \vec{H}_{p,n})^2 \tag{6-3}$$

where $n$ is the number of the prisms on the two plates.

(3) Selected Results

A section of the grooved magnetic plate with a structured hexahedral mesh is shown in Figure 6.6a. The resulting square of the strength of the magnetic field due to induced magnetism of the grooved plates is shown in Figure 6.6b. Figure 6.6c and Figure 6.6d show the concentrations and velocity vectors of the magnetic particles and non-magnetic particles in the mid-plane cut in the $z$ direction, respectively. These results clear show that most of the magnetic particles are trapped on the magnetic plate, which agree well with the observations in experimental studies reported by Mohanty *et al.*[220]
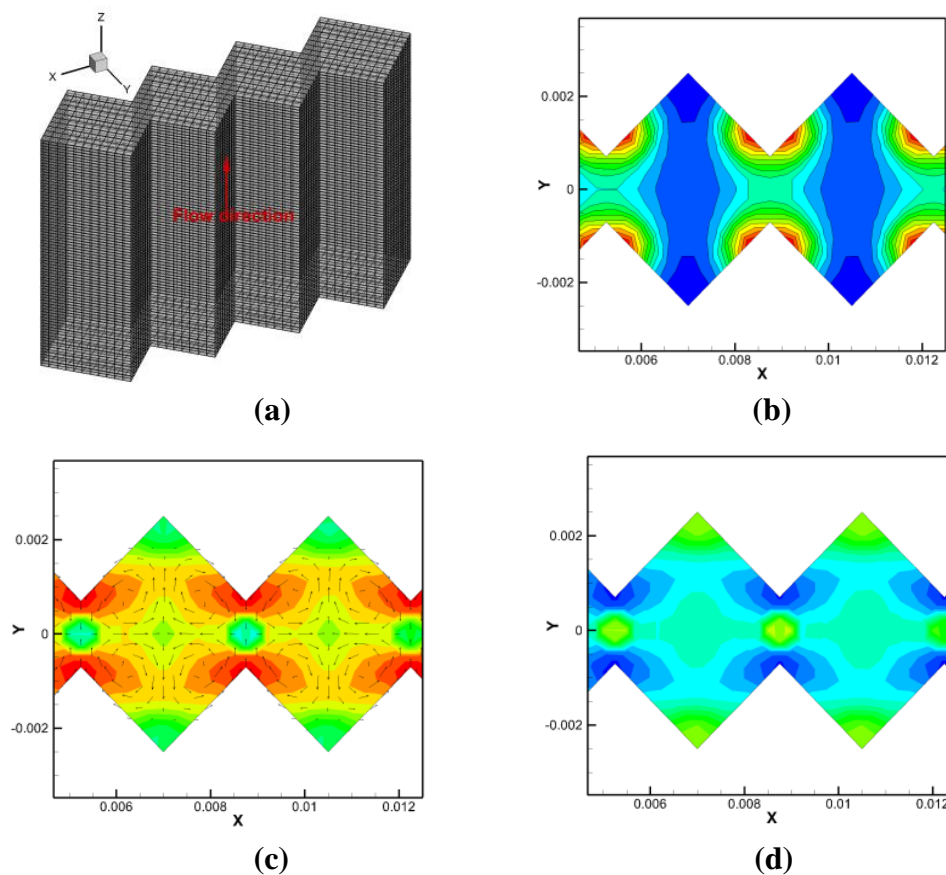


**Figure 6.6** Results of predicting magnetic separation using CFD (mid-plane cut in z; red and blue color indicates regions with high and low concentrations, respectively).

**6.4 CFD Simulation of static magnetic separation**

**6.4.1 Experimental setup and available experimental data**

The static magnetic separation experiment was carried out in a small glass vial with different types of magnetic nanoparticles homogenous suspended in water. The glass vial was held by two Nd-B permanent magnets (12.5 mm $\times$ 12.5 mm) on each side of the vial, which produced a 0.5 T of magnetic field induction at the surface, as illustrated in Figure 6.7. Different lengths of vials (20–60 mm) were used to achieve the different magnetic field gradients across the tube. By placing the magnets next to the vial, the magnetic particles started moving toward the magnets due to the magnetic force exerted on them. The separation time was recorded when all the particles got captured at the two edges of vial. The experiment results were summarized in Figure 6.8, which indicated that magnetic nanosorbents can be quickly separated from the contaminated water in less than 1 min by applying a magnetic field larger than 3500 gauss/cm, which can be easily provided by a commercial magnet.
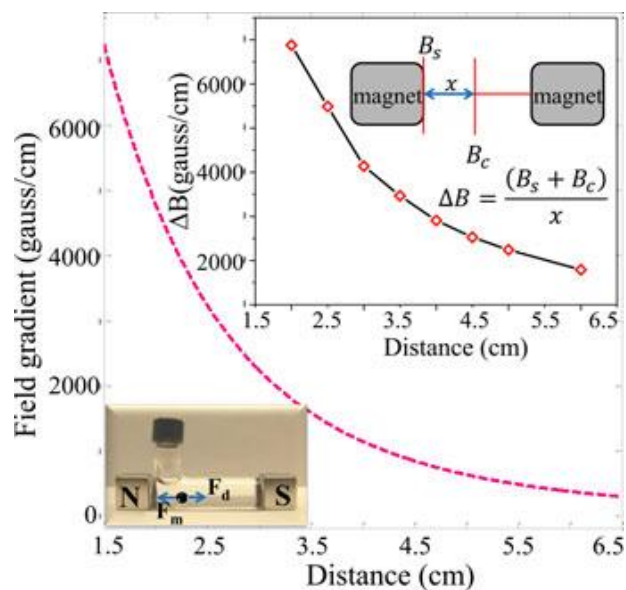
**Figure 6.7** The calculated and measured (inset) magnetic field gradient ($\Delta B$) along the symmetry axis of a cubic Nd-B magnet as a function of the distance from the magnet pole face (inset figure).[179]
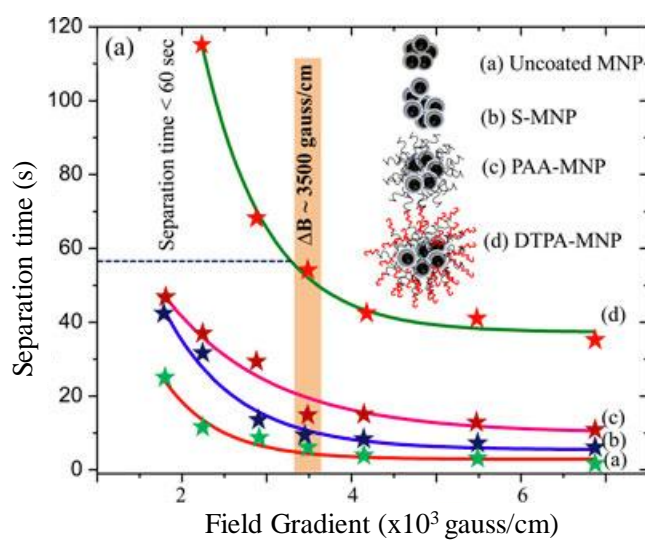


**Figure 6.8** Separation time of different MNPs as a function of magnetic field gradient.[179]

### 6.4.2 2D simulation in FLUENT

In the Eulerian 2-phase simulation, a 2D channel with a length of 0.03 m was first built up, and the domain was meshed with a structured mesh consisting of 50,000 hexahedral cells. All the four boundaries were set as the no-slip wall. Pure iron nanoparticles (750 nm, the hydrodynamic size) were chosen as the solid phase and water as liquid phase. The simulation was first initialized with zero velocity for both water and solid phase. The solid phase (magnetic particles) was initially homogeneously distributed across the whole tube with a volume fraction of 4E-5. After adding magnetic source term (calculated according to Eqn. 6-3) onto the magnetic particles, an unsteady state simulation was carried out and it was observed that the particles started to move to the regions with the maximum magnetic field gradient as shown in Figure 6.9a. The particles close to the magnets were first captured, and the particles in the middle of the channel were relatively slowly moving to the two magnets due to the weakness of the magnetic forces in that region. Due to mass conservation, the motion of fluid particles caused two vortex bubbles near each end of the tube. After 4 seconds, all the particles were accumulated near the two ends and the particle concentration for most of the regions in the tube is zero (Fig. 9b). The predicted separation time 4s agrees well with the experimental data.
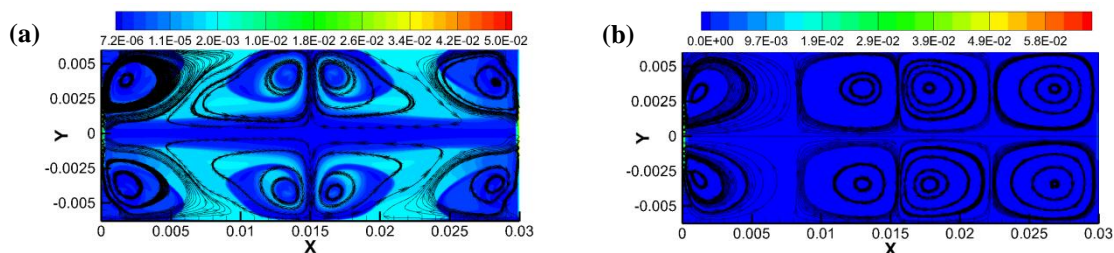


**Figure 6.9** Streamline and contour of magnetic particle concentration in the tube: (a) $t = 2$ s; (b) $t = 4$ s.

### 6.4.3 3D simulation in FLUENT

With the similar solution setup used in 2D simulation, a 3D tube with a length of 0.03 m was built up, and the domain was meshed with a structured mesh consisting of 228,000 hexahedral cells (Figure 6.10a). As shown in Figure 6.10b and c, non-uniform distribution resolution in $x$-axis was chosen to better resolve the magnetic field at the two ends as well as to save the computational cost. The 3D simulation results were compared with the 2D ones. At the beginning, both 3D and 2D showed the similar streamline and concentration contour of magnetic particles as shown in Figure 6.11. However, as the time extended, significant differences were observed between 3D and 2D simulations (Figure 6.12). This is likely due to the addition of another dimension which introduces the complexity of the flow movement. In both cases at any time, the maximum concentrations of magnetic particles were near the center of the two ends, which was in agreement with the experimental observation.
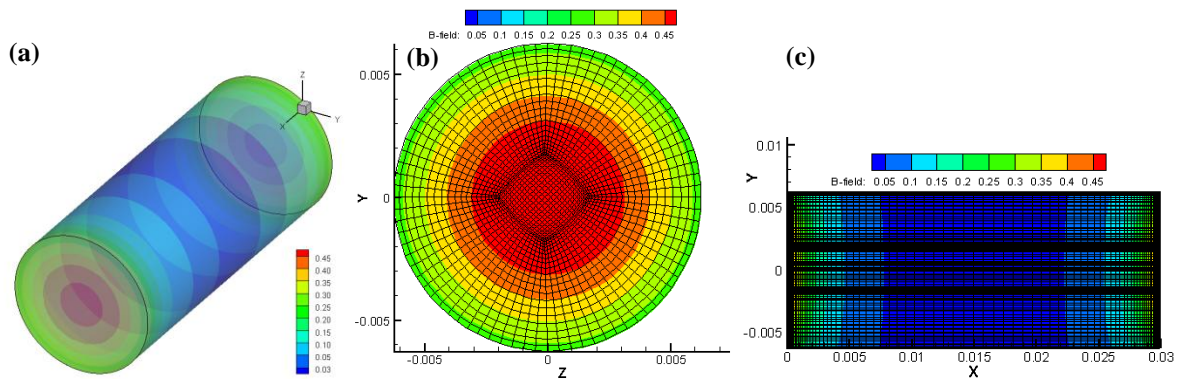


**Figure 6.10** (a) Contour of magnetic field in 3D tube; (b) Contour of magnetic field of the tube cross-section at $x=0$ (with mesh); (c) Contour of magnetic field of the plane cut along the tube centerline (with mesh).
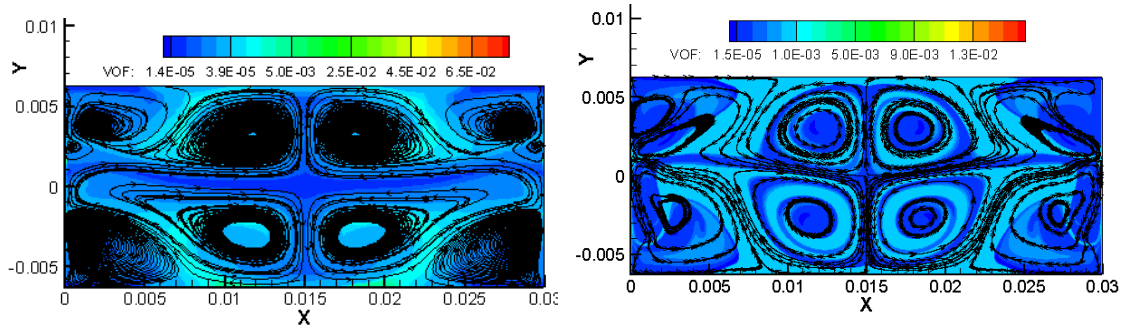
**Figure 6.11** (a) Streamline and contour of magnetic particle concentration in 3D simulation (left, the plane view cut along the tube centerline), and 2D simulation (right) at $t$=2 s.
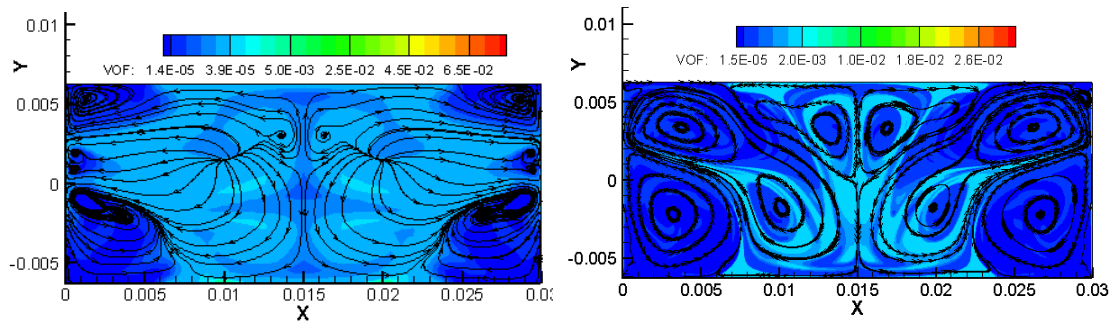


**Figure 6.12** (a) Streamline and contour of magnetic particle concentration in 3D simulation (left, the plane view cut along the tube centerline), and 2D simulation (right) at $t$=4 s.

## 6.5 Summary

In this study, advanced CFD models were implemented to simulate magnetic separation process and to explore the dynamic behavior of MNPs in a continuous flow. 2D and 3D Eulerian models have been established on the platform of ANSYS FLUENT, and user defined functions (UDFs) written in $C^{++}$ has been compiled and incorporated into the software solver for the source term for the momentum balance equation of MNPs to account for the magnetic force. The models were verified and validated using experimental data

from literatures and our own research. To achieve the continuous operation, specific quadrupole magnets were required to generate a magnetic field whose magnitude grows rapidly with the radial distance from its longitudinal axis, so that particles and water coming from the same inlet can be separated from different outlets. The CFD study of continuous flow in a quadrupole magnetic system is not as simple as the study of a steady flow in the applied field generated by permanent magnets. More intensive studies are needed to improve and optimize the currently established CFD models to be used for the continuous separation system design. Using the simulation tools prior to build the lab-scale equipment is necessary as it will save time, economic cost, and manpower for a new type of device design. Once the CFD models are validated, parametric studies can be performed to elucidate the correlation between the flow rate, particle concentration, magnetic field geometry, magnetic field strength, and types of MNPs to optimize the dynamic separation system for achieving the highest removal efficiency.

**References**

(1)     Gunther, C. G. *Electro-Magnetic Ore Separation*; Hill Publishing Company: New York, 1909.

(2)     Parker, M. R. The physics of magnetic separation. *Contemporary Physics* **1977**, *18* (3), 279–306.

(3)     Bronkala, W. J. Magnetic Separation. In *Ullmann's Encyclopedia of Industrial Chemistry*; Wiley-VCH Verlag GmbH & Co. KGaA, 2000.

(4)     Oberteuffer, J. High gradient magnetic separation. *IEEE Transactions on Magnetics* **1973**, *9* (3), 303–306.

(5)     Oder, R. High gradient magnetic separation theory and applications. *IEEE Transactions on Magnetics* **1976**, *12* (5), 428–435.

(6)     Magnetic separation - From Wikipedia, the free encyclopedia http://en.wikipedia.org/wiki/Magnetic_separation.

(7)     Pankhurst, Q. A.; Connolly, J.; Jones, S. K.; Dobson, J. Applications of magnetic nanoparticles in biomedicine. *Journal of Physics D: Applied Physics* **2003**, *36*, R167–R181.

(8)     Birss, R.; Gerber, R.; Parker, M.; Sheerer, T. Theory and performance of axial magnetic filters in laminar flow conditions. *IEEE Transactions on Magnetics* **1978**, *14* (5), 389–391.

(9)     Abbasov, T.; Ceylan, K. Filter Performance and Velocity Distribution Relation in Magnetic Filtration of Non-Newtonian Liquids. *Separation Science and Technology* **1999**, *34*, 2177–2189.

(10)    Eskandarpour, A.; Iwai, K.; Asai, S. Superconducting Magnetic Filter: Performance, Recovery, and Design. *IEEE Transactions on Applied Superconductivity* **2009**, *19* (2), 84–95.

(11)    Yano, J.; Eguchi, I. Application of high gradient magnetic separation for water treatment in steel industry. *Ind. Appl. Magn. Separation* **1978**, 134–136.

(12)    Paul A. Beharrell. Applications of superconducting magnetic sepation. QuantumDesign September 2012.

(13)    Vedavyasan, C. V. Pontential use of magnetic fields — a perspective. *Desalination* **2001**, *134* (1–3), 105–108.

(14)  Yavuz, C. T.; Prakash, A.; Mayo, J. T.; Colvin, V. L. Magnetic separations: From steel plants to biotechnology. *Chemical Engineering Science* **2009**, *64* (10), 2510–2521.

(15)  Maxwell, E.; Kelland, D. High gradient magnetic separation in coal desulfurization. *IEEE Transactions on Magnetics* **1978**, *14* (5), 482–487.

(16)  Uslu, T.; Atalay, U.; Arol, A. I. Effect of microwave heating on magnetic separation of pyrite. *Colloids and Surfaces A: Physicochemical and Engineering Aspects* **2003**, *225* (1), 161–167.

(17)  Kerkdijk, C.; Dijkhuis, J.; Segal, H.; Van Kleef, R.; Van der Sloot, H. High gradient magnetic separation of fly ash. *IEEE Trans. Magn.* **1982**, *18* (3), 858–861.

(18)  Shoumkova, A. S. Magnetic separation of coal fly ash from Bulgarian power plants. *Waste Management & Research* **2011**, *29* (10), 1078–1089.

(19)  Ambashta, R. D.; Sillanpää, M. Water purification using magnetic assistance: a review. *J. Hazard. Mater* **2010**, *180* (1–3), 38–49.

(20)  Harland, J.; Nilsson, L.; Wallin, M. Pilot scale high gradient magnetic filtration of steel mill wastewater. *IEEE Transactions on Magnetics* **1976**, *12* (6), 904–906.

(21)  Worl, L. A.; Devlin, D.; Hill, D.; Padilla, D.; Prenger, F. C. Particulate capture of plutonium by high gradient magnetic separation with advanced matrices. *Separation Science and Technology* **2001**, *36* (5–6), 1335–1349.

(22)  Rupp, G. Secondary-loop water purification at a pressurized-water reactor by a mesh-type high-gradient magnetic test separator. *IEEE Transactions on Magnetics* **1984**, *20* (5), 1192–1194.

(23)  Gerber, R.; Birss, R. R. *High gradient magnetic separation*; Research Studies Press, 1983.

(24)  Gokon, N.; Shimada, A.; Hasegawa, N.; Kaneko, H.; Kitamura, M.; Tamaura, Y. Ferrimagnetic coagulation process for phosphate ion removal using high-gradient magnetic separation. *Separation Science and Technology* **2002**, *37* (16), 3781–3791.

(25)  Li, Y.; Wang, J.; Zhao, Y.; Luan, Z. Research on magnetic seeding flocculation for arsenic removal by superconducting magnetic separation. *Separation and Purification Technology* **2010**, *73* (2), 264–270.

(26)  Phanapavudhikul, P.; Waters, J. A.; Perez de Ortiz, E. S. Design and performance of magnetic composite particles for the separation of heavy metals from water. *J Environ Sci Health A Tox Hazard Subst Environ Eng* **2003**, *38* (10), 2277–2285.

(27)    Suleiman, J. S.; Hu, B.; Peng, H.; Huang, C. Separation/preconcentration of trace amounts of Cr, Cu and Pb in environmental samples by magnetic solid-phase extraction with Bismuthiol-II-immobilized magnetic nanoparticles and their determination by ICP-OES. *Talanta* **2009**, *77* (5), 1579–1583.

(28)    Yamashita, H.; Fujita, K.; Nakajima, F.; Ozawa, Y.; Murata, T. Extraction of Uranium from Seawater Using Magnetic Adsorbents. *Separation Science and Technology* **1981**, *16* (9), 987–998.

(29)    Gruttner, C.; Bohmer, V.; Casnati, A.; Dozol, J.; Reinhoudt, D.; Reinosogarcia, M.; Rudershausen, S.; Teller, J.; Ungaro, R.; Verboom, W. Dendrimer-coated magnetic particles for radionuclide separation. *Journal of Magnetism and Magnetic Materials* **2005**, *293* (1), 559–566.

(30)    Machado, L. C. R.; Lima, F. W. J.; Paniago, R.; Ardisson, J. D.; Sapag, K.; Lago, R. M. Polymer coated vermiculite–iron composites: Novel floatable magnetic adsorbents for water spilled contaminants. *Applied Clay Science* **2006**, *31* (3–4), 207–215.

(31)    Leslie-Pelecky, D. L.; Rieke, R. D. Magnetic Properties of Nanostructured Materials. *Chem. Mater.* **1996**, *8* (8), 1770–1783.

(32)    Lu, A.-H.; Salabas, E. L.; Schüth, F. Magnetic Nanoparticles: Synthesis, Protection, Functionalization, and Application. *Angew. Chem. Int. Ed.* **2007**, *46* (8), 1222–1244.

(33)    Kim, J. H. Preparation of magnetic nanoclusters for adsorption and separation system of lanthanide, Korea Advanced Institute of Science and Technology (KAIST), 2012.

(34)    Moffat, G.; Williams, R. A.; Webb, C.; Stirling, R. Selective separations in environmental and industrial processes using magnetic carrier technology. *Minerals Engineering* **1994**, *7* (8), 1039–1056.

(35)    Warner, M. G.; Warner, C. L.; Addleman, R. S.; Yantasee, W. Magnetic Nanomaterials for Environmental Applications. In *Nanotechnologies for the Life Sciences*; Kumar, C. S. S. R., Ed.; Wiley-VCH Verlag GmbH & Co. KGaA: Weinheim, Germany, 2011.

(36)    Huber, D. Synthesis, Properties, and Applications of Iron Nanoparticles. *Small* **2005**, *1* (5), 482–501.

(37)    Laurent, S.; Forge, D.; Port, M.; Roch, A.; Robic, C.; Vander Elst, L.; Muller, R. N. Magnetic iron oxide nanoparticles: synthesis, stabilization, vectorization, physicochemical characterizations, and biological applications. *Chem. Rev* **2008**, *108* (6), 2064–2110.

(38) Lu, A.-H.; Salabas, E. L.; Schüth, F. Magnetic Nanoparticles: Synthesis, Protection, Functionalization, and Application. *Angew. Chem. Int. Ed.* **2007**, *46* (8), 1222–1244.

(39) Antony, J.; Qiang, Y.; Baer, D. R.; Wang, C. Synthesis and characterization of stable iron-iron oxide core-shell nanoclusters for environmental applications. *J Nanosci Nanotechnol* **2006**, *6* (2), 568–572.

(40) Warner, M. G.; Warner, C. L.; Addleman, R. S.; Yantasee, W. Magnetic Nanomaterials for Environmental Applications. In *Nanotechnologies for the Life Sciences*; Kumar, C. S. S. R., Ed.; Wiley-VCH Verlag GmbH & Co. KGaA: Weinheim, Germany, 2011.

(41) Liu, Q.; Xu, Z.; Finch, J. A.; Egerton, R. A Novel Two-Step Silica-Coating Process for Engineering Magnetic Nanocomposites. *Chem. Mater.* **2011**, *10* (12), 3936–3940.

(42) Deng, Y.; Wang, C.; Hu, J.; Yang, W.; Fu, S. Investigation of formation of silica-coated magnetite nanoparticles via sol–gel approach. *Colloids and Surfaces A: Physicochemical and Engineering Aspects* **2005**, *262* (1–3), 87–93.

(43) Han, H.; Johnson, A.; Kaczor, J.; Kaur, M.; Paszczynski, A.; Qiang, Y. Silica coated magnetic nanoparticles for separation of nuclear acidic waste. *J. Appl. Phys.* **2010**, *107* (9), 09B520.

(44) Kryszewski, M.; Jeszka, J. Nanostructured conducting polymer composites — superparamagnetic particles in conducting polymers. *Synthetic Metals* **1998**, *94* (1), 99–104.

(45) Harris, L. A.; Goff, J. D.; Carmichael, A. Y.; Riffle, J. S.; Harburn, J. J.; St. Pierre, T. G.; Saunders, M. Magnetite Nanoparticle Dispersions Stabilized with Triblock Copolymers. *Chem. Mater.* **2011**, *15* (6), 1367–1377.

(46) Nies, D. H. Microbial heavy-metal resistance. *Appl. Microbiol. Biotechnol.* **1999**, *51*, 730–750.

(47) Lenntech Water Treatment and Air Purification http://www.excelwater.com/thp/filters/Water-Purification.htm (accessed Oct 31, 2011).

(48) *Handbook on the toxicology of metals*; Friberg, L., Nordberg, G. R., Vouk, V. B., Eds.; Elsevier/North-Holland Biomedical Press: New York, 1979.

(49) Devi, M.; Fingerman, M. Inhibition of acetylcholinesterase activity in the central nervous system of the red swamp crayfish, procambarus clarkii, by mercury, cadmium, and lead. *Bull. Environ. Contam. Toxicol.* **1995**, *55* (5).

(50)  Mukherjee, A.; Sengupta, M. K.; Hossain, M. A.; Ahamed, S.; Das, B.; Nayak, B.;
      Lodh, D.; Rahman, M. M.; Chakraborti, D. Arsenic contamination in groundwater: a
      global perspective with emphasis on the Asian scenario. *J Health Popul Nutr* **2006**,
      *24* (2), 142–163.

(51)  Ho, Y. S.; Porter, J. F.; McKay, G. Equilibrium Isotherm Studies for the Sorption of
      Divalent Metal Ions onto Peat: Copper, Nickel and Lead Single Component Systems.
      *Water, Air, and Soil Pollution* **2002**, *141* (1–4), 1–33.

(52)  Miller, J. R.; Hudson-Edwards, K. A.; Lechler, P. J.; Preston, D.; Macklin, M. G.
      Heavy metal contamination of water, soil and produce within riverine communities of
      the Río Pilcomayo basin, Bolivia. *Science of The Total Environment* **2004**, *320* (2–3),
      189–209.

(53)  Zietz, B. P.; Dieter, H. H.; Lakomek, M.; Schneider, H.; Kessler-Gaedtke, B.;
      Dunkelberg, H. Epidemiological investigation on chronic copper toxicity to children
      exposed via the public drinking water supply. *Sci. Total Environ* **2003**, *302* (1–3),
      127–144.

(54)  Rai, P. K. Heavy metal pollution in aquatic ecosystems and its phytoremediation
      using wetland plants: an ecosustainable approach. *Int J Phytoremediation* **2008**, *10*
      (2), 131–158.

(55)  Wildgoose, G. G.; Leventis, H. C.; Simm, A. O.; Jones, J. H.; Compton, R. G.
      Cysteine methyl ester modified glassy carbon spheres for removal of toxic heavy
      metals from aqueous media. *Chem. Commun.* **2005**, No. 29, 3694.

(56)  Sgarlata, C.; Arena, G.; Longo, E.; Zhang, D.; Yang, Y.; Bartsch, R. A. Heavy metal
      separation with polymer inclusion membranes. *Journal of Membrane Science* **2008**,
      *323* (2), 444–451.

(57)  Fergusson, J. *The heavy elements : chemistry, environmental impact and health
      effects*; Pergamon press: Oxford ;;New York ;;Seoul [etc.], 1990.

(58)  Glover-Kerkvliet, J. Environmental assault on immunity. *Environ. Health Perspect*
      **1995**, *103* (3), 236–239.

(59)  Almeida, P.; Stearns, L. B. Political Opportunities and Local Grassroots
      Environmental Movements: The Case of Minamata. *Social Problems* **1998**, *45* (1),
      37–60.

(60)  Code of Federal Regulations (CFR), 40, 141, 261, 268.40. US Government Printing
      Office, Superintendent of Documents, Washington, DC.

(61)  Kiefer, R.; Höll, W. H. Sorption of Heavy Metals onto Selective Ion-Exchange Resins with Aminophosphonate Functional Groups. *Industrial & Engineering Chemistry Research* **2001**, *40* (21), 4570–4576.

(62)  Motsi, T.; Rowson, N. A.; Simmons, M. J. H. Adsorption of heavy metals from acid mine drainage by natural zeolite. *International Journal of Mineral Processing* **2009**, *92* (1–2), 42–48.

(63)  Kang, S. Competitive adsorption characteristics of Co2+, Ni2+, and Cr3+ by IRN-77 cation exchange resin in synthesized wastewater. *Chemosphere* **2004**, *56* (2), 141–147.

(64)  Inglezakis, V. J.; Grigoropoulou, H. Effects of operating conditions on the removal of heavy metals by zeolite in fixed bed reactors. *Journal of Hazardous Materials* **2004**, *112* (1–2), 37–43.

(65)  Jusoh, A.; Sushiung, L.; Ali, N.; Noor, M. A simulation study of the removal efficiency of granular activated carbon on cadmium and lead. *Desalination* **2007**, *206* (1–3), 9–16.

(66)  Babel, S.; Kurniawan, T. A. Low-cost adsorbents for heavy metals uptake from contaminated water: a review. *J. Hazard. Mater* **2003**, *97* (1–3), 219–243.

(67)  Baltpurvins, K. Effect of electrolyte composition on zinc hydroxide precipitation by lime. *Water Research* **1997**, *31* (5), 973–980.

(68)  Ozverdi, A.; Erdem, M. Cu2+, Cd2+ and Pb2+ adsorption from aqueous solutions by pyrite and synthetic iron sulphide. *J. Hazard. Mater* **2006**, *137* (1), 626–632.

(69)  Huang, J.-H.; Zeng, G.-M.; Zhou, C.-F.; Li, X.; Shi, L.-J.; He, S.-B. Adsorption of surfactant micelles and Cd2+/Zn2+ in micellar-enhanced ultrafiltration. *Journal of Hazardous Materials* **2010**, *183* (1–3), 287–293.

(70)  Benito, Y.; Ruiz, M. Reverse osmosis applied to metal finishing wastewater. *Desalination* **2002**, *142* (3), 229–234.

(71)  Sadrzadeh, M.; Mohammadi, T.; Ivakpour, J.; Kasiri, N. Separation of lead ions from wastewater using electrodialysis: Comparing mathematical and neural network modeling. *Chemical Engineering Journal* **2008**, *144* (3), 431–441.

(72)  Yavuz, C. T.; Prakash, A.; Mayo, J. T.; Colvin, V. L. Magnetic separations: From steel plants to biotechnology. *Chemical Engineering Science* **2009**, *64* (10), 2510–2521.

(73)   *Commercial Spent Nuclear Fuel: Observations on the Key Attributes and Challenges of Storage and Disposal Options*; GAO-13-532T; U.S. Government Accountability Office, 2013; pp 1–17.

(74)   Processing of Used Nuclear Fuel http://www.world-nuclear.org/info/nuclear-fuel-cycle/fuel-recycling/processing-of-used-nuclear-fuel/ (accessed Oct 28, 2015).

(75)   International Atomic Energy Agency. *Spent fuel reprocessing options*; IAEA-TECDOC-1587; 2008.

(76)   Beaver, W. *The Demise of Yucca Mountain*; The Independent Review, 2010.

(77)   NRC: Nuclear Fuel Pool Capacity, Energy Resources International and DOE/RW-0431 – Revision 1 http://www.nrc.gov/waste/spent-fuel-storage/nuc-fuel-pool.html (accessed Apr 22, 2013).

(78)   *Application of ion exchange processes for the treatment of radioactive waste and management of spent ion exchangers*; International Atomic Energy Agency, Ed.; Technical reports series / International Atomic Energy Agency; International Atomic Energy Agency: Vienna, 2002.

(79)   Othman, S. H.; Sohsah, M. A.; Ghoneim, M. M.; Sokkar, H. H.; Badawy, S. M.; El-Anadouli, B. E. Adsorption of hazardous ions from radioactive waste on chelating cloth filter. *Radiation Physics and Chemistry* **2006**, *75* (2), 278–285.

(80)   *Chemical precipitation processes for the treatment of aqueous radioactive waste*; International Atomic Energy Agency, Ed.; Technical reports series / International Atomic Energy Agency; Vienna, 1992.

(81)   Chmielewski, A. G.; Harasimowicz, M.; Zakrzewska-Trznadel, G. Membrane technologies for liquid radioactive waste treatment. *Czech J Phys* **1999**, *49* (1), 979–985.

(82)   Godbee, H. W. Use of Evaporation for the Treatment of Liquids in the Nuclear Industry. *ORNL-4790* **1973**.

(83)   International Atomic Energy Agency. *Handling and processing of radioactive waste from nuclear applications*; TRS No. 402; Vienna, 2001.

(84)   Rahman, R. O. A.; Ibrahium, H. A.; Hung, Y.-T. Liquid Radioactive Wastes Treatment: A Review. *Water* **2011**, *3* (4), 551–565.

(85)   Kaur, M.; Zhang, H.; Martin, L.; Todd, T.; Qiang, Y. Conjugates of Magnetic Nanoparticle—Actinide Specific Chelator for Radioactive Waste Separation. *Environ. Sci. Technol.* **2013**, *47* (21), 11942–11959.

(86) Anderson, H. H.; Asprey, L. B. Solvent extraction process for plutonium. US2924506 (A), February 9, 1960.

(87) Birkett, J. E.; Carrott, M. J.; Fox, O. D.; Jones, C. J.; Maher, C. J.; Roube, C. V.; Taylor, R. J.; Woodhead, D. A. Recent Developments in the Purex Process for Nuclear Fuel Reprocessing: Complexant Based Stripping for Uranium/Plutonium Separation. *CHIMIA International Journal for Chemistry* **2005**, *59* (12), 898–904.

(88) Chamberlain, D. B.; Conner, C.; Hutter, J. C.; Leonard, R. A.; Wygmans, D. G.; Vandegrift, G. F. *Truex Processing of Plutonium Analytical Solutions at Argonne National Laboratory*; ANL/CMT/CP--86178; CONF-951057--11; Argonne National Lab., IL (United States), 1995.

(89) Weaver, B.; Kappelmann, F. A. *Talspeak: A New Method of Separating Americium and Curium from the Lanthanides by Extraction from an Aqueous Solution of an Aminopolyacetic Acid Complex with a Monoacidic Organophosphate or Phosphonate*; ORNL-3559; Oak Ridge National Lab., Tenn., 1964.

(90) Nuñez, L.; Buchholz, B. A.; Vandegrift, G. F. Waste Remediation Using in Situ Magnetically Assisted Chemical Separation. *Separation Science and Technology* **1995**, *30* (7–9), 1455–1471.

(91) Nuñez, L.; Kaminski, M.; Bradley, C.; Buchholz, B. A.; Aase, S. B.; Tuazon, H. E.; Vandegrift, G. F.; Landsberger, S. *Magnetically assisted chemical separation (MACS) process: Preparation and optimization of particles for removal of transuranic elements*; ANL--95/1, 167221; 1995.

(92) Nuñez, L.; Buchholz, B. A.; Kaminski, M.; Aase, S. B.; Brown, N. R.; Vandegrift, G. F. Actinide Separation of High-Level Waste Using Solvent Extractants on Magnetic Microparticles. *Separation Science and Technology* **1996**, *31* (10), 1393–1407.

(93) Nuñez, L.; Kaminski, M. D. Transuranic separation using organophosphorus extractants adsorbed onto superparamagnetic carriers. *Journal of Magnetism and Magnetic Materials* **1999**, *194* (1–3), 102–107.

(94) Fryxell, G. E.; Lin, Y.; Fiskum, S.; Birnbaum, J. C.; Wu, H.; Kemner, K.; Kelly, S. Actinide sequestration using self-assembled monolayers on mesoporous supports. *Environ. Sci. Technol* **2005**, *39* (5), 1324–1331.

(95) Yantasee, W.; Warner, C. L.; Sangvanich, T.; Addleman, R. S.; Carter, T. G.; Wiacek, R. J.; Fryxell, G. E.; Timchalk, C.; Warner, M. G. Removal of Heavy Metals from Aqueous Systems with Thiol Functionalized Superparamagnetic Nanoparticles. *Environ. Sci. Technol.* **2007**, *41* (14), 5114–5119.

(96)  Warner, C. L.; Addleman, R. S.; Cinson, A. D.; Droubay, T. C.; Engelhard, M. H.; Nash, M. A.; Yantasee, W.; Warner, M. G. High-Performance, Superparamagnetic, Nanoparticle-Based Heavy Metal Sorbents for Removal of Contaminants from Natural Waters. *ChemSusChem* **2010**, *3* (6), 749–757.

(97)  Fryxell, G. E.; Mattigod, S. V.; Lin, Y.; Wu, H.; Fiskum, S.; Parker, K.; Zheng, F.; Yantasee, W.; Zemanian, T. S.; Addleman, R. S.; et al. Design and synthesis of self-assembled monolayers on mesoporous supports (SAMMS): The importance of ligand posture in functional nanomaterials. *J. Mater. Chem.* **2007**, *17* (28), 2863.

(98)  Huang, S.-H.; Chen, D.-H. Rapid removal of heavy metal cations and anions from aqueous solutions by an amino-functionalized magnetic nano-adsorbent. *Journal of Hazardous Materials* **2009**, *163* (1), 174–179.

(99)  Chang, Y.-C.; Chen, D.-H. Preparation and adsorption properties of monodisperse chitosan-bound Fe3O4 magnetic nanoparticles for removal of Cu(II) ions. *Journal of Colloid and Interface Science* **2005**, *283* (2), 446–451.

(100) Chang, Y.-C.; Chen, D.-H. Recovery of gold(III) ions by a chitosancoated magnetic nano-adsorbent. *Gold Bull* **2006**, *39* (3), 98–102.

(101) Grass, R. N.; Athanassiou, E. K.; Stark, W. J. Covalently Functionalized Cobalt Nanoparticles as a Platform for Magnetic Separations in Organic Synthesis. *Angew. Chem. Int. Ed.* **2007**, *46* (26), 4909–4912.

(102) Koehler, F. M.; Rossier, M.; Waelle, M.; Athanassiou, E. K.; Limbach, L. K.; Grass, R. N.; Günther, D.; Stark, W. J. Magnetic EDTA: coupling heavy metal chelators to metal nanomagnets for rapid removal of cadmium, lead and copper from contaminated water. *Chem. Commun.* **2009**, No. 32, 4862.

(103) Senel, S.; Uzun, L.; Kara, A.; Denizli, A. Heavy Metal Removal from Synthetic Solutions with Magnetic Beads Under Magnetic Field. *Journal of Macromolecular Science, Part A* **2008**, *45* (8), 635–642.

(104) MAHMOUD NASEF, M.; SAIDI, H.; UJANG, Z.; MOHD DAHLAN, K. Z. REMOVAL OF METAL IONS FROM AQUEOUS SOLUTIONS USING CROSSLINKED POLYETHYLENE -GTMFJ-POLYSTYRENE SULFONIC ACID ADSORBENT PREPARED BY RADIATION GRAFTING. *Journal of the Chilean Chemical Society* **2010**, *55* (4), 421–427.

(105) Shiraishi, Y.; Nishimura, G.; Hirai, T.; Komasawa, I. Separation of Transition Metals Using Inorganic Adsorbents Modified with Chelating Ligands. *Industrial & Engineering Chemistry Research* **2002**, *41* (20), 5065–5070.

(106) Kaur, M.; Johnson, A.; Tian, G.; Jiang, W.; Rao, L.; Paszczynski, A.; Qiang, Y. Separation nanotechnology of diethylenetriaminepentaacetic acid bonded magnetic nanoparticles for spent nuclear fuel. *Nano Energy* **2013**, *2* (1), 124–132.

(107) Zhao, Y.; Li, J.; Zhang, S.; Wang, X. Amidoxime-functionalized magnetic mesoporous silica for selective sorption of U(VI). *RSC Adv.* **2014**, *4* (62), 32710–32717.

(108) Rezaei, A.; Khani, H.; Masteri-Farahani, M.; Rofouei, M. K. A novel extraction and preconcentration of ultra-trace levels of uranium ions in natural water samples using functionalized magnetic-nanoparticles prior to their determination by inductively coupled plasma-optical emission spectrometry. *Analytical Methods* **2012**, *4* (12), 4107.

(109) Sadeghi, S.; Azhdari, H.; Arabi, H.; Moghaddam, A. Z. Surface modified magnetic Fe3O4 nanoparticles as a selective sorbent for solid phase extraction of uranyl ions from water samples. *Journal of Hazardous Materials* **2012**, *215–216*, 208–216.

(110) Zhao, Y.; Li, J.; Zhao, L.; Zhang, S.; Huang, Y.; Wu, X.; Wang, X. Synthesis of amidoxime-functionalized Fe3O4@SiO2 core–shell magnetic microspheres for highly efficient sorption of U(VI). *Chemical Engineering Journal* **2014**, *235*, 275–283.

(111) Fan, F.-L.; Qin, Z.; Bai, J.; Rong, W.-D.; Fan, F.-Y.; Tian, W.; Wu, X.-L.; Wang, Y.; Zhao, L. Rapid removal of uranium from aqueous solutions using magnetic Fe3O4@SiO2 composite particles. *Journal of Environmental Radioactivity* **2012**, *106*, 40–46.

(112) Afsar, A.; Laventine, D. L.; Harwood, L. M.; Hudson, M. J.; Geist, A. Immobilisation of phenanthroline-bis triazine(c1-btphen) on magnetic nanoparticles for co-extraction of americium(III) and europium(III). *Heterocycles* **2013**, *88* (1), 613–620.

(113) Afsar, A.; Harwood, L. M.; Hudson, M. J.; Distler, P.; John, J. Effective separation of Am( III ) and Eu( III ) from HNO 3 solutions using CyMe 4 -BTPhen-functionalized silica-coated magnetic nanoparticles. *Chem. Commun.* **2014**, *50* (95), 15082–15085.

(114) Lewis, F. W.; Harwood, L. M.; Hudson, M. J.; Drew, M. G. B.; Desreux, J. F.; Vidick, G.; Bouslimani, N.; Modolo, G.; Wilden, A.; Sypula, M.; et al. Highly Efficient Separation of Actinides from Lanthanides by a Phenanthroline-Derived Bis-triazine Ligand. *J. Am. Chem. Soc.* **2011**, *133* (33), 13093–13102.

(115) Lewis, F. W.; Harwood, L. M.; Hudson, M. J.; Drew, M. G. B.; Wilden, A.; Sypula, M.; Modolo, G.; Vu, T.-H.; Simonin, J.-P.; Vidick, G.; et al. From BTBPs to BTPhens: The Effect of Ligand Pre-Organization on the Extraction Properties of Quadridentate Bis-Triazine Ligands. *Procedia Chemistry* **2012**, *7*, 231–238.

(116) Basualto, C.; Gaete, J.; Molina, L.; Valenzuela, F.; Ya ñez, C.; Marco, J. F. Lanthanide sorbent based on magnetite nanoparticles functionalized with organophosphorus extractants. *Science and Technology of Advanced Materials* **2015**, *16* (3), 35010.

(117) Dupont, D.; Brullot, W.; Bloemen, M.; Verbiest, T.; Binnemans, K. Selective Uptake of Rare Earths from Aqueous Solutions by EDTA-Functionalized Magnetic and Nonmagnetic Nanoparticles. *ACS Appl. Mater. Interfaces* **2014**, *6* (7), 4980–4988.

(118) Technical data sheet for Nanofer 25 product http://www.nanoiron.cz/en/nanofer-25 (accessed Nov 2, 2015).

(119) Han, H.; Johnson, A.; Kaczor, J.; Kaur, M.; Paszczynski, A.; Qiang, Y. Silica coated magnetic nanoparticles for separation of nuclear acidic waste. *Journal of Applied Physics* **2010**, *107*, 09B520.

(120) St öber, W. Controlled growth of monodisperse silica spheres in the micron size range. *Journal of Colloid and Interface Science* **1968**, *26*, 62–69.

(121) Sun, Z. Novel sol-gel nanoporous materials, nanocomposites and their applications in bioscience, Drexel University, 2005.

(122) Sumper, M.; Brunner, E. Learning from Diatoms: Nature's Tools for the Production of Nanostructured Silica. *Advanced Functional Materials* **2006**, *16*, 17–26.

(123) Johnson, A. K. Application of magnetic nanoparticles for nuclear waste cleanup and biotechnology, University of Idaho, 2011.

(124) Pentetic acid - Wikipedia, the free encyclopedia http://en.wikipedia.org/wiki/Pentetic_acid (accessed Nov 3, 2011).

(125) Johnson, A. K.; Kaczor, J.; Han, H.; Kaur, M.; Tian, G.; Rao, L.; Qiang, Y.; Paszczynski, A. J. Highly hydrated poly(allylamine)/silica magnetic resin. *J. Nanopart. Res.* **2011**, *13*, 4881–4895.

(126) Transmission electron microscopy - Wikipedia, the free encyclopedia http://en.wikipedia.org/wiki/Transmission_electron_microscopy (accessed Nov 5, 2011).

(127) Berne, B. J.; Pecora, R. *Dynamic light scattering*; John Wiley & Sons: New York, 1976.

(128) Sartor, M. Dynamic light scattering - to determin the radius of small beads in Brownian motion in a solution. University of California, San Diego.

http://physics.ucsd.edu/neurophysics/courses/physics_173_273/dynamic_light_scattering_03.pdf (accessed November 5, 2011).

(129) Reis, B. M.; Armes, S. P.; Fujii, S.; Biggs, S. Characterisation of the dispersion stability of a stimulus responsive core–shell colloidal latex. *Colloids and Surfaces A: Physicochemical and Engineering Aspects* **2010**, *353*, 210–215.

(130) Johnson, A. K.; Kaczor, J.; Han, H.; Kaur, M.; Tian, G.; Rao, L.; Qiang, Y.; Paszczynski, A. J. Highly hydrated poly(allylamine)/silica magnetic resin. *J. Nanopart. Res.* **2011**, *13*, 4881–4895.

(131) Zhang, H.; Johnson, A. K.; Kaur, M.; Paszczynski, A. J.; Qiang, Y. Fast separation of cadmium and lead ions from contaminated water using conjugates of magnetic nanoparticle-DTPA. In *2011 11th IEEE Conference on Nanotechnology (IEEE-NANO)*; Portland, OR, USA, 2011; pp 1504–1507.

(132) Reis, B. M.; Armes, S. P.; Fujii, S.; Biggs, S. Characterisation of the dispersion stability of a stimulus responsive core–shell colloidal latex. *Colloids and Surfaces A: Physicochemical and Engineering Aspects* **2010**, *353*, 210–215.

(133) Li, J.; Liu, R.; Yu, J.; Jiang, F. A gold electrode modified with self-assembled diethylenetriaminepentaacetic acid via charge-based discrimination. *Anal. Sci.* **2009**, *25* (11), 1289–1293.

(134) US EPA, O. Final National Priorities List (NPL) Sites - by State http://www2.epa.gov/superfund/final-national-priorities-list-npl-sites-state (accessed Oct 21, 2015).

(135) USGS, Water-Resources Investigations Report 96-4257 http://ca.water.usgs.gov/archive/reports/penn (accessed Nov 8, 2011).

(136) Reece, D. E.; Felkey, J. R.; Wai, C. M. Heavy metal pollution in the sediments of the Coeur d'Alene River, Idaho. *Geo* **1978**, *2* (5), 289–293.

(137) Moberly, J. G.; Borch, T.; Sani, R. K.; Spycher, N. F.; Şengör, S. S.; Ginn, T. R.; Peyton, B. M. Heavy Metal–Mineral Associations in Coeur d'Alene River Sediments: A Synchrotron-Based Analysis. *Water Air Soil Pollut* **2009**, *201* (1–4), 195–208.

(138) Harrington, J. M.; LaForce, M. J.; Rember, W. C.; Fendorf, S. E.; Rosenzweig, R. F. Phase Associations and Mobilization of Iron and Trace Elements in Coeur d'Alene Lake, Idaho. *Environ. Sci. Technol.* **1998**, *32* (5), 650–656.

(139) Rastogi, G.; Barua, S.; Sani, R. K.; Peyton, B. M. Investigation of Microbial Populations in the Extremely Metal-Contaminated Coeur d'Alene River Sediments. *Microb Ecol* **2011**, *62* (1), 1–13.

(140) Godt, J.; Scheidig, F.; Grosse-Siestrup, C.; Esche, V.; Brandenburg, P.; Reich, A.; Groneberg, D. A. The toxicity of cadmium and resulting hazards for human health. *J Occup Med Toxicol 1*, 22–22.

(141) US Environmental Protection Agency, 816F03016, www.epa.gov.

(142) Inglezakis, V. J.; Grigoropoulou, H. Effects of operating conditions on the removal of heavy metals by zeolite in fixed bed reactors. *Journal of Hazardous Materials* **2004**, *112* (1–2), 37–43.

(143) Benito, Y.; Ruiz, M. Reverse osmosis applied to metal finishing wastewater. *Desalination* **2002**, *142* (3), 229–234.

(144) Yantasee, W.; Warner, C. L.; Sangvanich, T.; Addleman, R. S.; Carter, T. G.; Wiacek, R. J.; Fryxell, G. E.; Timchalk, C.; Warner, M. G. Removal of Heavy Metals from Aqueous Systems with Thiol Functionalized Superparamagnetic Nanoparticles. *Environmental Science & Technology* **2007**, *41* (14), 5114–5119.

(145) Xu, Z.; Dong, J. Synthesis, Characterization, and Application of Magnetic Nanocomposites for the Removal of Heavy Metals from Industrial Effluents. In *Emerging Environmental Technologies*; Shah, V., Ed.; Springer Netherlands: Dordrecht, 2008; pp 105–148.

(146) Kaur, M.; Huijin Zhang; You Qiang. Magnetic Separation Dynamics of Colloidal Magnetic Nanoparticles. *IEEE Magnetics Letters* **2013**, *4*, 4000204–4000204.

(147) Farghali, A. A.; Bahgat, M.; Enaiet Allah, A.; Khedr, M. H. Adsorption of Pb(II) ions from aqueous solutions using copper oxide nanostructures. *Beni-Suef University Journal of Basic and Applied Sciences* **2013**, *2* (2), 61–71.

(148) McKay, G.; Otterburn, M. S.; Sweeney, A. G. The removal of colour from effluent using various adsorbents--IV. Silica: Equilibria and column studies. *Water Research* **1980**, *14* (1), 21–27.

(149) Arshadi, M.; Amiri, M. J.; Mousavi, S. Kinetic, equilibrium and thermodynamic investigations of Ni(II), Cd(II), Cu(II) and Co(II) adsorption on barley straw ash. *Water Resources and Industry* **2014**, *6*, 1–17.

(150) Akpomie, K. G.; Dawodu, F. A.; Adebowale, K. O. Mechanism on the sorption of heavy metals from binary-solution by a low cost montmorillonite and its desorption potential. *Alexandria Engineering Journal* **2015**, *54* (3), 757–767.

(151) Horsfall, M.; Spiff, A. I.; Abia, A. A. Studies on the Influence of Mercaptoacetic Acid (MAA) Modification of Cassava (Manihot sculenta Cranz) Waste Biomass on the

Adsorption of Cu $^{2+}$ and Cd $^{2+}$ from Aqueous Solution. *Bulletin of the Korean Chemical Society* **2004**, *25* (7), 969–976.

(152) Li, Y.; Xia, B.; Zhao, Q.; Liu, F.; Zhang, P.; Du, Q.; Wang, D.; Li, D.; Wang, Z.; Xia, Y. Removal of copper ions from aqueous solution by calcium alginate immobilized kaolin. *Journal of Environmental Sciences* **2011**, *23* (3), 404–411.

(153) Phanapavudhikul, P.; Waters, J. A.; de Ortiz, E. S. P. Design and Performance of Magnetic Composite Particles for the Separation of Heavy Metals from Water. *Journal of Environmental Science and Health, Part A* **2003**, *38* (10), 2277–2285.

(154) Mahmoud Nasef, M.; Saidi, H.; Ujang, Z.; Mohd Dahlan, K. Z. Removal of metal ions from aqueous solutions using crosslinked polyethylene-graft-polystyrene sulfonic acid adsorbent prepared by radiation grafting. *Journal of the Chilean Chemical Society* **2010**, *55* (4), 421–427.

(155) Smiciklas, I.; Dimović, I.; Mitrić, M. Removal of Co2+ from aqueous solutions by hydroxyapatite. *Water Res.* **2006**, *40* (12), 2267–2274.

(156) Gautam, R. K.; Mudhoo, A.; Lofrano, G.; Chattopadhyaya, M. C. Biomass-derived biosorbents for metal ions sequestration: Adsorbent modification and activation methods and adsorbent regeneration. *Journal of Environmental Chemical Engineering* **2014**, *2* (1), 239–259.

(157) Nash, K. L.; Lumetta, G. J. *Advanced Separation Techniques for Nuclear Fuel Reprocessing and Radioactive Waste Treatment*; Elsevier, 2011.

(158) Ronda, C. R.; Jüstel, T.; Nikol, H. Rare earth phosphors: fundamentals and applications. *J. Alloys Compd.* **1998**, *275–277*, 669–676.

(159) Xu, C.; Qu, X. Cerium oxide nanoparticle: a remarkably versatile rare earth nanomaterial for biological applications. *NPG Asia Mater.* **2014**, *6* (3), e90.

(160) Rare Earth Elements. http://www.rareelementresources.com/rare-earth-elements#.VH-xFsm9b7x (accessed Dec 4, 2014).

(161) Koodynska, D.; Hubicki, Z. Investigation of Sorption and Separation of Lanthanides on the Ion Exchangers of Various Types. In *Ion Exchange Technologies*; Kilislioglu, A., Ed.; InTech, 2012.

(162) Humphries, M. *Rare Earth Elements: The Global Supply Chain*; CRS Report for Congress R41347; 2013.

(163) *Critical Materials Strategy*; U.S. Department of Energy Report; 2011.

(164) Binnemans, K.; Jones, P. T.; Blanpain, B.; Van Gerven, T.; Yang, Y.; Walton, A.; Buchert, M. Recycling of rare earths: a critical review. *J. Cleaner Prod.* **2013**, *51*, 1–22.

(165) Binnemans, K.; Jones, P. T. Perspectives for the recovery of rare earths from end-of-life fluorescent lamps. *J. Rare Earths* **2014**, *32* (3), 195–200.

(166) Hower, J. C.; Ruppert, L. F.; Eble, C. F. Lanthanide, yttrium, and zirconium anomalies in the Fire Clay coal bed, Eastern Kentucky. *International Journal of Coal Geology* **1999**, *39* (1–3), 141–153.

(167) Bechtel, A.; Ghazi, A. M.; Elliott, W. C.; Oszczepalski, S. The occurrences of the rare earth elements and the platinum group elements in relation to base metal zoning in the vicinity of Rote Fäule in the Kupferschiefer of Poland. *Applied Geochemistry* **2001**, *16* (3), 375–386.

(168) Tong, S.-L.; Zhu, W.-Z.; Gao, Z.-H.; Meng, Y.-X.; Peng, R.-L.; Lu, G.-C. Distribution characteristics of rare earth elements in children's scalp hair from a rare earths mining area in southern China. *J Environ Sci Health A Tox Hazard Subst Environ Eng* **2004**, *39* (9), 2517–2532.

(169) Zhang, H.; Feng, J.; Zhu, W.; Liu, C.; Xu, S.; Shao, P.; Wu, D.; Yang, W.; Gu, J. Chronic toxicity of rare-earth elements on human beings: implications of blood biochemical indices in REE-high regions, South Jiangxi. *Biol Trace Elem Res* **2000**, *73* (1), 1–17.

(170) Weltje, L.; Heidenreich, H.; Zhu, W.; Wolterbeek, H. T.; Korhammer, S.; de Goeij, J. J. M.; Markert, B. Lanthanide concentrations in freshwater plants and molluscs, related to those in surface water, pore water and sediment. A case study in The Netherlands. *Sci. Total Environ.* **2002**, *286* (1–3), 191–214.

(171) Hirano, S.; Suzuki, K. T. Exposure, metabolism, and toxicity of rare earths and related compounds. *Environ Health Perspect* **1996**, *104* (Suppl 1), 85–95.

(172) Gupta, C. K.; Krishnamurthy, N. *Extractive Metallurgy of Rare Earths*; CRC Press: Boca Raton, 2004.

(173) Liao, B. Q.; Wang, J.; Wan, C. R. Separation and Recovery of Rare Earths in Reciprocating Extraction Columns. *Sep. Sci. Technol.* **2005**, *40* (8), 1685–1700.

(174) Murakami, H.; Ishihara, S. Carbonatite related light REE-rich deposit: Mountain Pass deposit, California, USA. *Shigen-Chishitsu* **2006**, *56* (2), 197–204.

(175) Xie, F.; Zhang, T. A.; Dreisinger, D.; Doyle, F. A critical review on solvent extraction of rare earths from aqueous solutions. *Miner. Eng.* **2014**, *56*, 10–28.

(176) Yantasee, W.; Warner, C. L.; Sangvanich, T.; Addleman, R. S.; Carter, T. G.; Wiacek, R. J.; Fryxell, G. E.; Timchalk, C.; Warner, M. G. Removal of Heavy Metals from Aqueous Systems with Thiol Functionalized Superparamagnetic Nanoparticles. *Environ. Sci. Technol.* **2007**, *41* (14), 5114–5119.

(177) Koehler, F. M.; Rossier, M.; Waelle, M.; Athanassiou, E. K.; Limbach, L. K.; Grass, R. N.; Günther, D.; Stark, W. J. Magnetic EDTA: coupling heavy metal chelators to metal nanomagnets for rapid removal of cadmium, lead and copper from contaminated water. *Chem. Commun.* **2009**, No. 32, 4862–4864.

(178) Kaminski, M.; Landsberger, S.; Nuñez, L.; Vandegrift, G. F. Sorption Capacity of Ferromagnetic Microparticles Coated with CMPO. *Sep. Sci. Technol.* **1997**, *32* (1–4), 115–126.

(179) Kaur, M.; Johnson, A.; Tian, G.; Jiang, W.; Rao, L.; Paszczynski, A.; Qiang, Y. Separation nanotechnology of diethylenetriaminepentaacetic acid bonded magnetic nanoparticles for spent nuclear fuel. *Nano Energy* **2013**, *2* (1), 124–132.

(180) Kaur, M.; Zhang, H.; Martin, L.; Todd, T.; Qiang, Y. Conjugates of Magnetic Nanoparticle—Actinide Specific Chelator for Radioactive Waste Separation. *Environ. Sci. Technol.* **2013**, *47* (21), 11942–11959.

(181) Polido Legaria, E. Hybrid nanoadsorbents for extraction and separation of rare earth elements in solution. Licenciate Thesis, Swedish University of Agricultural Sciences: Uppsala, Sweden, 2016.

(182) Tian, G.; Martin, L. R.; Zhang, Z.; Rao, L. Thermodynamic, Spectroscopic, and Computational Studies of Lanthanide Complexation with Diethylenetriaminepentaacetic Acid: Temperature Effect and Coordination Modes. *Inorg. Chem.* **2011**, *50* (7), 3087–3096.

(183) Nash, K. L.; Brigham, D.; Shehee, T. C.; Martin, A. The kinetics of lanthanide complexation by EDTA and DTPA in lactate media. *Dalton Trans.* **2012**, *41* (48), 14547–14556.

(184) Brigham, D. M. Lanthanide-Polyaminopolycarboxylate Complexation Kinetics in High Lactate Media: Investigating the Aqueous Phase of TALSPEAK. Dissertation, Washington State University: Pullman, WA, USA, 2013.

(185) Thakur, P.; Conca, J. L.; Dodge, C. J.; Francis, A. J.; Choppin, G. R. Complexation thermodynamics and structural studies of trivalent actinide and lanthanide complexes with DTPA, MS-325 and HMDTPA. *Radiochim. Acta* **2013**, *101* (4), 221–232.

(186) Grimes, T. S.; Nash, K. L. Acid Dissociation Constants and Rare Earth Stability Constants for DTPA. *J. Solution Chem.* **2014**, *43* (2), 298–313.

(187) Roosen, J.; Spooren, J.; Binnemans, K. Adsorption performance of functionalized chitosan–silica hybrid materials toward rare earths. *J. Mater. Chem. A* **2014**, *2* (45), 19415–19426.

(188) Li, W.; Wang, X.; Zhang, H.; Meng, S.; Li, D. Solvent extraction of lanthanides and yttrium from nitrate medium with CYANEX 925 in heptane. *J. Chem. Technol. Biotechnol.* **2007**, *82* (4), 376–381.

(189) Radhika, S.; Kumar, B. N.; Kantam, M. L.; Reddy, B. R. Liquid–liquid extraction and separation possibilities of heavy and light rare-earths from phosphoric acid solutions with acidic organophosphorus reagents. *Sep. Purif. Technol.* **2010**, *75* (3), 295–302.

(190) Sui, N.; Huang, K.; Zhang, C.; Wang, N.; Wang, F.; Liu, H. Light, Middle, and Heavy Rare-Earth Group Separation: A New Approach via a Liquid–Liquid–Liquid Three-Phase System. *Ind. Eng. Chem. Res.* **2013**, *52* (17), 5997–6008.

(191) Lanthanide contraction. *Wikipedia, the free encyclopedia*; 2014.

(192) Shannon, R. D. Revised effective ionic radii and systematic studies of interatomic distances in halides and chalcogenides. *Acta Crystallogr., Sect. A* **1976**, *32* (5), 751–767.

(193) D'Angelo, P.; Zitolo, A.; Migliorati, V.; Chillemi, G.; Duvail, M.; Vitorge, P.; Abadie, S.; Spezia, R. Revised Ionic Radii of Lanthanoid(III) Ions in Aqueous Solution. *Inorg. Chem.* **2011**, *50* (10), 4572–4579.

(194) Zhang, H.; Zhou, H.; Qiang, Y. Kinetics, Thermodynamics and Reusability of DTPA-Functionalized Magnetic Nanosorbents for Cadmium Removal from Wastewater. *(To be submitted)*.

(195) Moeller, T.; Thompson, L. C. Observations on the rare Earths—LXXV(1): The stabilities of diethylenetriaminepentaacetic acid chelates. *J. Inorg. Nucl. Chem.* **1962**, *24* (5), 499–510.

(196) Richens, D. T. *The chemistry of aqua ions: synthesis, structure, and reactivity: a tour through the periodic table of the elements*; J. Wiley: Chichester ; New York, 1997.

(197) Lewis, G. N.; Randall, M. The Activity Coefficient of Strong Electrolytes[1]. *J. Am. Chem. Soc.* **1921**, *43* (5), 1112–1154.

(198) Shehee, T. C. The americium/lanthanide separation conundrum: Selective oxidation or soft donor complexants?, WASHINGTON STATE UNIVERSITY, 2010.

(199) Qiu, H.; Lv, L.; Pan, B.; Zhang, Q.; Zhang, W.; Zhang, Q. Critical review in adsorption kinetic models. *J. Zhejiang Univ. Sci. A* **2009**, *10* (5), 716–724.

(200) Lagergren, S. About the theory of so-called adsorption of soluble substances. *K. Sven. Vetenskapsakad. Handl.* **1898**, *24* (4), 1–39.

(201) Ho, Y. S.; McKay, G. Pseudo-second order model for sorption processes. *Process Biochem.* **1999**, *34* (5), 451–465.

(202) Ho, Y. S. Review of second-order models for adsorption systems. *J. Hazard. Mater.* **2006**, *136* (3), 681–689.

(203) Weber, W. J.; Morris, J. C. Kinetics of Adsorption on Carbon from Solution. *J. Sanit. Eng. Div.* **1963**, *89* (2), 31–60.

(204) Boyd, G. E.; Adamson, A. W.; Myers, L. S. The Exchange Adsorption of Ions from Aqueous Solutions by Organic Zeolites. II. Kinetics[1]. *J. Am. Chem. Soc.* **1947**, *69* (11), 2836–2848.

(205) Sheha, R. R.; El-Zahhar, A. A. Synthesis of some ferromagnetic composite resins and their metal removal characteristics in aqueous solutions. *J. Hazard. Mater.* **2008**, *150* (3), 795–803.

(206) Itodo, A. U.; Abdulrahman, F. W.; Hassan, L. G.; Maigandi, S. A.; Itodo, H. U. Intraparticle Diffusion and Intraparticulate Diffusivities of Herbicide on Derived Activated Carbon. *Researcher* **2010**, *2* (2), 74–86.

(207) Abdel-Ghani, N. T.; El-Chaghaby, G. A.; Zahran, E. M. Pentachlorophenol (PCP) adsorption from aqueous solution by activated carbons prepared from corn wastes. *Int. J. Environ. Sci. Technol.* **2015**, *12* (1), 211–222.

(208) Mollinedo-Ponce-de-León, H. R.; Martínez-Delgadillo, S. A.; Mendoza-Escamilla, V. X.; Gutiérrez-Torres, C. C.; Jiménez-Bernal, J. A. Evaluation of the Effect of the Rotational Electrode Speed in an Electrochemical Reactor Using Computational Fluid Dynamics (CFD) Analysis. *Industrial & Engineering Chemistry Research* **2012**, *51* (17), 5947–5952.

(209) Stamou, A. I.; Theodoridis, G.; Xanthopoulos, K. Design of Secondary Settling Tanks Using a CFD Model. *Journal of Environmental Engineering* **2009**, *135* (7), 551–561.

(210) Xu, N.; Fan, L.; Pang, H.; Shi, H. Feasibility study and CFD-aided design for a new type oxidation ditch based on airlift circulation. *The Canadian Journal of Chemical Engineering* **2010**, n/a-n/a.

(211) Brannock, M.; Wang, Y.; Leslie, G. Mixing characterisation of full-scale membrane bioreactors: CFD modelling with experimental validation. *Water Research* **2010**, *44* (10), 3181–3191.

(212) Le Moullec, Y.; Gentric, C.; Potier, O.; Leclerc, J. P. CFD simulation of the hydrodynamics and reactions in an activated sludge channel reactor of wastewater treatment. *Chemical Engineering Science* **2010**, *65* (1), 492–498.

(213) Hriberšek, M.; Žajdela, B.; Hribernik, A.; Zadravec, M. Experimental and numerical investigations of sedimentation of porous wastewater sludge flocs. *Water Research* **2011**, *45* (4), 1729–1735.

(214) Qi, N.; Zhang, H.; Jin, B.; Zhang, K. CFD modelling of hydrodynamics and degradation kinetics in an annular slurry photocatalytic reactor for wastewater treatment. *Chemical Engineering Journal* **2011**, *172* (1), 84–95.

(215) Khashan, S. A.; Elnajjar, E.; Haik, Y. CFD simulation of the magnetophoretic separation in a microchannel. *Journal of Magnetism and Magnetic Materials* **2011**, *323* (23), 2960–2967.

(216) Khashan, S. A.; Elnajjar, E.; Haik, Y. Numerical simulation of the continuous biomagnetic separation in a two-dimensional channel. *International Journal of Multiphase Flow* **2011**, *37* (8), 947–955.

(217) Khashan, S. A.; Haik, Y.; Elnajjar, E. CFD simulation for biomagnetic separation involving dilute suspensions. *Can. J. Chem. Eng.* **2012**, *90* (6), 1450–1456.

(218) Fukui, S.; Nakajima, H.; Ozone, A.; Hayatsu, M.; Yamaguchi, M.; Sato, T.; Imaizumi, H.; Nishijima, S.; Watanabe, T. Study on open gradient magnetic separation using multiple magnetic field sources. *IEEE Transactions on Applied Superconductivity* **2002**, *12* (1), 959–962.

(219) S. Fukui, M. T. Analytical Study on Open Gradient Magnetic Separation Using Quadrupole Magnetic Field. *Applied Superconductivity, IEEE Transactions on* **2004**, *14* (2), 1572–1575.

(220) Mohanty, S.; Das, B.; Mishra, B. K. A preliminary investigation into magnetic separation process using CFD. *Minerals Engineering* **2011**, *24* (15), 1651–1657.